

R.P.I. Technical Report MP-23

A Progress Report for
July 1, 1970 to June 30, 1971

ANALYSIS AND DESIGN OF A CAPSULE
LANDING SYSTEM AND SURFACE VEHICLE
CONTROL SYSTEM FOR MARS EXPLORATION

National Aeronautics and Space
Administration

Grant NGL 33-018-091

Submitted by the Special Projects Committee

D.K. Frederick
P.K. Lashmet
G.N. Sandor
C.N. Shen
E.J. Smith
S.W. Yerazunis

June 30, 1971

School of Engineering
Rensselaer Polytechnic Institute

ABSTRACT

Investigation of problems related to control of a mobile planetary vehicle according to a systematic plan for the exploration of Mars has been undertaken. Problem areas receiving attention include: overall systems analysis; vehicle configuration, dynamics and attitude control; vehicle power systems analysis; on-board navigation systems; satellite-vehicle navigation systems; terrain sensing, interpretation and modeling; and chromatographic systems design concept studies. The specific tasks which have been undertaken are defined and the progress which has been achieved during the period July 1, 1970 to June 30, 1971 is summarized. Projections of the work to be undertaken in certain areas during the period July 1, 1971 to June 30, 1972 are included.

TABLE OF CONTENTS

	Page
INTRODUCTION.....	1
DEFINITION OF TASKS.....	1
A. Vehicle Configuration, Control, Dynamics, Systems and Propulsion.....	1
B. General Systems Analysis.....	2
C. Surface Navigation and Path Control.....	2
D. Chemical Analysis of Specimens.....	2
SUMMARY OF RESULTS.....	2
A. Vehicle Configuration, Control, Dynamics, Systems and Propulsion.....	2
A.1. Roving Vehicle Configuration and Dynamics.....	2
A.1.a. Dynamics Study.....	3
A.1.b. Obstacle Capability.....	11
A.1.c. Maneuverability.....	12
A.1.d. Payload Study.....	18
A.2. Flexible Toroidal Wheel Design.....	18
A.2.a. Model Wheel Redesign.....	23
A.2.b. Wheel and Hoop Testing.....	24
A.2.c. Computer Analysis of Wheel.....	24
A.2.d. Full-Sized Wheel Prototype.....	27
A.2.e. Hinge Design.....	28
A.3. Vehicle Steering Control System.....	28
A.3.a. Differential Drive Control.....	32
A.3.b. Steering Control Sub-System.....	36
B. Systems Analysis.....	38
C. Navigation, Terrain Modeling and Path Selection.....	52
C.1. Navigation Systems.....	52
C.1.a. Satellite Navigation System.....	54
C.1.b. Vehicle Navigation System.....	63
C.1.c. Preliminary Design of an Automatic Device for the Location of the Pole Star and/or True Pole of Mars.....	69
C.1.d. Local Vertical Sensor.....	75

C.2.	Terrain Modeling and Path Selection.....	80
D.	Chromatographic Systems Analysis.....	90
D.1.	Test Facility.....	90
D.2.	System Model Verification.....	91
D.3.	Transport Parameter Estimation.....	101
REFERENCES.	103

Analysis and Design of a Capsule Landing System and Surface Vehicle Control System for Mars Exploration

I. Introduction

Current national goals in space exploration include a detailed study and examination of the planet Mars. The effectiveness of Mars exploration missions would be enhanced according to the extent to which the investigative devices which are landed are mobile, to the range of their mobility, and to the ability to control their motion. In order to achieve basic mission objectives, and beyond that, to maximize the return on the commitment of resources to the mission, formidable technical problems must be resolved. The major factor contributing to these problems is the round trip communications time delay between martian and earth control stations which varies from a minimum of about 9 minutes to a maximum of 25 minutes. This time delay imposes stringent requirements on the vehicle, on its control and communication systems and on those systems included on board to make the scientific measurements, in terms of their ability to function autonomously. These systems must be able to operate with a high degree of reliability and must be capable of calling for earth control under appropriate circumstances.

A number of important problems originating with these factors and relating directly the basic mission objectives of an unmanned exploration of Mars have been and are currently being investigated by a faculty-student project team at Rensselaer Polytechnic Institute with the support of NASA NGL-33-018-091.

This progress report describes the tasks which have been undertaken and documents the progress which has been achieved in the interval July 1, 1970 to June 30, 1971.

II. Definition of Tasks

The delay time in round trip communication between Mars and Earth gives rise to unique problems relevant to martian and/or other planetary explorations. All phases of the mission from landing the capsule in the neighborhood of a desired position to the systematic traversing of the surface and the attendant detection, measurement, and analytical operations must be consummated with a minimum of control and instruction by earth based units. The delay time requires that on board systems capable of making rational decisions be developed and that suitable precautions be taken against potential catastrophic failures. Four major task areas, which are in turn divided into appropriate sub-tasks, have been defined and are listed below.

- A. Vehicle Configuration, Control, Dynamics, Systems and Propulsion.
The objectives of this task are to investigate problems related to the design of a roving vehicle for Mars exploration with respect to configuration; motion and attitude control; obstacle avoidance; control, information and power systems; and propulsion systems. In addition, the design concepts must accommodate the equipment and instruments required to automate the vehicle and to perform the scientific objectives of the mission.

- B. General Systems Analysis. The objective of this task is to develop a framework within which decisions in design involving conflicting requirements can be made rationally and in the context of the whole system and mission. Relationships between alternative mission profiles and specifications and weight, energy and space allocation and management will be sought.
- C. Surface Navigation and Path Control. Once the capsule is landed and the roving vehicle is in an operational state, it is necessary that the vehicle can be directed to proceed under remote control from the landing site to specified positions on the martian surface. This task is concerned with the problems of terrain modeling, path selection and navigation between the initial and terminal sites when major terrain features precluding direct paths are to be anticipated. On board decision making capability must be designed to minimize earth control responsibility except in the most adverse circumstances.
- D. Chemical Analysis of Specimens. A major objective of martian surface exploration will be to obtain chemical, biochemical or biological information. Most experiments proposed for the mission require a general duty, chromatographic separator prior to chemical analysis by some device. The objective of this task is to generate fundamental data and concepts required to optimize such a chromatographic separator according to the anticipated mission.

III. Summary of Results

Task A. Vehicle Configuration, Control, Dynamics, Systems and Propulsion

The objectives of this task are to investigate problems related to the design of a roving vehicle for Mars exploration with respect to configuration, motion and attitude control, obstacle avoidance, control, information and power systems and propulsion systems. In addition, the design concepts which are developed must accommodate the equipment and instruments required to automate the vehicle and to perform the scientific objectives of the mission.

Three major sub-tasks have been defined: (a) roving vehicle configuration and dynamics, (b) wheel analysis and design, and (c) vehicle steering control system.

The progress achieved to date is described in the sections immediately following.

Task A.1. Roving Vehicle Configuration and Dynamics -

W. P. Rayfield, D. Caracappa, H. Goldberg, D. Walsh, J. Young
Faculty Advisor: Prof. G. N. Sandor

The major objective of this task is the development and optimization of a roving vehicle for Mars, hereafter designated as MRV. There were four main objectives for the previous period. First, the heave and pitch dynamics of the MRV were to be studied. Secondly, the obstacle capabilities of the rover were to be studied and tested. Thirdly, the vehicle maneuverability was to be evaluated. And

fourthly, a payload study was to be initiated.

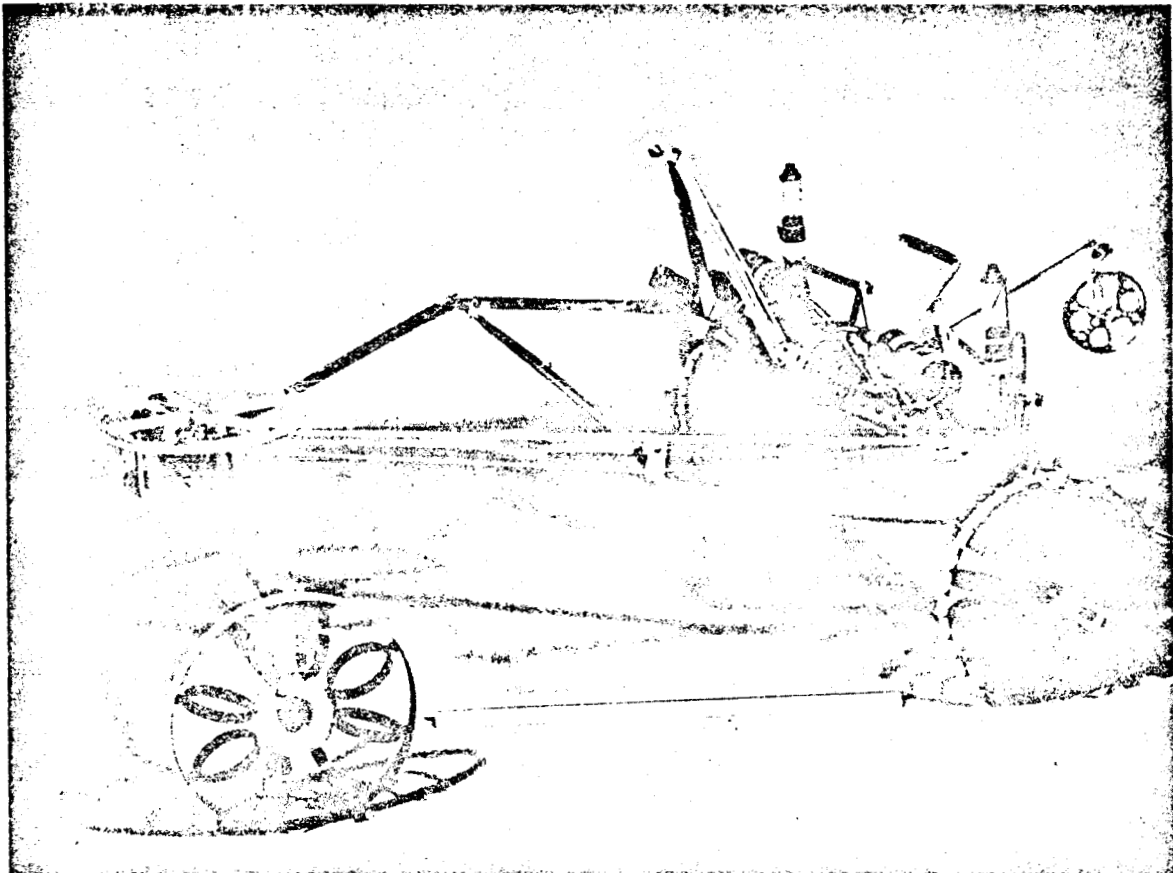
The MRV concept, which has been described in detail in References 1 and 2 is shown in Figure 1. In brief, the proposed MRV is a five-wheeled vehicle which would normally operate in a four-wheel mode but which could also maneuver in a three-wheel mode using the swivel wheel by a shift in the center of gravity of the vehicle.

Task A.1.a. Dynamics Study.

An outline of the dynamics study has been prepared as shown in Figure 2. Progress has been made in the following four areas:

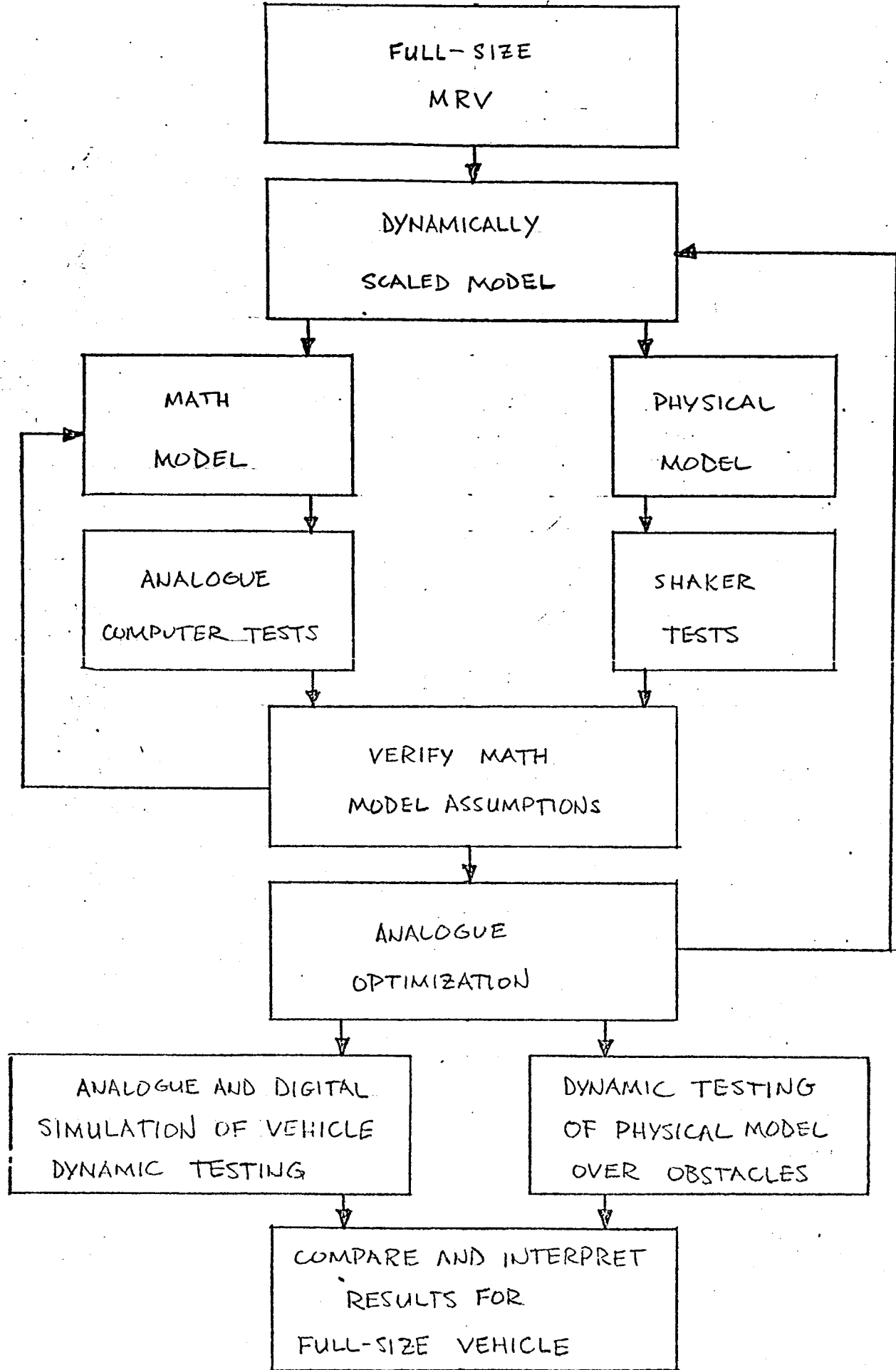
- (1) The MRV dynamically-scaled operational model has been debugged and revised as shown in Table 1. In addition, a straight-line, path-generating four-bar linkage has been designed to replace the original, single-pivot rear suspension, as shown in Figures 3 and 4.
- (2) The MRV dynamically-scaled operational vehicle has been analyzed and refined to reduce the total vehicle weight and maintain the proper mass distribution. Major weight reductions were achieved by machining the flanges off the four control motors, milling down the wheel hubs, adding lightening holes to most elements of the main vehicle frame, and replacing the rear swivel wheel with a lighter design.
- (3) Dynamic test apparatus has been prepared for testing the MRV model. A shaker platform was designed and constructed which is capable of providing a vehicle displacement input to the two rear wheels, the two front wheels or the left or right side of the MRV. The amplitude and frequency of the input can be adjusted to study vehicle response to different terrains.
- (4) A mathematical model of the heave and pitch dynamics of the MRV has been developed as follows:

The vehicle is considered to move only in the vertical plane, which can be justified by its symmetry. An oscillating vertical displacement input is applied to the rear wheels simulating a terrain disturbance. The vehicle can be represented schematically as a lumped spring-mass system with four masses and moments of inertia, four linear spring constants, three torsional spring constants, and a one-way damping coefficient, as shown in Figure 5. Taking the five rigid sections individually, and constructing free-body diagrams, Figure 6, three differential equations can be written for each since each section has three degrees of freedom. This yields a total of fifteen equations. Eight of the fifteen equations must be used to determine the "internal" forces between each pair of connected sections of the vehicle, i.e. force equations. This leaves seven equations in the seven unknowns necessary to



DYNAMIC SCALED DOWN MODEL OF
MARS ROVING VEHICLE

Figure 1

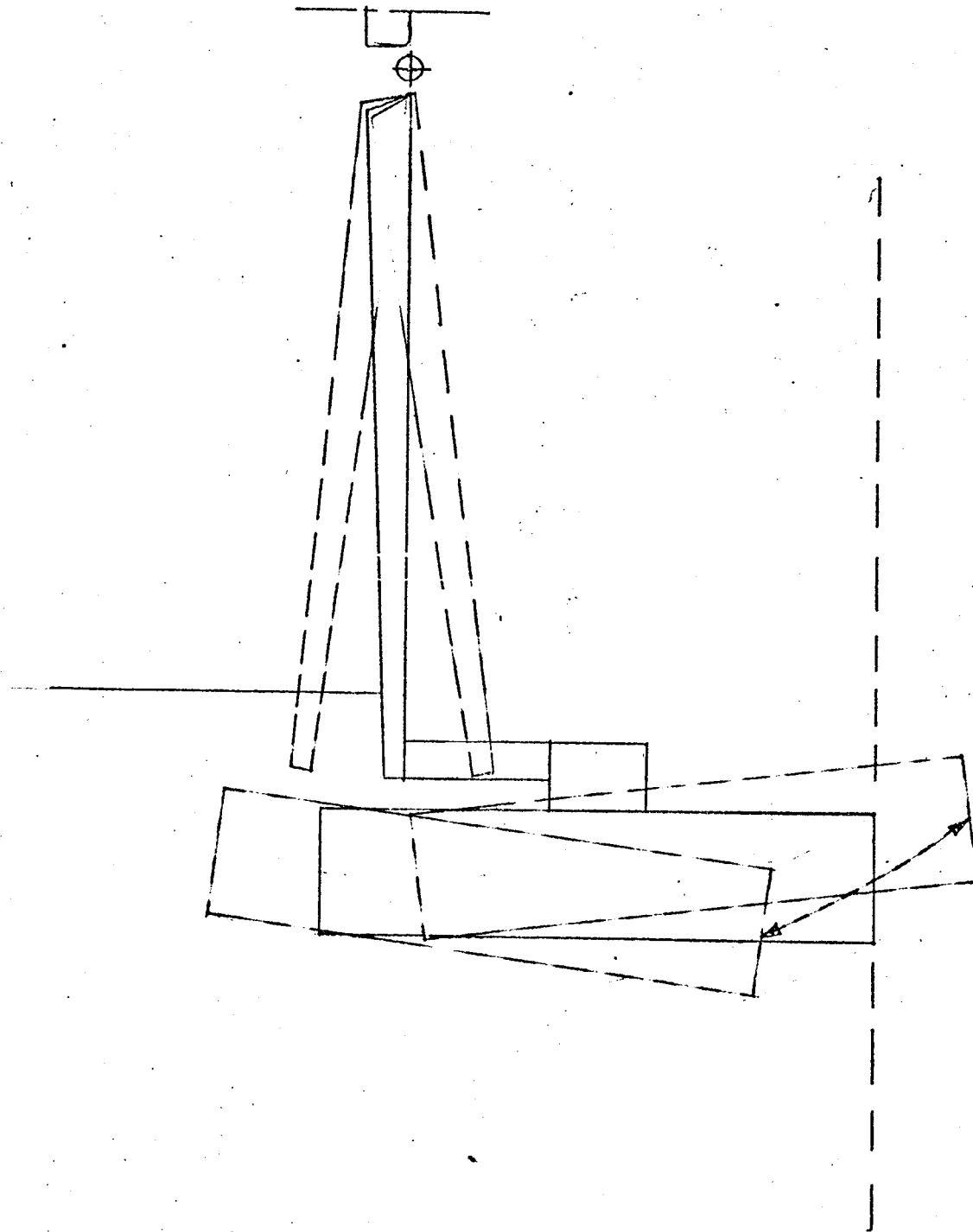


PROPOSED MRV DYNAMICS STUDY

Figure 2.

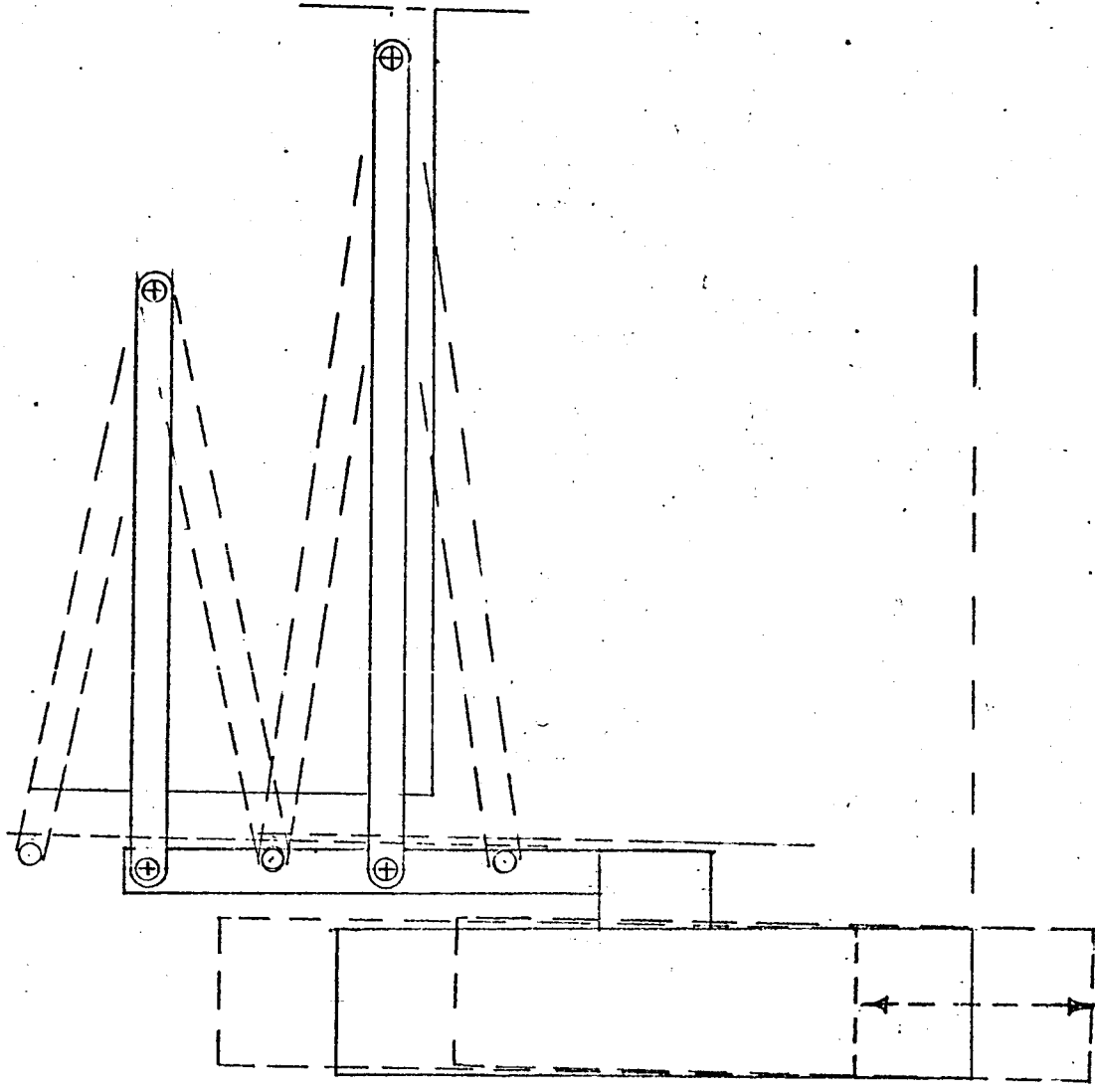
TABLE 1: DESIGN IMPROVEMENTS ON MRV DYNAMIC MODEL SINCE MAY, 1970

<u>Vehicle Elements</u>	<u>Problems Existing in May, 1970</u>	<u>Solutions Implemented</u>
Frame:	Angles twisted under spring load Forward support structure susceptible to buckling Epoxy weak on front cross brace	Brace added Rectangular cross-section replaced with angle Epoxied joint riveted
Suspension:	Rear vertical deflection spring too weak Rear horizontal deflection springs permitted twisting during tilt-back Rear suspension needed damping Rear suspension strut interfered with vehicle frame Rear suspension strut twisted on tilt-back maneuver	Spring steel replaced phosphor bronze Shorter spring used Air dampers added Slide added to guide free end of struts Larger, closer fitted slide added
Tilting:	Tilt actuator lever slipped on tilt shaft Spring tension too low on down slopes Tilting shaft interfered with Drive motor support braces	Larger set-screws used Cable spring tilting system redesigned Support braces redesigned
Drive Motors:	Minimum speed too high, maximum torque too low Difficult to control while steering	New motors purchased to be interchangeable with present high speed motors Pulley and cable system added to power supplies
Steering:	Cable slips on spool, tangles Pulleys slip off bearings Cable slacks on obstacle negotiation, slips off pulleys	Larger spool added, cable fixed to spool Plastic pulleys replaced with aluminum Tension element added to cable system



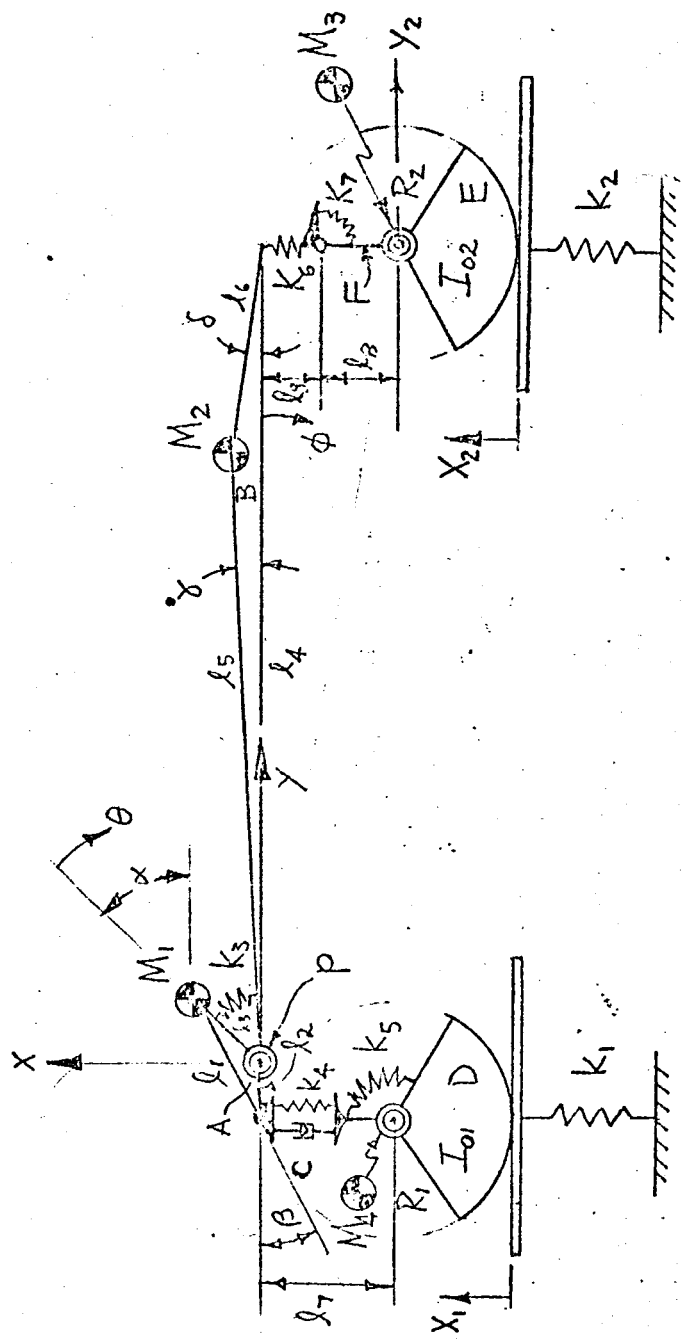
MRV -- ORIGINAL REAR SUSPENSION

FIGURE 3



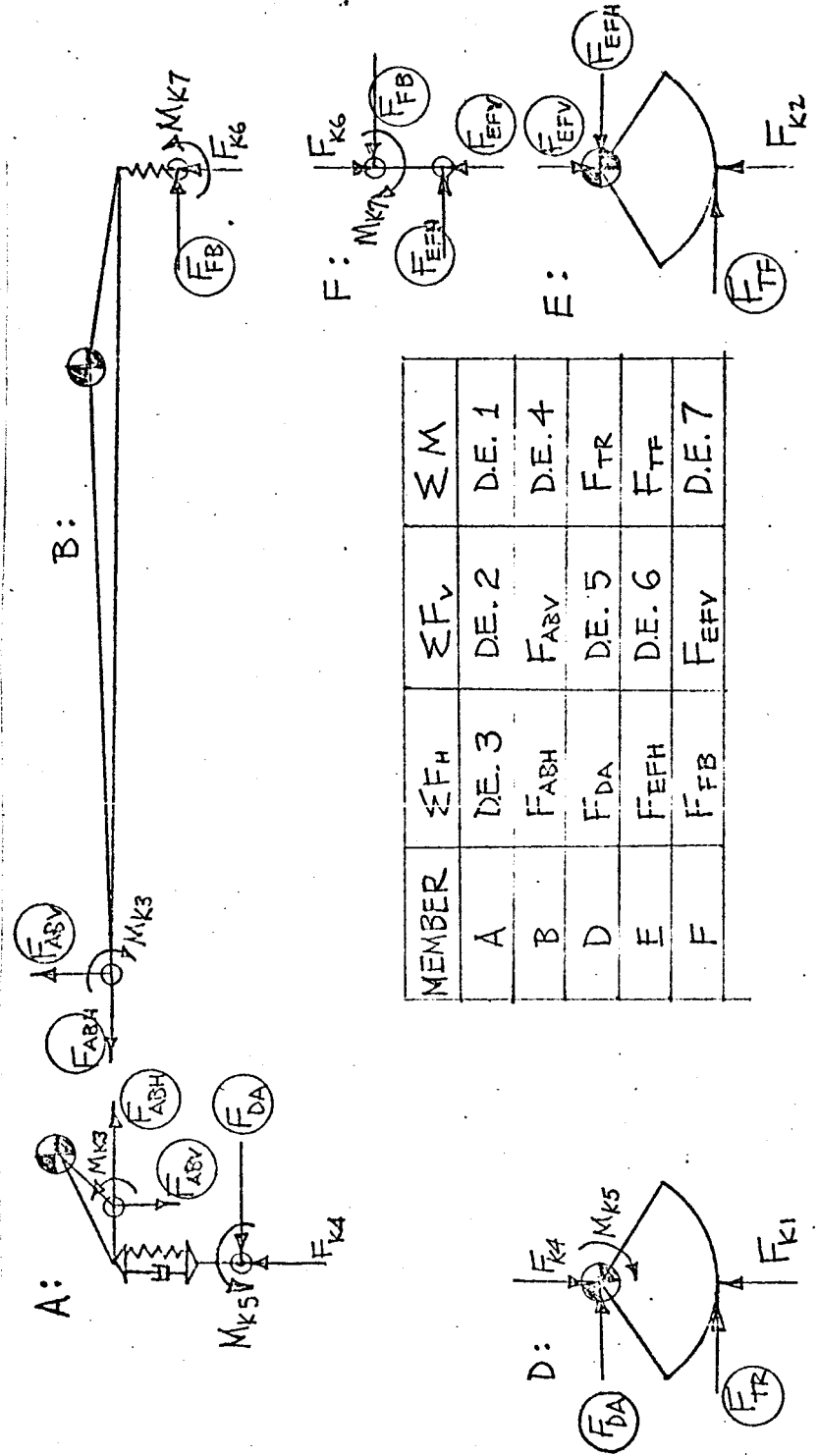
MRV -- IMPROVED REAR SUSPENSION

FIGURE 4



SCHEMATIC OF VEHICLE FOR HEAVE AND PITCH DYNAMICS
(7 DEGREES-OF-FREEDOM)

FIGURE 5



FREE-BODY DIAGRAMS: INTERNAL FORCES
(INERTIA FORCES OMITTED)

FIGURE 6

describe the position of all parts of the vehicle at any one time. Since the seven equations are linear in all acceleration terms, the equations can be expressed in matrix form as shown in Figures 7 and 8 where matrices A and B contain displacements and velocity terms and products, but no acceleration terms. By using a fourth-order Runge-Kutta iteration technique on the computer, all seven displacements and velocities can be calculated for each time increment; thus all the matrix elements of both A and B can be evaluated. Inverting A and multiplying the result by B yields the acceleration terms. The computer can then print out graphs of the displacement, velocity, and acceleration of each of the seven independent variables, Figures 9 and 10. The program is flexible to permit adjustment of the input amplitude and frequency as well as any of the vehicle parameters.

The mathematical model was developed to simulate the scaled operational model, and all spring constants, masses and dimensions for the computer input were measured from it. Thus, the natural frequencies and any instabilities predicted by the computer can be experimentally substantiated. The model can then predict the maximum acceleration at any point of the vehicle for each excitation frequency.

This effort will be aimed at developing relationships between vehicle speed and payload excitation, obstacle size, and suspension elements, with the anticipated results that this vehicle, with optimized suspension design and set payload excitation limits will have a higher speed capability over rough terrain than the segmented configurations proposed by others.

Task A.1.b. Obstacle Capability.

Progress has been made in the following three areas:

(1) A theoretical analysis was made of the vehicle's obstacle negotiation capabilities including step, crevasse, up-slope, down-slope, side-slope, cliff, and ridge. To evaluate the results of this study, a vehicle test area was prepared. The area was designed to provide all the basic obstacles, each adjustable in magnitude. A high friction traction surface was applied to all the obstacles, since the purpose of the facility was to study the obstacle capability and stability limitations.

An MRV with an adjustable center-of-gravity can easily negotiate step obstacles less than the wheel radius and crevasse obstacles less than the wheel diameter. Free-body diagrams of the front and rear wheels are shown in Figure 11.

The track width of 119 inches and the ground clearance of 29 inches permit the vehicle to straddle a maximum ridge formed by two intersecting 28° opposite slopes. The vehicle can climb

$$\begin{bmatrix} A \\ 7 \times 7 \end{bmatrix} \begin{bmatrix} \ddot{\theta} \\ \ddot{x} \\ \ddot{y} \\ \ddot{\phi} \\ \ddot{x}_1 \\ \ddot{x}_2 \\ \ddot{y}_2 \end{bmatrix} = \begin{bmatrix} B \\ 7 \times 1 \end{bmatrix}$$

$$\begin{aligned} a_{11} &= I_{MIP} + M_1 l_3^2 \\ &\quad - [M_4 (x_1 - x - l_7) - I_{O1} (x_1 - x - l_7) \frac{1}{R_1^2}] [l_7 + x + l_2 \theta - x_1] \\ a_{12} &= -M_1 l_3 \cos \alpha + (M_4 \theta + I_{O1} \theta \frac{1}{R_1^2}) (l_7 + x + l_2 \theta - x_1) \\ a_{13} &= +M_1 l_3 \sin \alpha - (M_4 + I_{O1} \frac{1}{R_1^2}) (l_7 + x + l_2 \theta - x_1) \\ a_{14} &= 0 \\ a_{15} &= -M_4 \theta (l_7 + x + l_2 \theta - x_1) \\ a_{16} &= 0 \\ a_{17} &= 0 \end{aligned}$$

$$\begin{aligned} a_{21} &= -M_1 l_3 \cos \alpha \\ a_{22} &= M_1 + M_2 \\ a_{23} &= -M_4 \theta - I_{O1} \theta \frac{1}{R_1^2} \\ a_{24} &= -M_2 l_5 \\ a_{25} &= 0 \\ a_{26} &= 0 \\ a_{27} &= 0 \end{aligned} \quad \begin{aligned} a_{31} &= M_1 l_3 \sin \alpha + M_4 (x_1 - x - l_7) + I_{O1} (x_1 - x - l_7) \frac{1}{R_1^2} \\ a_{32} &= -M_4 \theta - I_{O1} \theta \frac{1}{R_1^2} \\ a_{33} &= M_1 + M_4 + I_{O1} \frac{1}{R_1^2} + M_2 \\ a_{34} &= 0 \\ a_{35} &= M_4 \theta + I_{O1} \frac{1}{R_1^2} \\ a_{36} &= 0 \\ a_{37} &= M_3 + I_{O2} \frac{1}{R_2^2} \end{aligned}$$

EQUATIONS OF MOTION FOR HEAVE AND PITCH DYNAMICS (1 of 2)

Figure 7.

$$\begin{array}{l}
 \left[\begin{array}{l} a_{41} = 0 \\ a_{42} = -M_2 l_5 \\ a_{43} = +M_2 l_5 \delta \\ a_{44} = I_{M2P} + M_2 l_5^2 \\ a_{45} = 0 \\ a_{46} = 0 \\ a_{47} = -(M_3 + I_{02} \frac{1}{R_2^2}) (l_9 + x - l_4 \phi - x_L) \end{array} \right. \quad \left[\begin{array}{l} a_{51} = 0 \\ a_{52} = 0 \\ a_{53} = M_4 \theta + I_{01} \theta \frac{1}{R_1^2} \\ a_{54} = 0 \\ a_{55} = M_4 \\ a_{56} = 0 \\ a_{57} = 0 \end{array} \right. \quad \left[\begin{array}{l} a_{61} = 0 \\ a_{62} = 0 \\ a_{63} = 0 \\ a_{64} = 0 \\ a_{65} = 0 \\ a_{66} = M_3 \\ a_{67} = 0 \end{array} \right. \quad \left[\begin{array}{l} a_{71} = 0 \\ a_{72} = 0 \\ a_{73} = 0 \\ a_{74} = 0 \\ a_{75} = 0 \\ a_{76} = 0 \\ a_{77} = (M_3 + I_{02} \frac{1}{R_2^2}) \end{array} \right]
 \end{array}$$

$$\begin{aligned}
 b_1 = & k_4 l_2 (-x - l_2 \theta + x_1) + \{ M_4 [(2\dot{x}_1 - 2\dot{x})\dot{\theta}] - k_5 [(-y + l_7 \theta + x \theta - x_1 \theta) \frac{1}{R_1} + \theta] \frac{1}{R_1} \\
 & + I_{01} [(2\dot{x}_1 - 2\dot{x})\dot{\theta}] \frac{1}{R_1^2} + k_4 (-x - l_2 \theta + x_1) \theta \} (l_7 + x + l_2 \theta - x_1) \\
 & - k_5 [(-y + l_7 \theta + x \theta - x_1 \theta) \frac{1}{R_1} + \theta] - k_3 (\theta - \phi) + M_1 g l_7 \sin \alpha \theta
 \end{aligned}$$

$$b_2 = k_6 (x_2 - x + l_4 \phi) - k_5 (-y \theta) \frac{1}{R_1} + k_4 (-x - l_2 \theta + x_1)$$

$$\begin{aligned}
 b_3 = & -M_4 [(2\dot{x}_1 - 2\dot{x})\dot{\theta}] + k_5 [(-y - l_7 \theta + x \theta - x_1 \theta) \frac{1}{R_1} + \theta] \frac{1}{R_1} \\
 & - I_{01} [(2\dot{x}_1 - 2\dot{x})\dot{\theta}] \frac{1}{R_1^2} - k_4 (-x - l_2 \theta + x_1) \theta + k_4 (-x - l_2 \theta + x_1) \theta
 \end{aligned}$$

$$b_4 = -k_6 (x_2 - x + \phi l_4) l_4 + k_3 (\theta - \phi) - k_7 [(y_2 - y)/l_8 + \phi]$$

$$b_5 = -k_1 x_1 - k_4 (-x - l_2 \theta + x_1) + k_5 (-y \theta) \frac{1}{R_1} + k_1 A \sin \omega t$$

$$b_6 = -k_2 x_2 - k_6 (x_2 - x + \phi l_4)$$

$$b_7 = k_6 (x_2 - x + l_4 \phi) (y_2 - y)$$

EQUATIONS OF MOTION FOR HEAVE AND PITCH DYNAMICS (2 of 2)

Figure 8.

ACCELERATION OF VARIABLE X(5)	DISP	MEL	ACC
.....			
VA	2.35E-11	7.04E-08	1.41E-04
V A	1.88E-10	2.81E-07	2.81E-04
V A	6.32E-10	6.32E-07	4.20E-04
DV A	1.50E-09	1.12E-06	5.58E-04
DV A	2.92E-09	1.75E-05	6.93E-04
D V A	5.04E-09	2.51E-06	8.27E-04
D V A	7.98E-09	3.40E-06	9.57E-04
D V A	1.19E-08	4.42E-06	1.08E-03
D V A	1.69E-08	5.56E-06	1.21E-03
D V A	2.30E-08	6.83E-06	1.32E-03
D V A	3.06E-08	8.21E-06	1.44E-03
D V A	3.95E-08	9.71E-06	1.55E-03
D V A	5.00E-08	1.13E-05	1.65E-03
D V A	6.21E-08	1.30E-05	1.75E-03
D V A	7.60E-08	1.48E-05	1.84E-03
D V A	9.18E-08	1.67E-05	1.92E-03
D V A	1.09E-07	1.86E-05	2.00E-03
D V A	1.29E-07	2.07E-05	2.07E-03
D V A	1.51E-07	2.28E-05	2.13E-03
D V A	1.75E-07	2.49E-05	2.19E-03
D V A	2.01E-07	2.71E-05	2.23E-03
D V A	2.29E-07	2.94E-05	2.27E-03
D V A	2.59E-07	3.17E-05	2.30E-03
D V A	2.92E-07	3.40E-05	2.33E-03
D V A	3.28E-07	3.63E-05	2.34E-03
D V A	3.65E-07	3.87E-05	2.35E-03
D V A	4.05E-07	4.10E-05	2.34E-03
D V A	4.47E-07	4.34E-05	2.33E-03
D V A	4.92E-07	4.57E-05	2.31E-03
D V A	5.38E-07	4.80E-05	2.28E-03
D V A	5.88E-07	5.03E-05	2.25E-03
D V A	6.39E-07	5.25E-05	2.20E-03
D V A	6.93E-07	5.47E-05	2.15E-03
D V A	7.48E-07	5.68E-05	2.09E-03
D V A	8.06E-07	5.88E-05	2.03E-03
D V A	8.66E-07	6.08E-05	1.95E-03
D V A	9.28E-07	6.27E-05	1.87E-03
D V A	9.91E-07	6.46E-05	1.78E-03
D V A	1.06E-06	6.63E-05	1.69E-03
D V A	1.12E-06	6.79E-05	1.58E-03
D V A	1.19E-06	6.95E-05	1.48E-03
D V A	1.26E-06	7.09E-05	1.37E-03
D V A	1.33E-06	7.22E-05	1.25E-03
D V A	1.41E-06	7.34E-05	1.13E-03
D V A	1.48E-06	7.45E-05	1.00E-03
D V A	1.56E-06	7.54E-05	8.74E-04
COMPUTER OUTPUT			
.....			
Figure 9.			

[illegible]

25° up- and down-slopes and 45° side-slopes, while maintaining a constant ground clearance, as shown in Figure 13; 40° up-slopes can be negotiated with a loss of ground clearance, provided there exists good traction; 80° down-slopes are possible, with good traction. The MRV can cross a ridge formed by two intersecting 40° opposite-slopes.

Turning radii have been determined as shown in Figure 12. The center of gravity analysis shown in Figures 14 and 15 indicate, for example, a stability permitting the vehicle to climb its maximum step while on a 25° up-slope.

Static traction and torque equations were written as functions of the magnitudes of each of three major obstacles (step, crevasse, and slope), and the forward motion of the MRV while negotiating them. A computer program was written to solve these for the incrementally increasing forward movement of the vehicle, showing the positions of peak torque and traction requirements.

(2) A 16-mm movie was made using the operational model and the prepared test area. The film illustrates the following: maneuverability in the four- and three-wheel modes; the tilt-back maneuver; up-slope, down-slope, and side-slope maneuvering; step and crevasse negotiation; operation of all suspension elements; and a short traverse over a loose soil, outdoor test area.

(3) For the vehicle to tilt back into the three-wheel mode, the tilting motor simply shifts the vehicle CG aft of the rear wheels by tilting the vehicle body with respect to the forward structure as shown in Figure 16. However, this same method cannot be used to return the vehicle to the four-wheel mode since the front wheels are no longer in contact with the surface.

Therefore, a simple, lightweight forward jacking mechanism was designed and added to the vehicle, Figure 17. A small level, pivoted to the end of the tail-wheel strut, is lowered to the surface automatically as the raised front section is lowered; this is the first step in returning the vehicle to the four-wheel mode. The rear traction wheels are then driven forward, forcing the pointed jacking strut, equipped with a "basket" similar to a ski pole, to penetrate a soft terrain or "catch" on a harder rock surface. Thus, as the vehicle moves forward, the strut gently tilts the vehicle forward into its normal four-wheel mode.

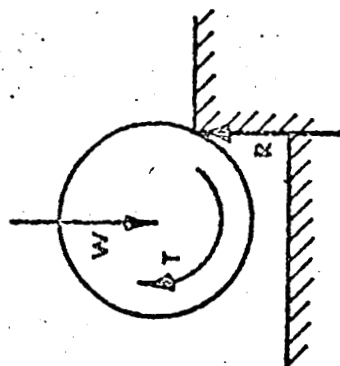
Task A.1.c. Maneuverability.

The most important "obstacle capability" of an unmanned roving vehicle is its maneuverability, since this can greatly reduce the number of difficult obstacles it must negotiate as well as provide recourse for non-negotiable obstacles.

The first problem of the maneuverability study was to establish meaningful parameters to measure maneuverability of various

STEP AND CREVASSE OBSTACLE NEGOTIATION

REAR WHEEL:



FRONT WHEEL:

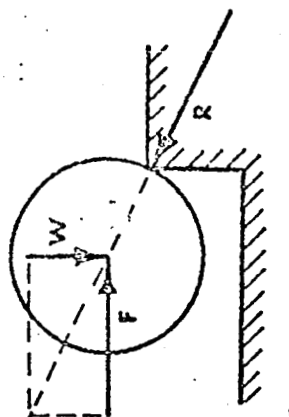


Figure 11

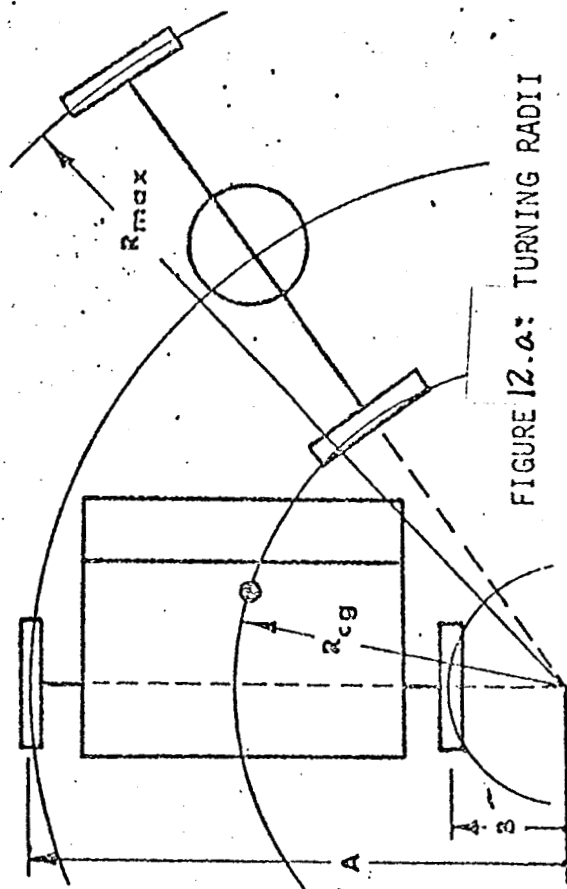


FIGURE 12.a: TURNING RADII

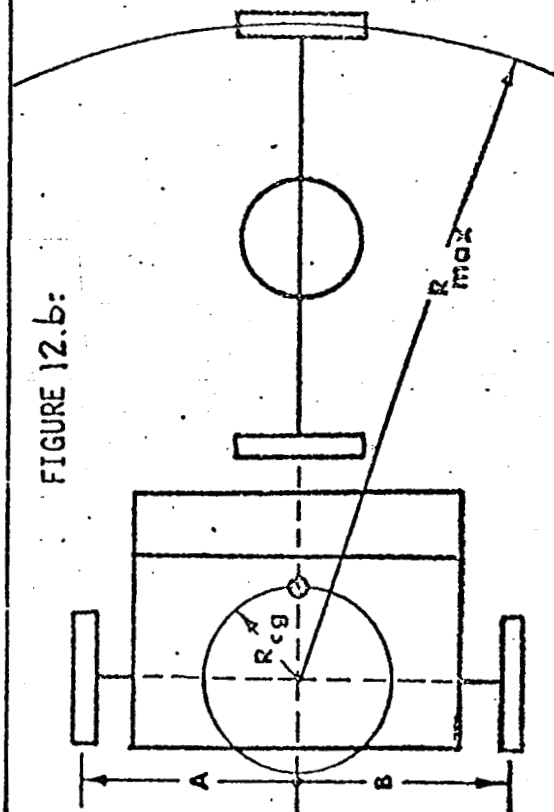


FIGURE 12.b:

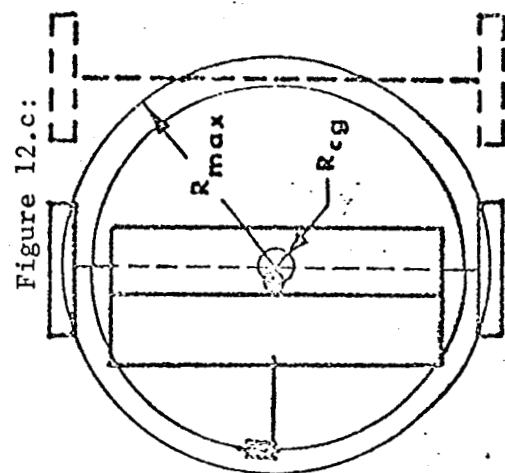
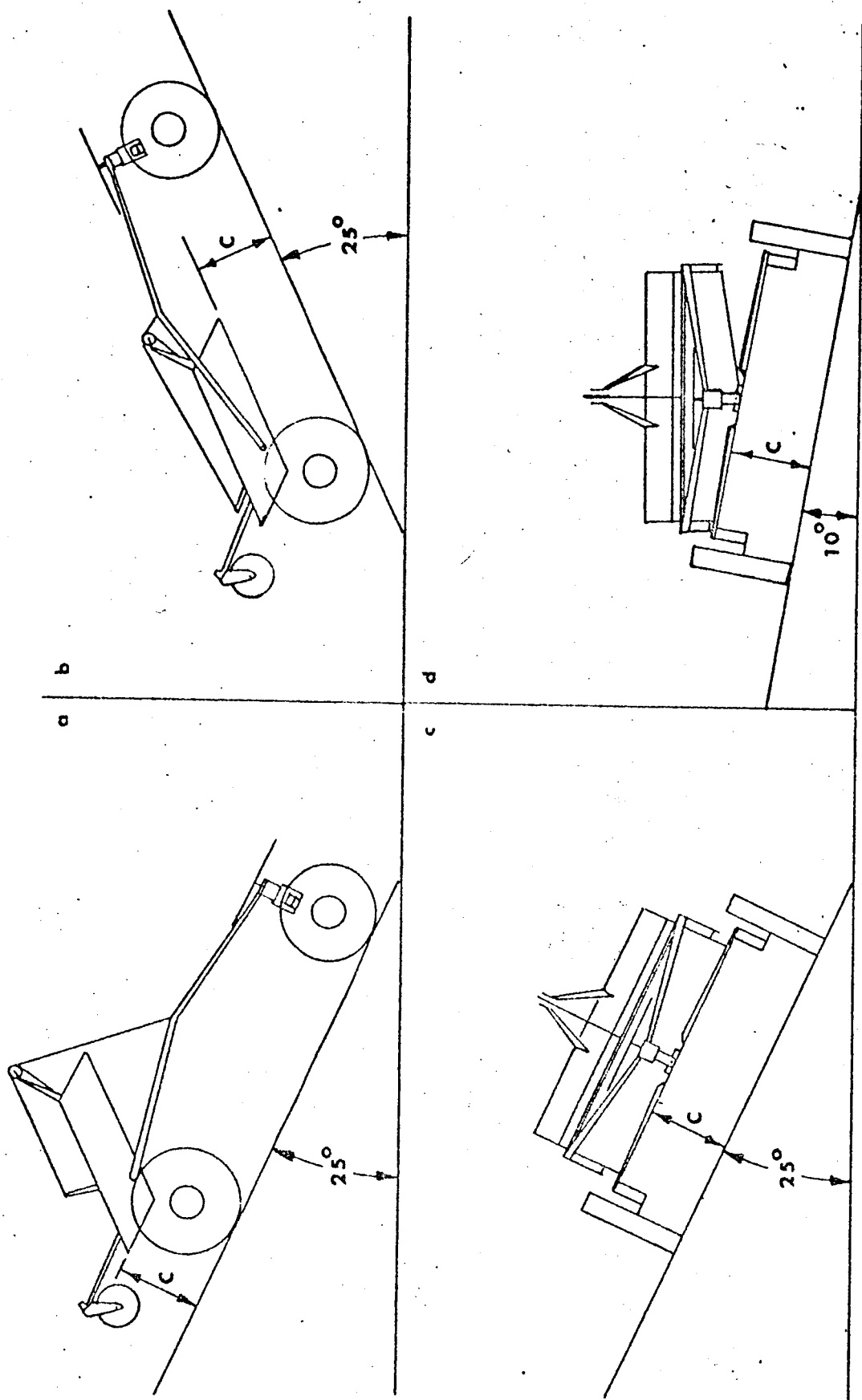


Figure 12.c:



SLOPE CAPABILITY

Figure 13.

FIGURE 14:
FOUR-WHEEL
MODE STABILITY

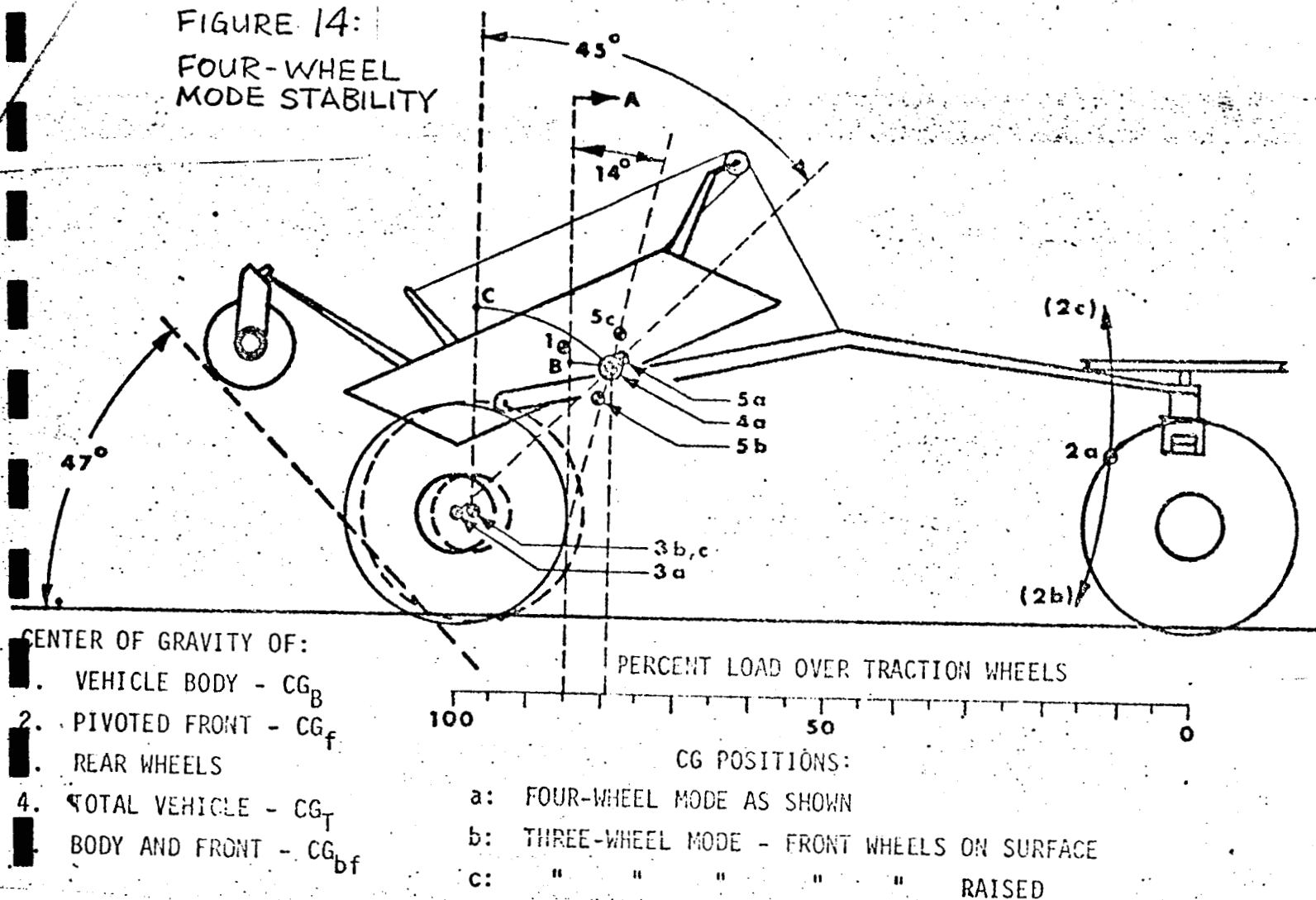
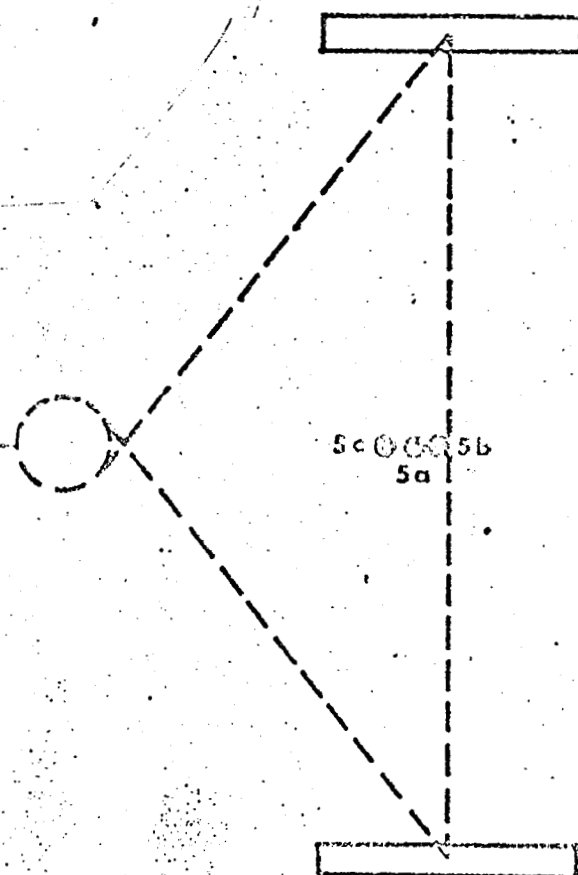
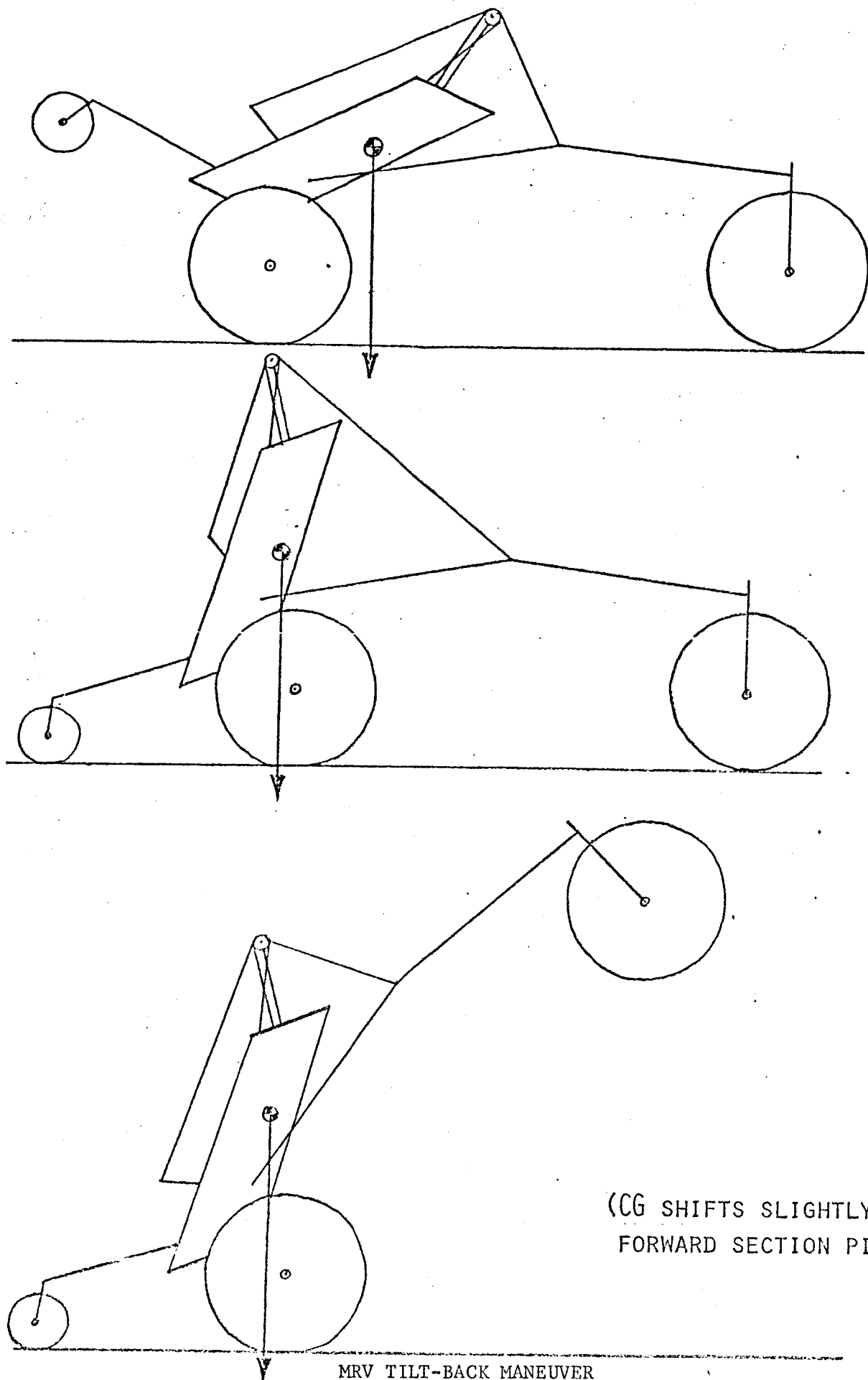


FIGURE 15:
THREE-WHEEL
MODE STABILITY

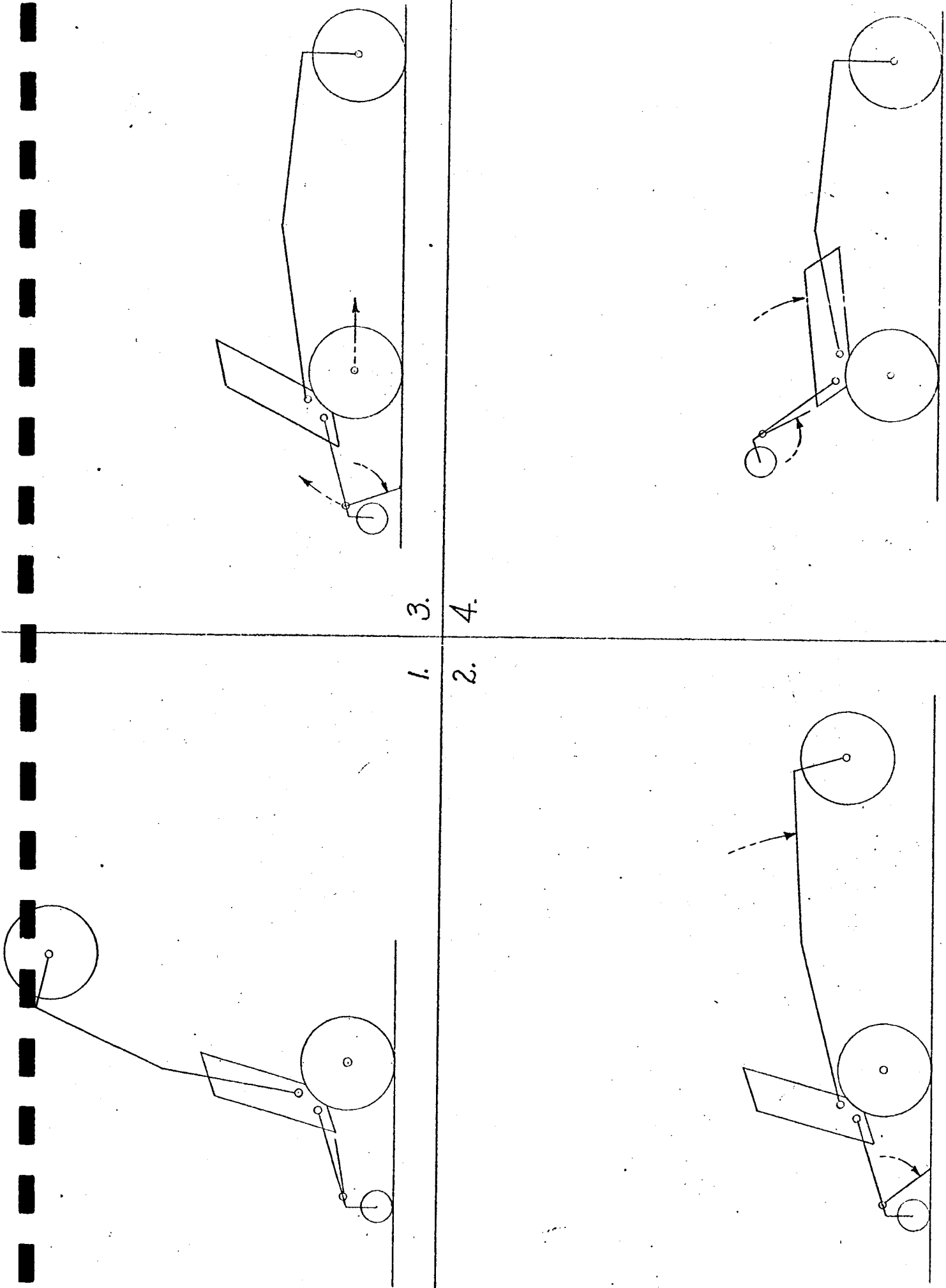
LOCUS OF SWIVEL WHEEL-GROUND CONTACT





MRV TILT-BACK MANEUVER

Figure 16.



FORWARD JACKING MECHANISM
Figure 17.

vehicle concepts. Five separate criteria were established as useful "yardsticks." These were then measured for two comparably sized rover configurations: a 6-wheeled, three-segmented vehicle design, similar to proposed unmanned, lunar rovers, and the RPI-MRV, in both four- and three-wheel modes. The results, as shown in Table 2, illustrate the maneuverability superiority of the MRV over segmented configurations in every category analyzed.

Task A.1.d. Payload Study.

A list of probable instrumentation for the science payload was compiled.

The value of each instrument was weighted according to its usefulness in each of the three major science objectives: atmosphere analysis, lithosphere analysis, and life-support capability study. The instruments were then listed according to this preliminary priority system, the most useful to the least useful, as shown in Table 3. Summing the maximum and minimum estimated earth weight and volume requirements according to the priority list, and comparing these summations to expected vehicle payload capacity gives a first approximation of instrument size requirements, Figure 18.

A study of the mission configuration was also initiated. Various missions using one or two landers in combination with one or two rovers were outlined. In addition, the use of two vehicles with individually distinct functions to complement each other has been proposed. For example, one vehicle could be designed as a pathfinder with exceptionally good obstacle detection and negotiation capabilities at the expense of the science payload and communications. It would be the task of this vehicle to search out the least treacherous or most efficient path for the second vehicle. The second vehicle, traveling on the surveyed path would need less obstacle detection and negotiation capability and could devote more weight to the scientific instruments and communications equipment. Other combinations of separate vehicle designs are also possible, such as a soil sample and rock gathering vehicle in conjunction with a fixed or moving sample analyzer and communicator.

Task A.2. Flexible Toroidal Wheel Design - F. L. Simon, G. Chapek, L. Cupreys, H. Goldberg Faculty Adviser: G. N. Sandor

The objective of this task is to design and evaluate a wheel suitable for the MRV. This task has extended earlier work in the development of a toroidal wheel concept, Figure 19, presented in Reference 3. This past year's effort is documented in more detail in Reference 4.

During the past period, five major activities have been pursued. First, the scaled model wheels were redesigned. Second, an extensive wheel and hoop testing program has been conducted. Third, the mathematical analysis initiated during the previous work period was extended

TABLE 2:

MANEUVERABILITY CRITERIA ANALYSIS RESULTS



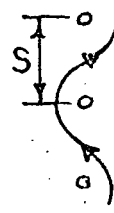
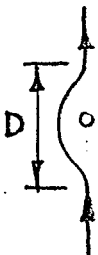
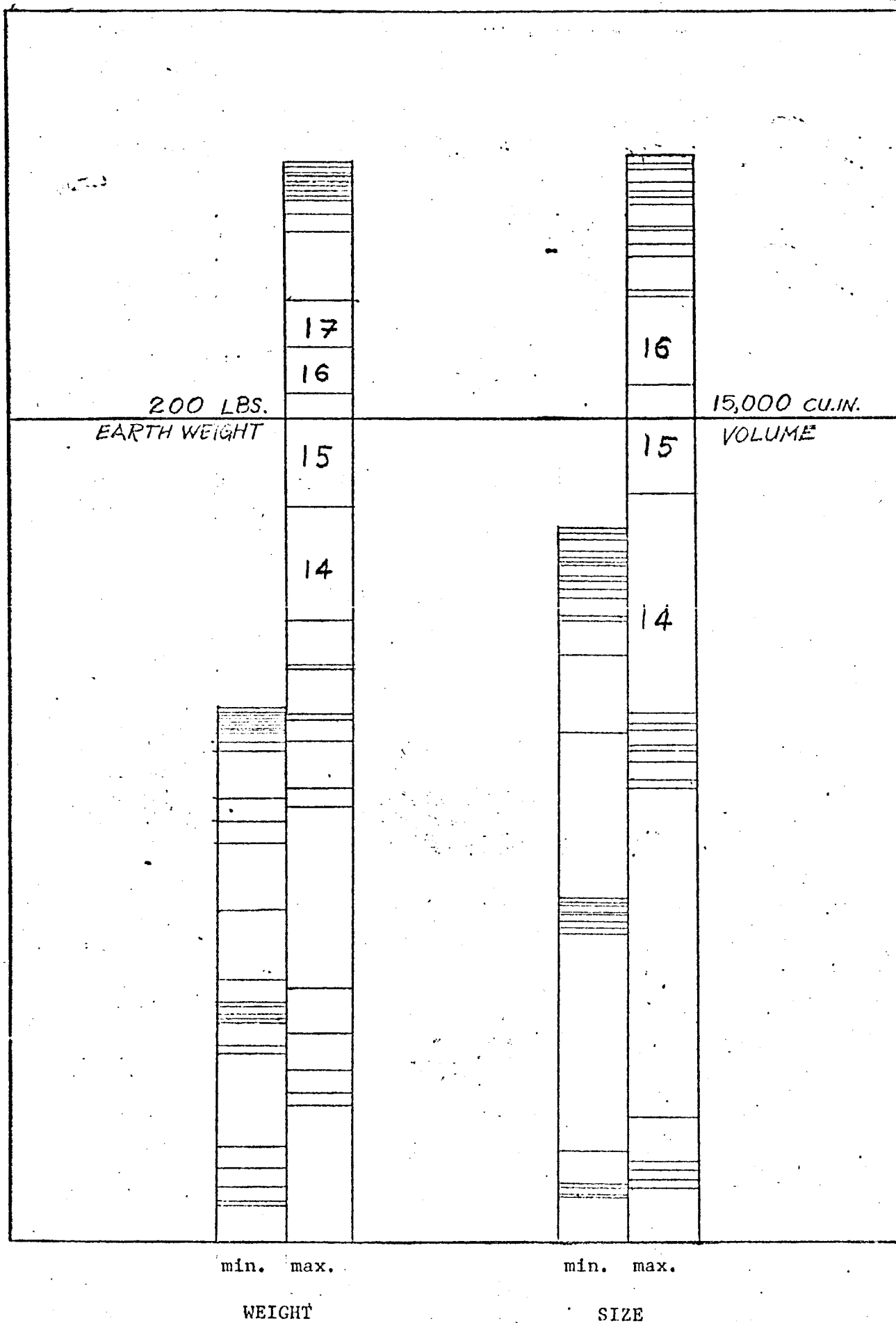
CRITERIA	6 WHEELED VEHICLE 90" x 120" (w x l)	MRV- 120" x 120" (w x l)	
		4 WHEEL MODE	3 WHEEL MODE
 MINIMUM TURNING RADIUS	$R = 156 \text{ in}$	$R = 0 \text{ in}$	$R = 0 \text{ in}$
 MINIMUM AREA COVERED IN 180° TURN	$A = 89,000 \text{ in}^2$	$A = 71,000 \text{ in}^2$	$A = 12,000 \text{ in}^2$
 MINIMUM SLALOM SPACING	$S = 220 \text{ in}$	$S = 190 \text{ in}$	$S = 120 \text{ in}$
 MINIMUM POINT OBSTACLE AVOIDANCE DISTANCE	$D = 260 \text{ in}$	$D = 120 \text{ in}$	$D = 120 \text{ in}$
MINIMUM 180° TURN ENERGY	$E = 45,000 \text{ in-lbs}$	$E = 19,000 \text{ in-lbs}$	$E = 17,000 \text{ in-lbs}$

TABLE 3:

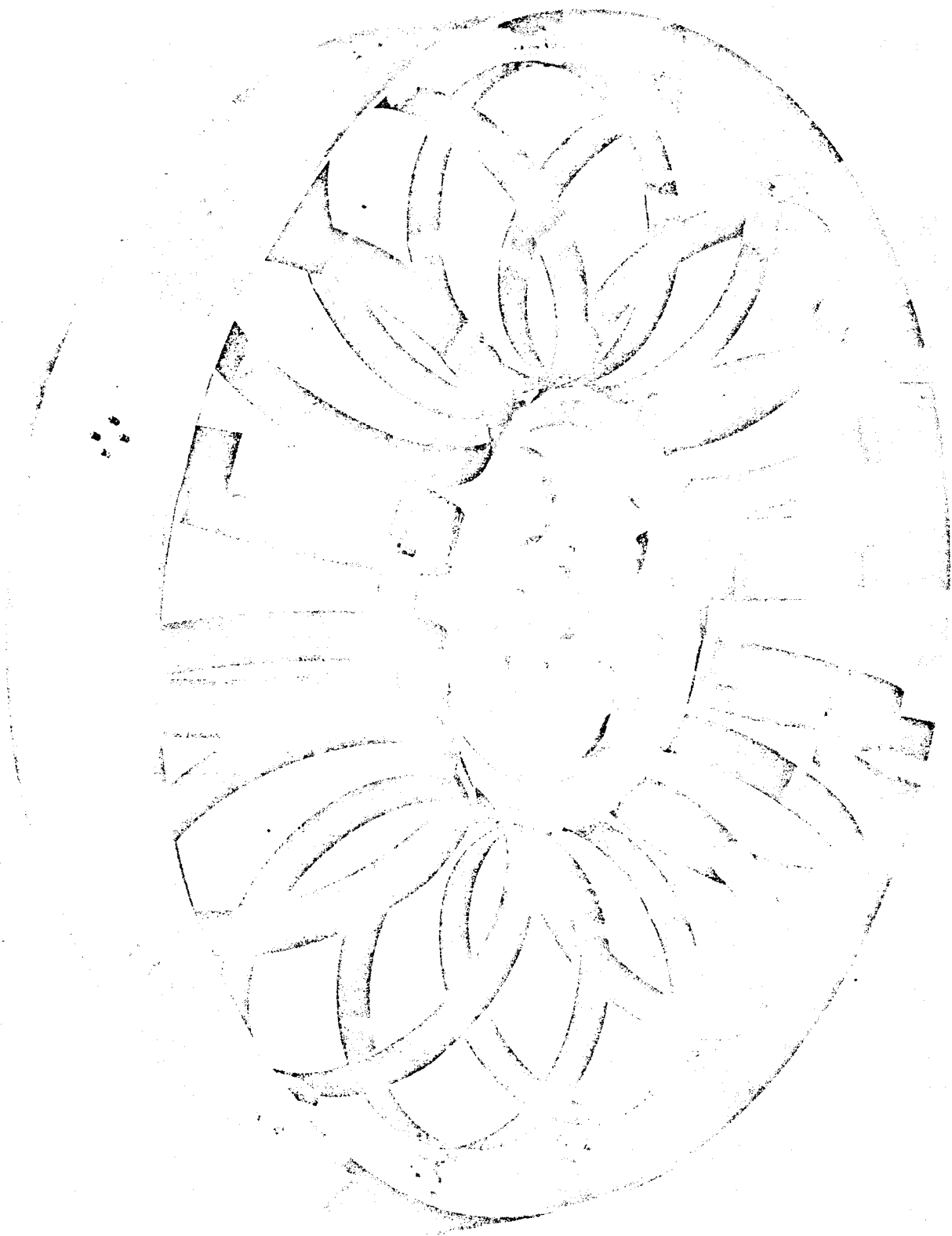
INSTRUMENT WEIGHT SIZE AND POWER REQUIREMENTS

Instrument	Weight in lbs.	Size in cu.in.	Power in watts
1. Oven	8-15	400-500	500
2. pH Meter	1-3	40-70	5-10
3. Flame Tester	3-5	60-100	0-1
4. Spectrograph	4-8	100-150	0-1
5. Centrifuge	5-10	300-400	5-10
6. Chromatograph	20-40	2000-3000	10-100
7. Filter	2-4	50-100	10-20
8. Reagent Tester	5-10	70-150	5-10
9. Camera	1-5	50-100	1-5
10. Microphone	1	30-50	0.5
11. Odor Tester	2-10	50-150	2-10
12. Thermometer	0.5	20-50	0.1
13. Density Equipment	5-10	50-100	5-10
14. Soil Scoop	15-25	1500-2000	10-100
15. Core Sampler	15-25	700-1000	50-500
16. Hardness Tester	5-10	300-800	30-70
17. Porosity Tester	5-10	40-70	10-20
18. Seismometer	10-15	150-300	1-5
19. Shock Tester	2-4	50-120	0-1
20. Bolometer	2-3	1-3	0-1
21. Field Detectors	0.5-1	10-30	1-5
22. Gieger Counter	0.5-1	100-200	0-1
23. Barometer	0.5-1	30-60	0-1
24. Hygrometer	0.5-1	30-60	0-1
25. Rain Gauge	0.5-1	30-80	1-5
26. Anemometer	0.5-1	100-120	0-1
27. Radio Sonde	0.5-1	50-80	0-1
28. Speaker	0.5-1	50-70	0-1



TOTAL SIZE AND WEIGHT OF THE INSTRUMENT PACKAGE

Figure 18.



FULL-SIZE SIXTEEN SPOKE TOROIDAL WHEEL

Figure 19.

to an N-spoke computer program. Fourth, a full-sized model wheel was designed, using the N-spoke computer program. And, fifth, an investigation of materials and design of the wheel's hoop-rim hinges.

Task A.2.a. Model Wheel Redesign

Beginning in June 1970, the major task was to improve on the design and fabrication of the scaled model toroidal wheel. The original wheels built for the dynamic model (see Task A.1) could not stand up to the rigors of dynamic testing. The deficiencies with these wheels lay in the following areas: The spring-tempered phosphor-bronze hoop and rim material was permanently deforming in normal usage, because of its insufficient elastic limit; the hinges connecting each hoop with the rim were fastened with epoxy resin, the strength of which was insufficient in normal usage causing failure; and the traction of the rear wheels needed improvement.

The first problem was resolved by selecting a material with a higher elastic limit. S.A.E. 1095 tempered spring steel was chosen with its elastic limit of 67,000 p.s.i. as compared to 12,000 p.s.i. for phosphor bronze. Assuming 80.0% of the load was supported by the bottom-most hoop, an analysis was carried out on the hoop using Castigliano's Theorem to determine deflections as a function of hoop dimensions, i.e. width and thickness. Hoop dimensions were chosen to match as closely as possible the desired deflections in the original phosphor bronze hoop under identical loading. This final choice was 0.280" wide and 0.010" thick.

The second major problem was concerned with the method of attaching the hinges to the hoops and rim. Several design alternatives were considered. The stronger types of epoxy were found to be too brittle. Since bolting or riveting cause stress concentrations in the vicinity of the hole, these alternatives were rejected. Tying with fine wire looked promising and could always be used should the remaining alternatives fail. Although solder would not have the needed strength, spot welding appeared to be a worthy concept. Experimentation with samples of the 0.010 inch thick S.A.E. 1095 steel showed that this method was fast and efficient. However, metallurgical changes in the welding sequence were causing the material in the vicinity of the weld to become brittle.

The spot welding problem was discussed with faculty of the Materials Division and it was concluded that the rapid cooling after spot welding was causing a quench. The welding process involving resistance heating raises the temp. to about 1300°F (Austenizing temperature) after which the rapid cooling allowed a martensitic transformation to take place. The martensite microstructure is very brittle.

Two courses of action were tried to alleviate the problem:

Solution I - Complete heat treatment by returning welded parts to austenizing temperature, oil quenching followed by tempering.

Solution II- tempering welded parts only.

It was found that Solution II was sufficient to strengthen the weld area. Tempering reduces the hardness and increases the overall strength of the joint.

With the spot welding problem solved, new hinges were made from untempered soft S.A.E. 1095 steel and welded to the steel hoops and rim. A set of four wheels were assembled and are performing excellently. The traction difficulty was solved by welding metal cleats to the rim.

Task A.2.b. Wheel and Hoop Testing

The hoop and wheel testing program served two purposes. First, the values of the hoop spring constants in the normal and tangential directions were required as data for the wheel analysis computer program. Second, the spring constants of the eight and sixteen spoke wheels were determined and compared with the results of the wheel analysis computer program. Experimental and theoretical results showed excellent correlation.

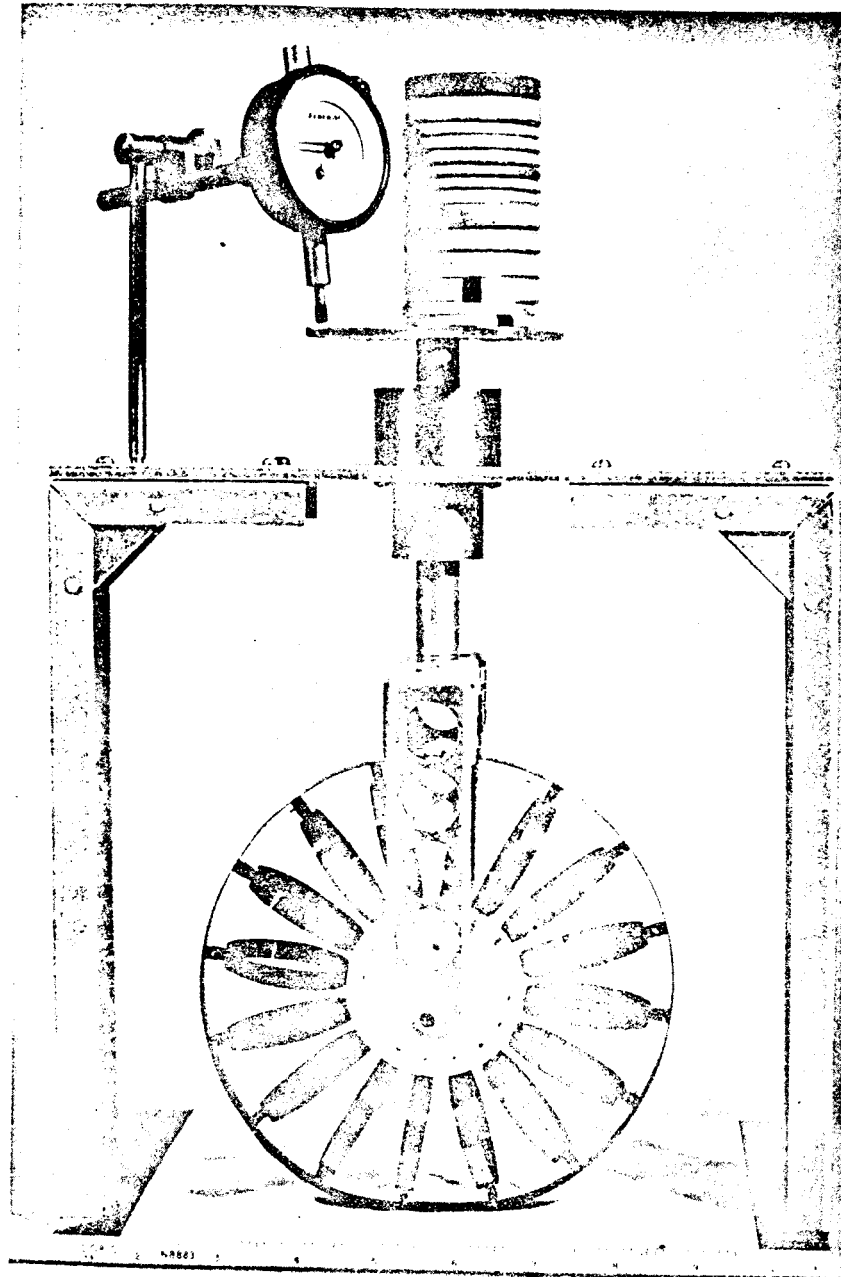
The test apparatus is shown in Figure 20. Loads were applied to the hoops and wheels by placing weights on the plunger. Various jigs and yokes were fabricated to meet the individual test requirements. Deflections were measured with a dial gauge. The experimental program called for three independent determinations of the various spring constants that were desired. Although sufficient data were not available for statistical analysis, investigation of the test results yielded values for the eight- and sixteen-spoke wheel spring constants that were in agreement with the values obtained by computer program.

The graph of the wheel spring constants are presented in Figure 21.

Task A.2.c. Computer Analysis of Wheel

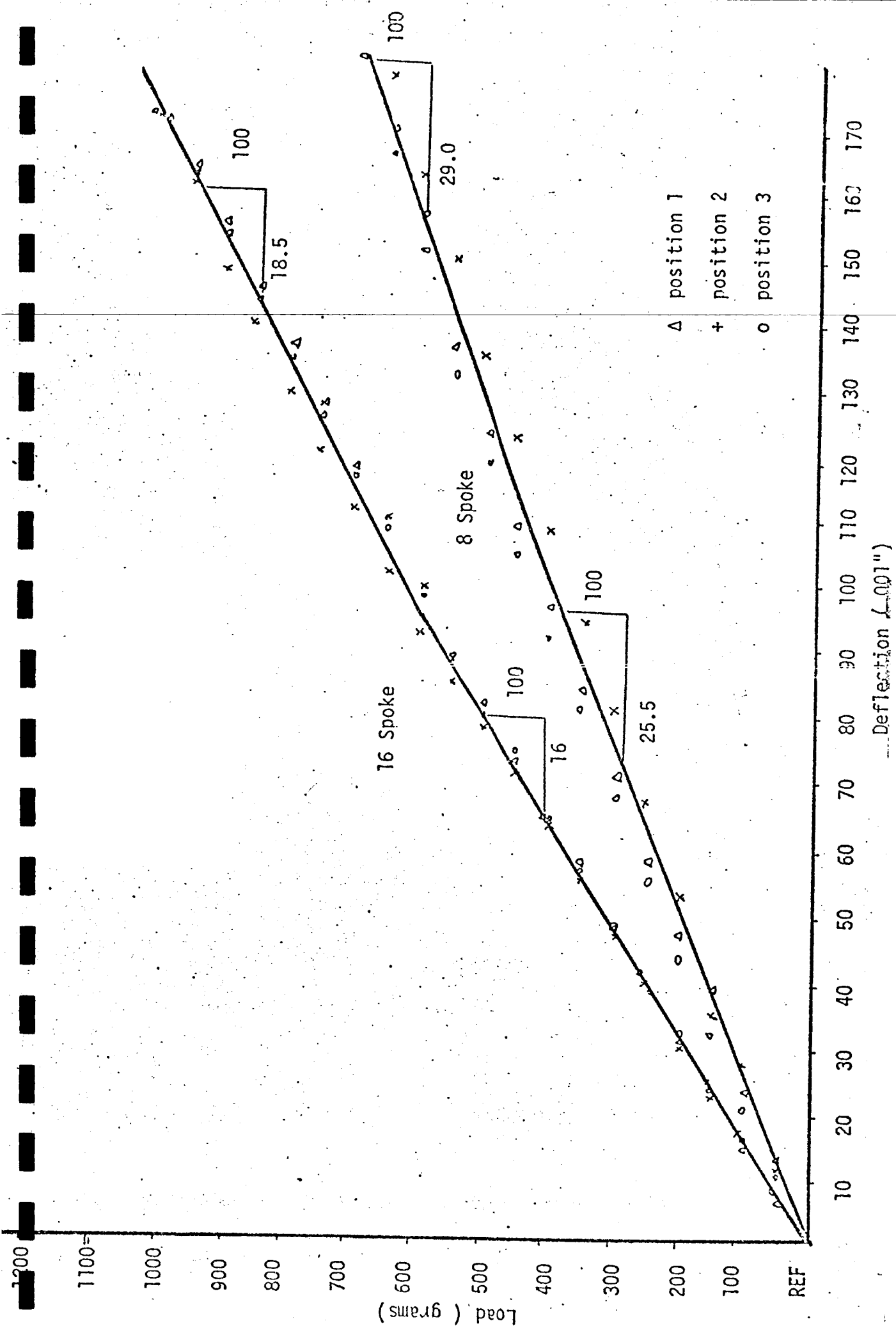
Preliminary work on the analysis was undertaken during the spring of 1970, Reference 3. Castigliano's Energy Theorem was used to analyze the individual hoops from all directions.

The present wheel analysis was developed by writing the force and moment equations for each rim segment. It was assumed that the continuous flexible rim was replaced by a finite number of infinitely rigid rim segments. They were assumed to be pin-jointed together and equaled the total number of hoops. A spring constant could be introduced at each pin joint to represent the stiffness of a continuous flexible rim over the length of a rim segment. Now loop closure equations could be written around each



WHEEL DEFLECTION TEST

Figure 20



LOAD VS. DEFLECTION FOR 8 AND 16 SPOKE WHEELS

Figure 21

hoop-rim-hoop-hub circuit. These efforts were stifled in an attempt to reduce the number of unknowns and equations. The difficulty lay in relating hoop deflections with rim rotations and the relations which were obtained were far too complicated.

Upon review of this earlier work, it was decided to treat hoop compressions as unknowns directly and use these and hoop relations in determining hoop cantilever deflections. The forces exerted by the hoop using these calculated deflections differ from those in reality. This, then, is the second important assumption which would render the equations solvable.

A proof of analysis principle was first tried with a modified Newton's method of solution. In this case there were 11 equations and 11 unknowns since only half of the wheel was analyzed (normal deflections on rim element 1 permit the use of symmetry). Failure of this method to converge introduced the Full Newton's Method. In this instance the equations converged and work was started on the 8-spoke analysis. After a long debugging period this program also worked.

Beginning in October work began on the N-spoke generalized program. The N-spoke program analyzes the entire wheel and enables the designer to control the following variables: hoop normal spring constant, hoop transverse spring constant, number of hoops, hoop and hub diameters, and thus wheel diameter. In addition, any combination of loading forces can be applied to the rim. The output of the program can be used to study the stresses in the hinges and other fastenings, determine the effect of wheel dimensions on the footprint and its associated pressure distribution, and optimize the number of spokes. Detailed descriptions of the mathematical analysis and computer programs used for wheel design may be found in Reference 4.

Task A.2.d. Full-Sized Wheel Prototype

The analysis program was used to determine the necessary dimensions for the full-size hoops. Hard temper (Rockwell 48c - 51c) spring steel, 0.072 inch thick, yielded a hoop width of 1.500 inches and a hoop radius of 7.705 inches. The corresponding spring constants for the steel hoops were as follows:

90.15 pounds per inch in the normal direction,
25.67 pounds per inch in the transverse direction, and
17.11 pounds per inch in the lateral direction.

Stronger, lower weight titanium of .078 inch thickness yielded a width of 1.75 and a hoop radius of 4.3 inches. The corresponding spring constants were, respectively as before, 90.55, 26.11, and 17.18 pounds per inch. However, due to the lower cost and availability, the spring steel was chosen for the first prototype, shown in Figure 19. The assembled prototype provided the desired wheel spring constant. The completed wheel was taken to the U.S. Army Waterways Experiment Station (W.E.S.) in

Vicksburg, Mississippi, to discuss and observe the testing of present lunar rover wheel designs, and to formulate a testing program for the R.P.I. toroidal wheel design. Engineers there expressed an interest in testing the R.P.I. when the design is optimized next spring. To obtain objective results it was suggested that N.A.S.A. contact with W.E.S. directly at that stage of the wheel development. A more detailed description of the full-size wheel design may be obtained from Reference 4.

Task A.2.e. Hinge Design

The three-piece mechanical hinge used for the small model wheels were inadequate for use on a full-size wheel due to the possibility of contamination during testing. This problem would be much more troublesome on the actual vehicle due to the low pressure environment which would tend to remove protective lubrication. One solution to this problem is to replace the mechanical hinge with a one-piece flexural element as shown in Figure 22. Another approach would be to protect the mechanical hinge with an encapsulating shell or boot, as shown in Figure 23. The first method was chosen because the integral hinge provided flexibility on two perpendicular axes, a useful feature for a good wheel footprint on side-slopes. Polyurethane was selected for use on the first full-size wheel prototype in order to demonstrate the integral hinge concept in laboratory operating conditions. Thus, such Martian conditions as temperature extremes were not considered. A stress analysis of the hinge design was made to allow the minimum weight design, since there could be approximately 64 hinges in the vehicle's four wheels.

A minimum weight mechanical hinge was also designed, and fabricated from Delrin, a nylon derivative. To determine the fatigue life of both the integral and mechanical hinges, a hinge testing machine was designed and constructed, as shown in Figure 24. The frequency and angle of flexure can be varied, and the test hinge can be loaded in either compression or tension. A 3,000,000 foot journey of the vehicle can be simulated by 400,000 flexes. Test hinges have all withstood this duration, first at 125 pounds compression and then at 70 pounds tension. Future tests are planned to determine the amount of creep in the hinge for the above test.

Task A.3. Vehicle Steering Control System - R. Koehler, D. Rosenthal Faculty Advisor: Prof. G. N. Sandor

The objective of this task is the design and construction of a steering control system for the Mars Roving Vehicle dynamic simulation model.

The system can be divided into two sub-systems. First, a rear wheel differential drive sub-system is needed to maintain the proper speed ratio between the rear wheels while the vehicle is turning. Second, a main steering control sub-system is required to regulate the turning angle of the vehicle. The vehicle employs wagon steering, i.e., a one-axle system connecting both front wheels pivots about its mid-point.

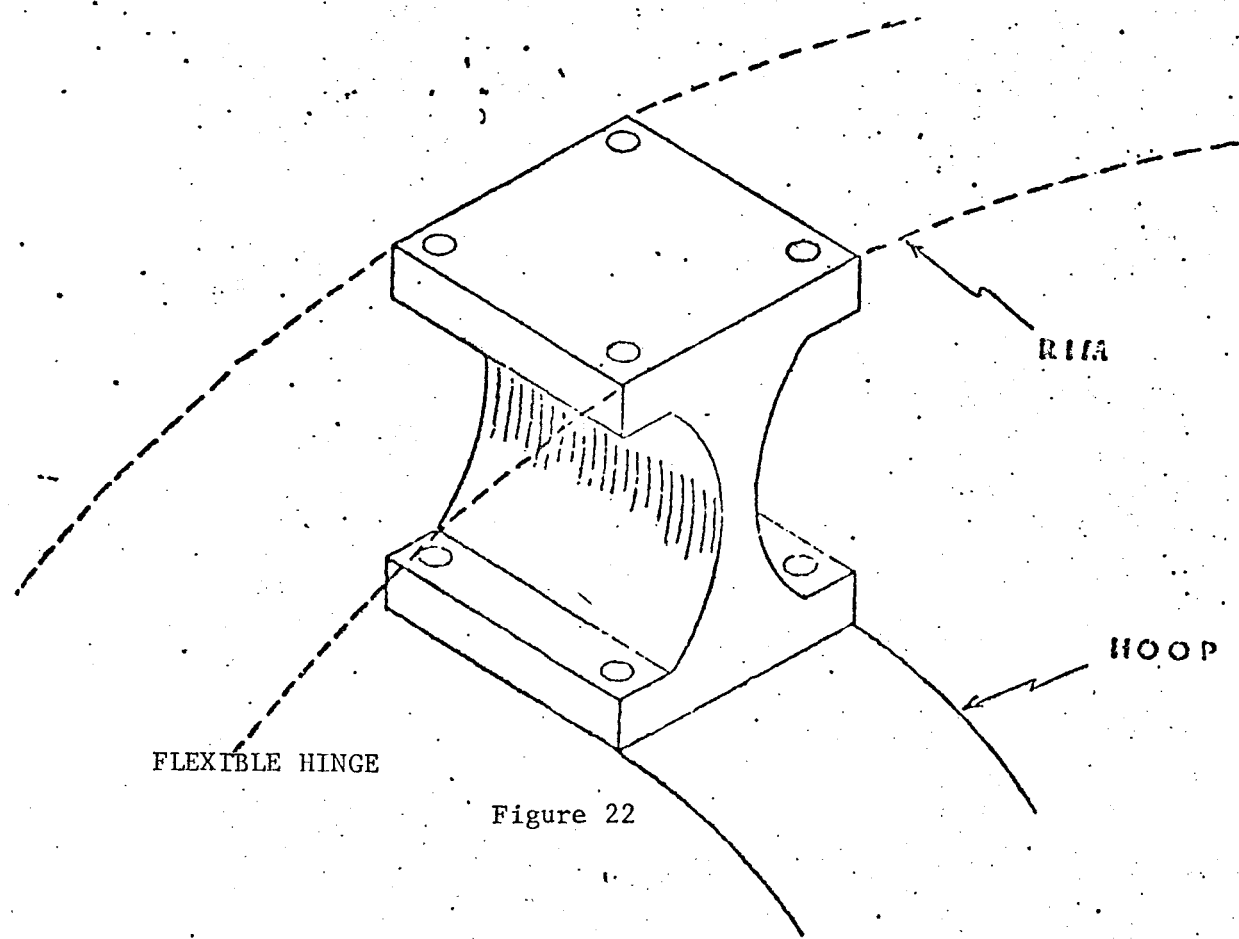
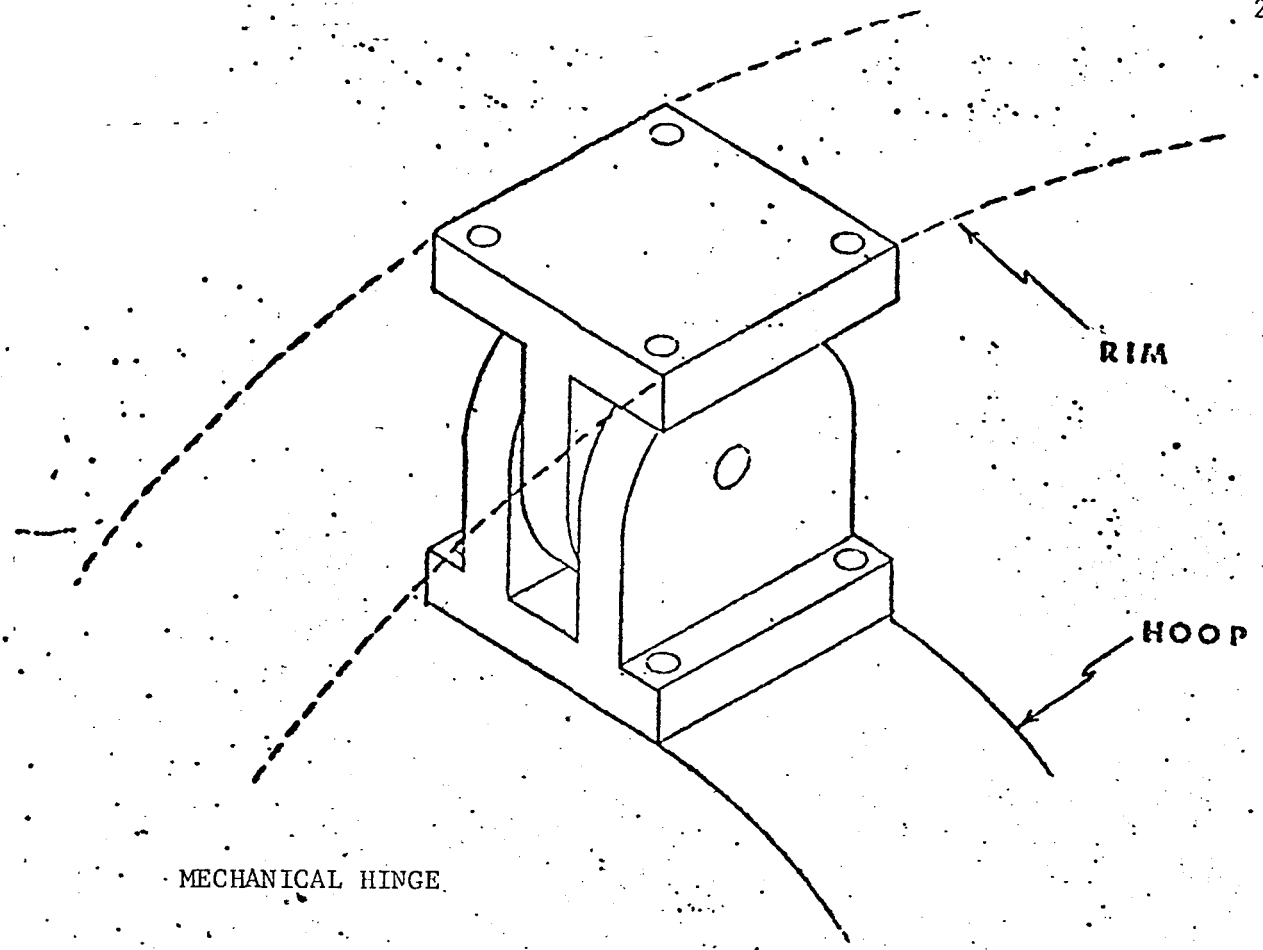
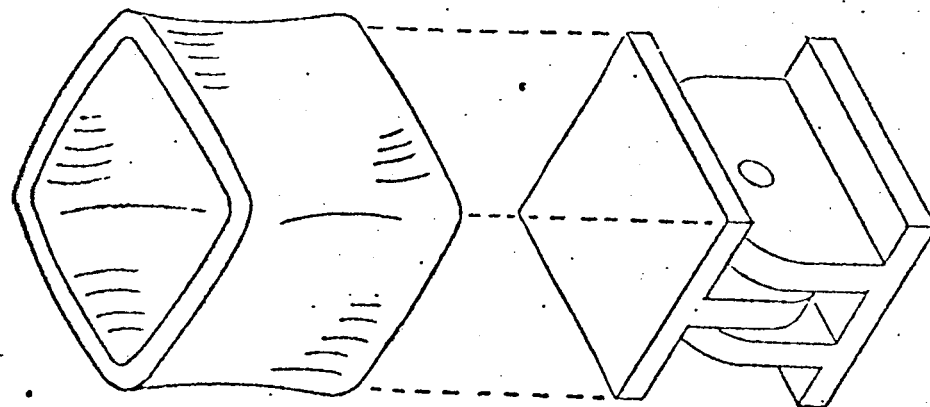
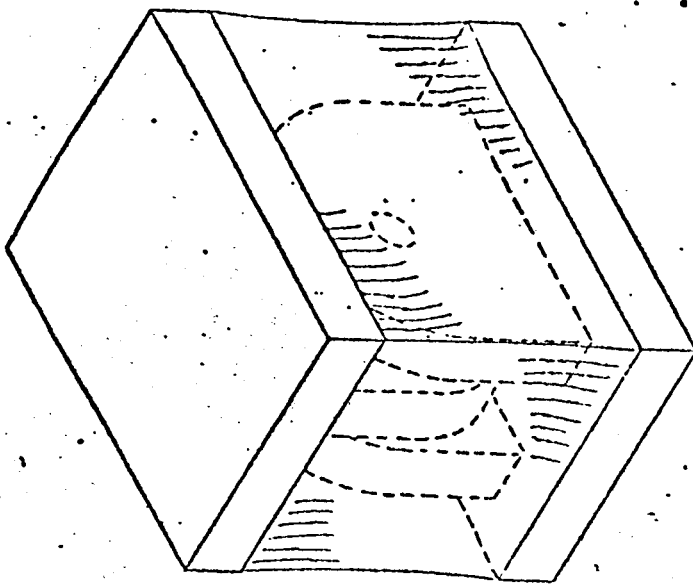


Figure 22



BOOTED HINGE



RTV HINGE

Figure 23



HINGE TESTER

Figure 24

Presently there is a manually regulated power supply to control the on-board steering motor which turns the front axle. It is desired to have a steering control for the operator to turn which would actuate the vehicle steering through a continuous feedback system.

Task A.3.a. Differential Drive Control

A geometric analysis of the turning operation is necessary to further specify the requirements of the rear wheel differential drive. To prevent the wheels from scuffing as the front axle turns, the appropriate rear wheel remains at the nominal speed while decelerating the inner rear wheel to a fractional ratio of the nominal speed. The ratio of the speeds is equivalent to the ratio of the turning radii, r_x and r_y , defined in the top view of the model, Figure 25. From geometrical analysis this ratio is

$$V_r = \frac{L \cot \theta - W/2}{L \cot \theta + W/2}$$

where L and W are the length and width of the vehicle, and θ is the turning angle.

This function is plotted in each of the four phases of turning, Figure 26; the rear rear wheel starts to slow down in Phase II as a right turn (positive θ) is initiated. When θ reaches 64° , r_x is zero and the right wheel is stopped. At 90° the right wheel is at full reverse speed and the left wheel remains at full forward speed. Continuing into Phase I, the left wheel decelerates while the right remains at full reverse speed. A similar description holds for left turns. Thus the turning angle varies over a full 360° range.

The vehicle is driven by its rear wheels, each having its own motor. These motors will be mounted in the hub of the wheels on the full size vehicle, although they are currently located in the payload section of this model for proper weight distribution. Thus, a purely mechanical differential is impractical. Also, weight and space restrictions for proper dynamic simulation of the vehicle prevents additional on-board equipment. A remote station will then directly supply the power to the motors through the existing connecting cable.

The rear wheel differential drive sub-system is shown in its block diagram, Figure 27. A potentiometer attached to the steering motor on the vehicle feeds a signal indicating the turning angle to the control circuit.

The functional relationship between the turning angle and the rear wheel speed is approximated by a piecewise-linear, diode-resistor circuit. A logic switching circuit has been designed to permit use of a single function-generating circuit for all four phases.

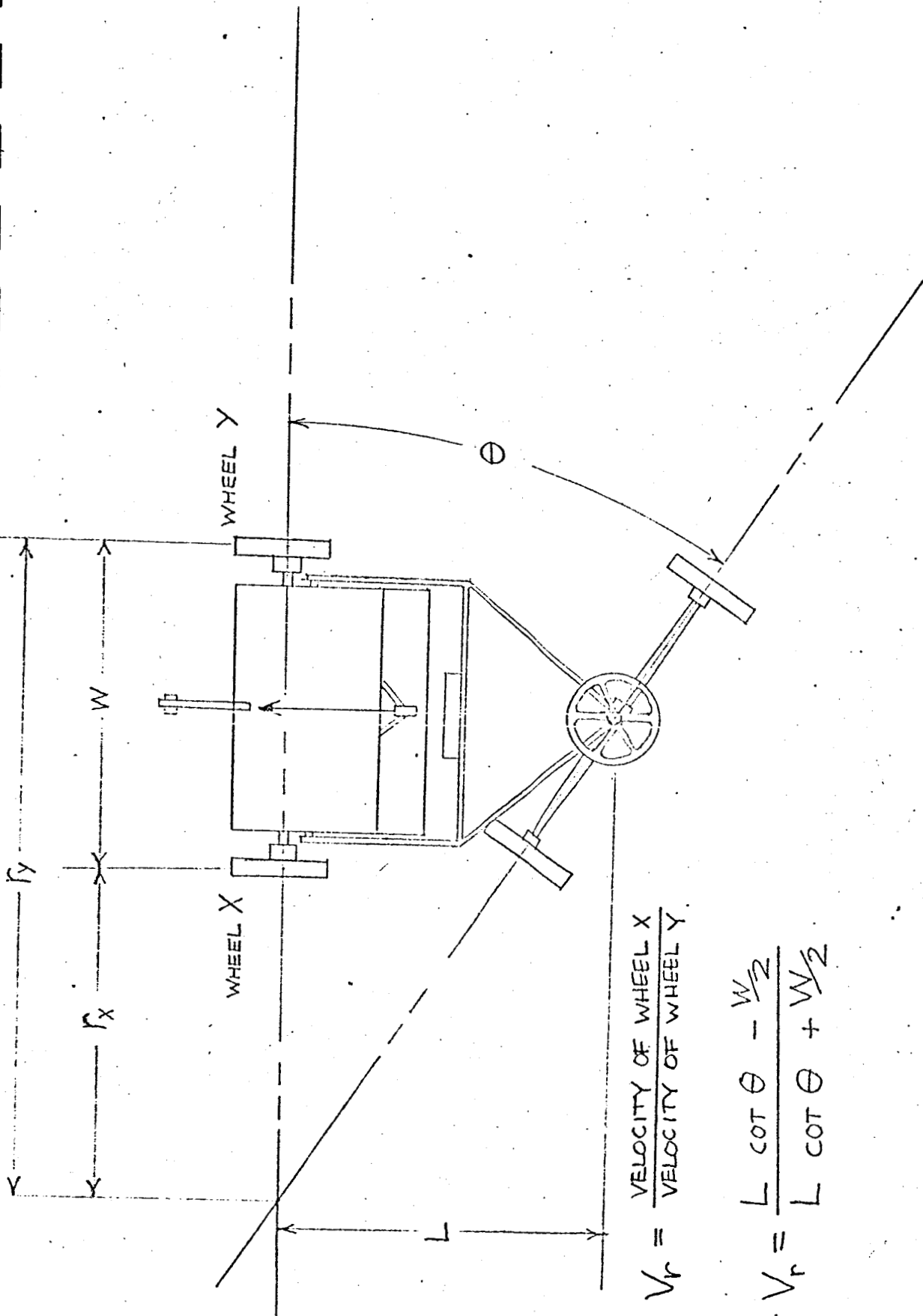
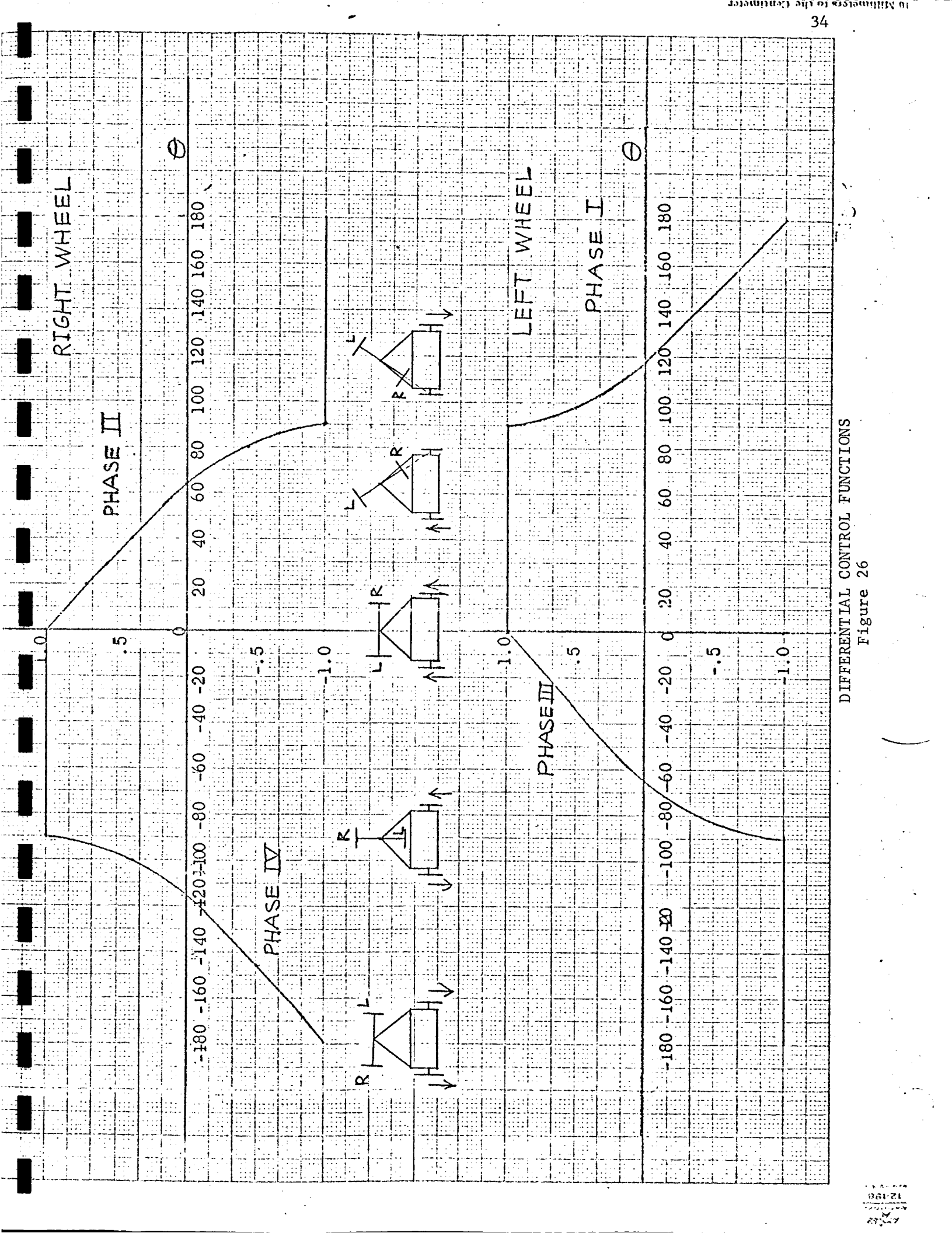
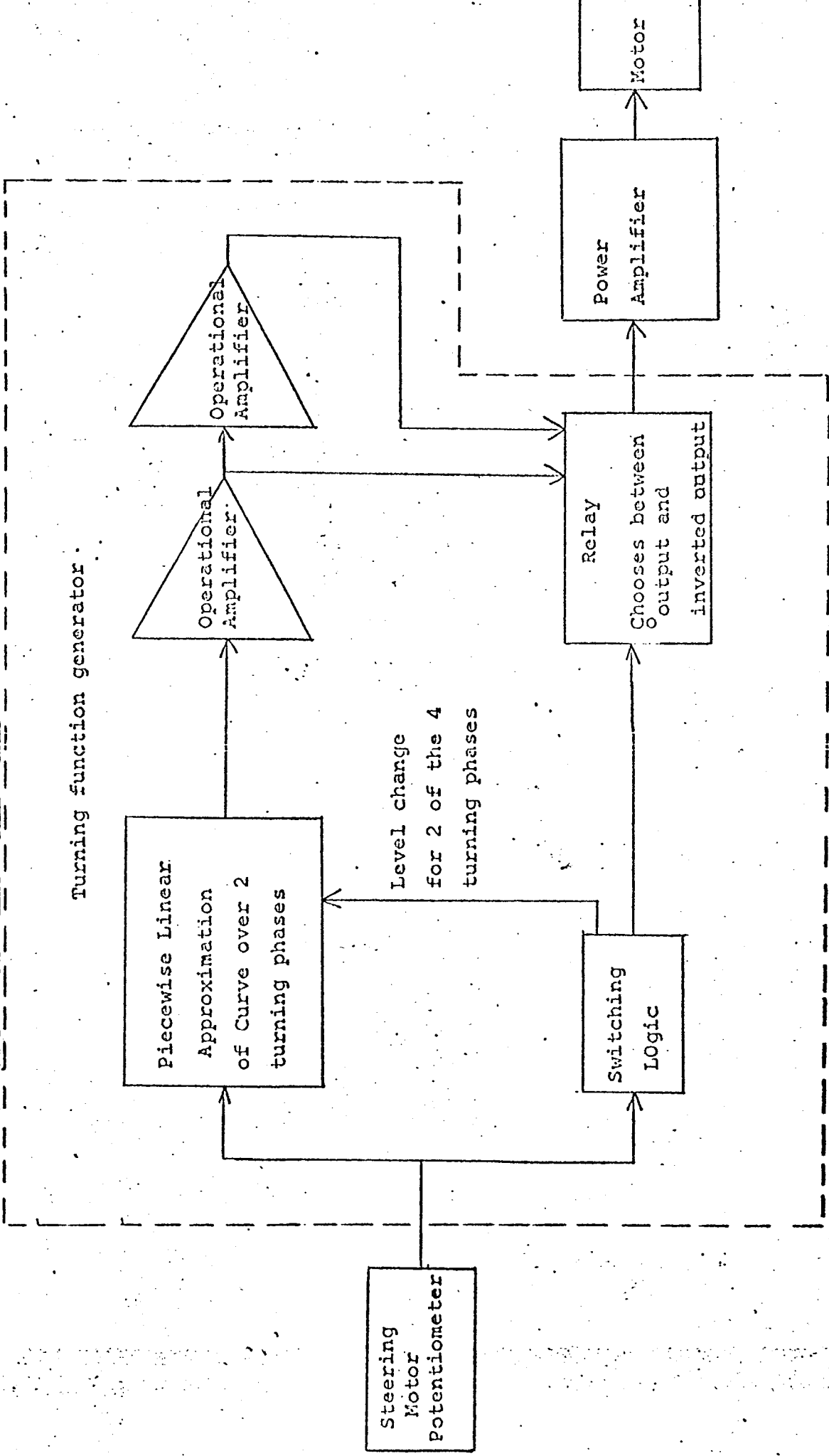


Figure 25



DIFFERENTIAL CONTROL FUNCTIONS
Figure 26



REAR WHEEL DIFFERENTIAL DRIVE CONTROL SYSTEM

Figure 27

Silicon control rectifier (SCR) circuits were constructed to operate the drive motors from the output of the function-generating circuit. However, upon testing the SCR control circuit did not perform properly. There was a large deadband when reversing the direction of the drive motors. And, since the SCR control uses only a portion of an alternating current, at slow speeds the geared-down drive motors reached a speed at which the internal mechanical backlash permitted excess vibration.

Therefore, a solid-state power amplifying circuit was designed which, upon testing, eliminated the above problems. However, electronic element parameters varied with head build-up as the system operated distorting the desired turning function. This is presently being studied and is expected to be resolved during the first part of the next period.

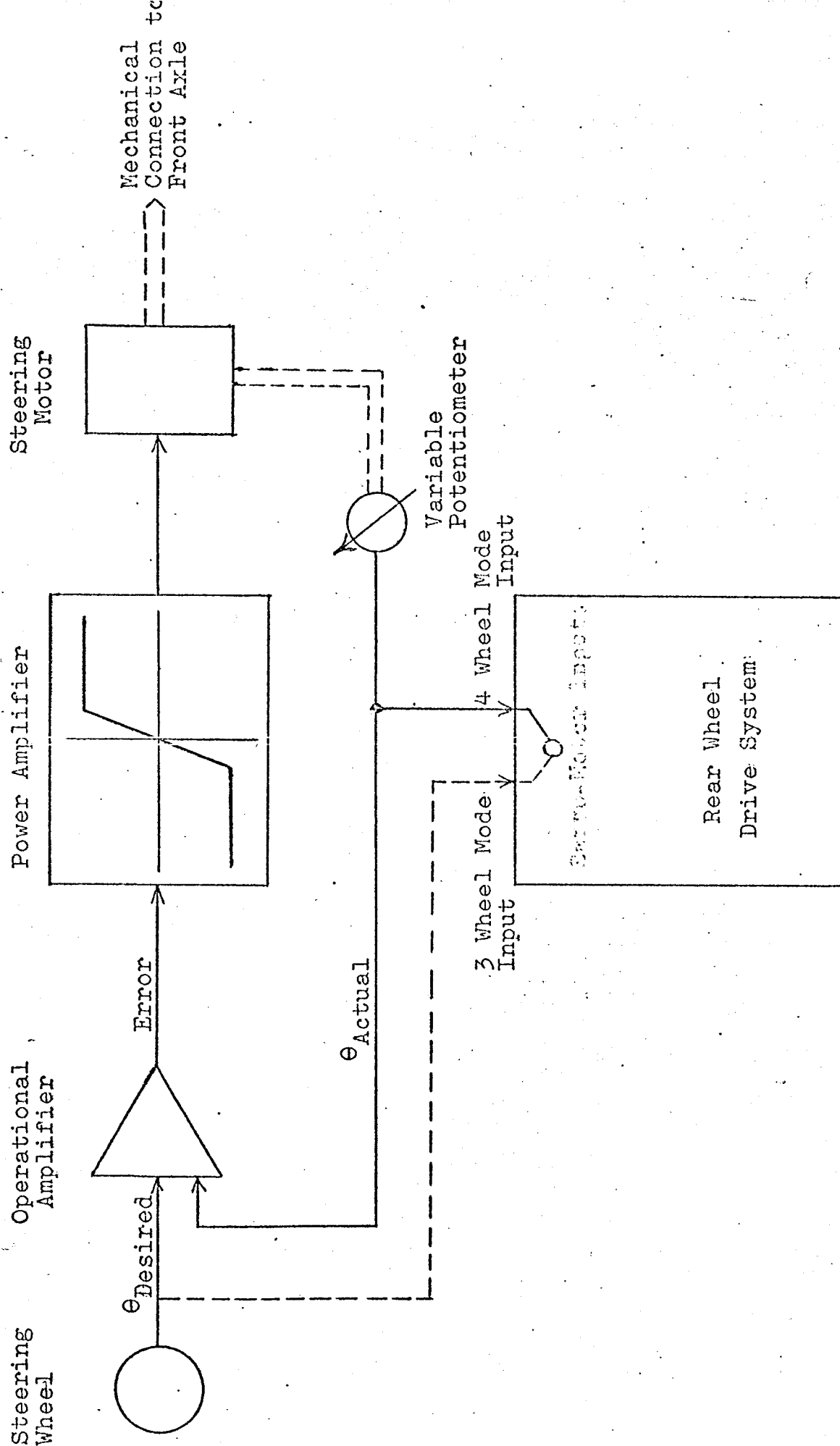
Task A.3.b. Steering Control Sub-System

The actual turning of the vehicle is regulated by the main steering control sub-system. It is essentially an error correcting feedback system with a high gain on the error, Figure 28. A manually operated steering wheel is connected to a potentiometer producing a signal proportional to the desired turning angle. The signal from the potentiometer on the steering motor, indicating the actual turning angle and which is fed to the servo-motor, is also fed back to a difference amplifier. The two signals are compared and the resultant error signal is fed to a power amplifier with a transfer function as shown in the block diagram. This power amplifier then drives the steering motor. It develops full power for small angle changes so that obstacles may be overcome.

The steering control system is easily adaptable to the 3-wheel mode, i.e., the contingency mode in which the vehicle tilts back onto a fifth wheel in the rear pivoting the front wheels off the ground. By throwing a switch, the signal from the steering wheel can be fed directly to the servo-motor system which controls the turning of the rear wheels. The front axle steering would be disengaged by the same switch.

The original design of the main steering control system called for use of a relay instead of a power amplifier to provide full power for a small error so that obstacles may be overcome for small turning angle changes. However, this would result in small chattering motion and, in some cases, instability. The power amplifier has nearly the same transfer function as a relay, but affords stability as well as a fast response time.

At the completion of this task, an off-vehicle system will be working that affords the vehicle model's operator two main controls: a steering wheel for turning and a knob for controlling the vehicle's over-all speed. On the actual vehicle, on-board computer logic would input these controls to the on-board control system.



STEERING CONTROL SYSTEM
Figure 28

Task B. Systems Analysis - John Baker, Alan Goldberg, Carl Pavarini,
Niles Van Denburg
Faculty Advisor: Prof. E. J. Smith

The objective of this task is to develop a framework within which vehicle design decisions involving conflicting requirements can be made. Analysis required the identification of the system model and the formulation of a method to examine design trade-offs by utilizing the model. Progress for the academic year included determination of both methodology and the system model subject to a number of simplifying assumptions. A computer program which identifies the optimal system design (subject to the assumptions) has been written. The present effort is directed toward implementing the program.

Progress achieved is described in detail under the four following sections: 1) An Overview of the Approach, 2) Method of Optimization, 3) Subsystem Modeling, and 4) System Modeling and Optimization. Finally, a projection of activities for the next period is included.

1. An Overview of the Approach

Design, in the systems sense, is the process of specifying the information required by subsystem designers. This information consists of the operating requirements to be met by the subsystem, and all constraints under which the designer must work. For the designer of a communications subsystem, such inputs might be that a pulse-code modulated subsystem capable of "x" data rate, not to exceed "y" weight, and limited to drawing "z" watts is needed.

Systems analysis is the task of determining the optimal system design. Required by this definition, is the examination of all the design trade-offs in the context of their effect upon the operation of the system. For a system of non-trivial size, the system design is composed of many parameters and constraints, the interrelationships of the parameters may be complex, and it is necessary to consider all of the parameters and constraints concurrently.

The task of optimization implies the use of a mathematical model of the system. It is infeasible to expect to be able to force the model to include all of the possible design variations. It becomes necessary then, to make certain assumptions about the system and subsystem configurations. This in turn means that optimization with respect to a single model is not the end product of systems analysis simply because there are probably other design alternatives not included in the model. To claim that the system design is indeed optimal, it is necessary to consider the models corresponding to the set of all possible assumptions.

The search for the optimum also implies that there is a standard by which the system quality can be measured. This "objective" (or objective function) may or may not be unique. Generally, the objective measures how well the system is fulfilling its purpose. If there are alternate ways of describing how well the system performs, these too are inputs to the optimization process and must be separately considered.

In addition there are assumptions that must be made about external constraints (funding, development of new technologies, time constraints,...) which may not be completely deterministic.

The many possible combinations of design assumptions, objectives, and external constraints make system optimization an iterative process in the sense that the problem must be run for many sets of inputs before confidence in the validity of the optimum is obtained. Schematically, the inputs to a single run of the optimization can be represented by Figure 29, where now, for a roving vehicle, mission goals are the determining factors in formulating the system objective.

2. Method of Optimization

In an attempt to identify and consider all possible system designs for a given set of assumptions, the optimization process consists of three parts:

- a) formulation of a mathematical model of the system (identification of constraints),
- b) determination of the objective function in terms of the model variables, and
- c) imbedding the problem in the nonlinear programming format and locating the optimum.

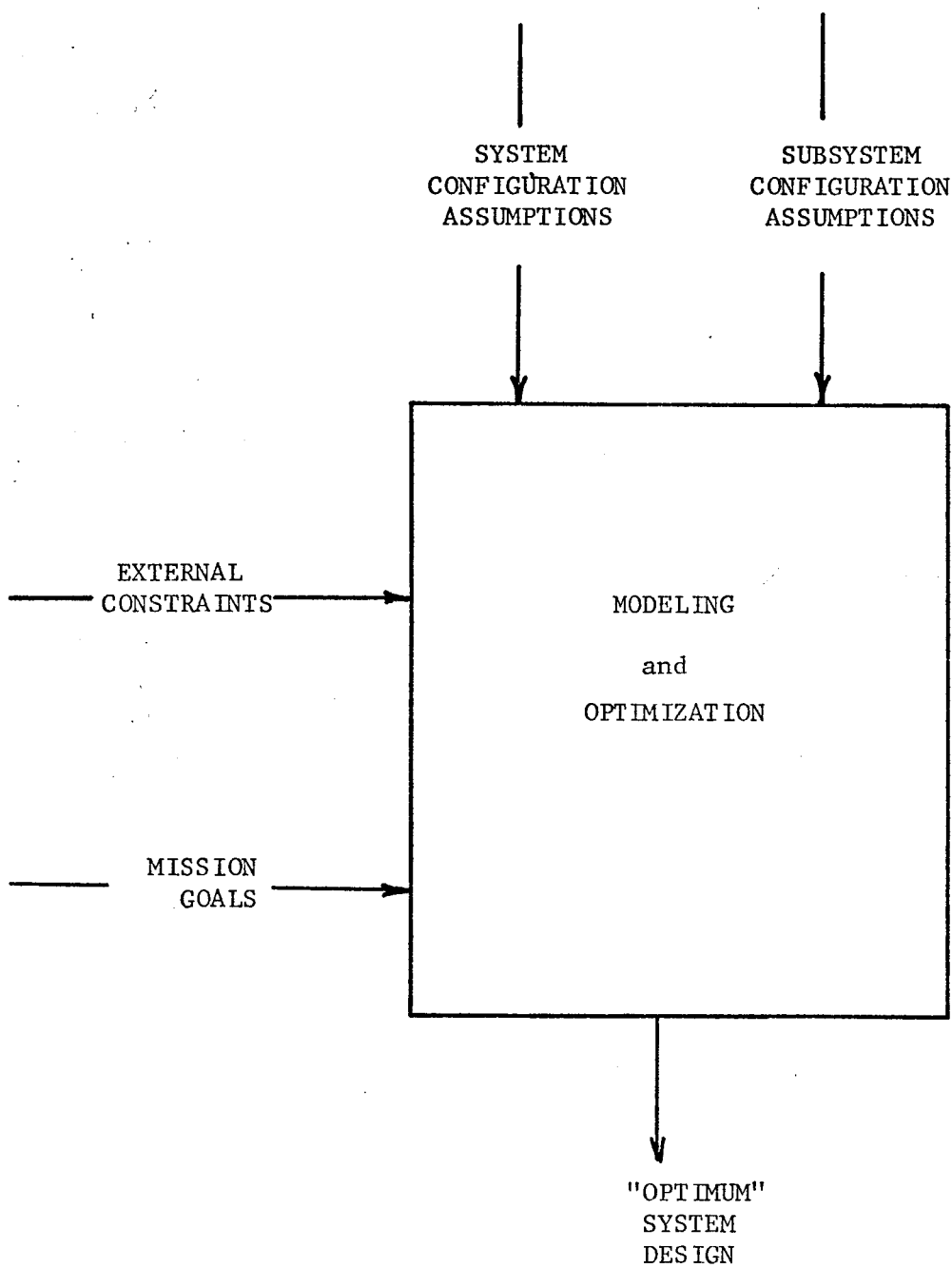
The nonlinear programming (NLP) problem is:

$$\begin{array}{ll}
 \text{extremize} & f(\underline{x}_n) \\
 & (\text{max or min}) \\
 \text{subject to} & g_i(\underline{x}_n) \geq 0 \quad i = 1, 2, \dots, m \\
 & h_i(\underline{x}_n) = 0 \quad i = m+1, \dots, k
 \end{array}$$

where \underline{x}_n is an n -vector of the variables to be chosen by the optimization. The f , g_i 's and h_i 's are all scalar functions of the components of \underline{x}_n . Unless the solution is unique (implying that there is only one way the system can be designed) or does not exist, it is necessary that the number of equality constraints be less than the number of variables (i.e., $k-m < n$).

The NLP problem is a natural way to describe the problem of optimal system design. If the system design can be formulated as the setting of n design parameters, then $f(\underline{x}_n)$ becomes the objective function previously discussed. In addition, the g_i and h_i functions (k in number) represent the physical and external constraints placed upon the choice of the n variables.

The modeling process is the determination of what the n variables (the x 's) are, and what relationships there must be between them (the



INPUTS TO OPTIMIZATION PROCESS

Figure 29

g_i 's and h_i 's) in order for the system design to be both realizable and to meet any outside constraints upon it. Suppose the results of modeling the system yield n variables of the system design, q inequality constraints, and r equality relationships of the variables. It is then generally possible (assuming no transcendental equations) to use the r equalities to eliminate r of the n variables both in $f(x_n)$ and in the $g_i(x_n)$ $i=1,2,\dots,q$ yielding a transformed objective $[f_1(x_{n-r})]$, q inequality constraints of $n-r$ variables, and no equality constraints. If r' of the r equalities are transcendental (i.e., not algebraically solvable), the number of variables can be reduced to $n-r+r'$, and there remain r' equality constraints. Call the reduced set of variables states. Then the order of the system design problem (number of states) is $n-r+r'$. The order represents the number of dependent decisions that must be made by the optimization process, and gives some idea as to the complexity of the optimal system design problem for a particular system. Note that the set of states is not unique, because the $r-r'$ variables that can be eliminated are likewise not unique.

It is not necessary to eliminate all, or for that matter any, of the $r-r'$ variables. While reducing the order of the problem would seem to simplify the optimization, this is not always the case. In the NLP solution, the partial derivatives of all the scalar functions must be taken with respect to each of the uneliminated variables, Reference 6. If the form of some of the h_i 's is not sufficiently simple, substitution using these equalities may serve to complicate the solution. Thus, it should remain the designer's option to utilize the substitution procedure for each of the inequalities.

Figure 30 shows the modeling and optimization process for a set of assumptions. Boxes 1 through 4 have been discussed. The method of NLP solution will be discussed later. The "optimum" output is in quotes because it is optimum only with respect to the validity of the input assumptions. The iteration is with respect to changes in these inputs.

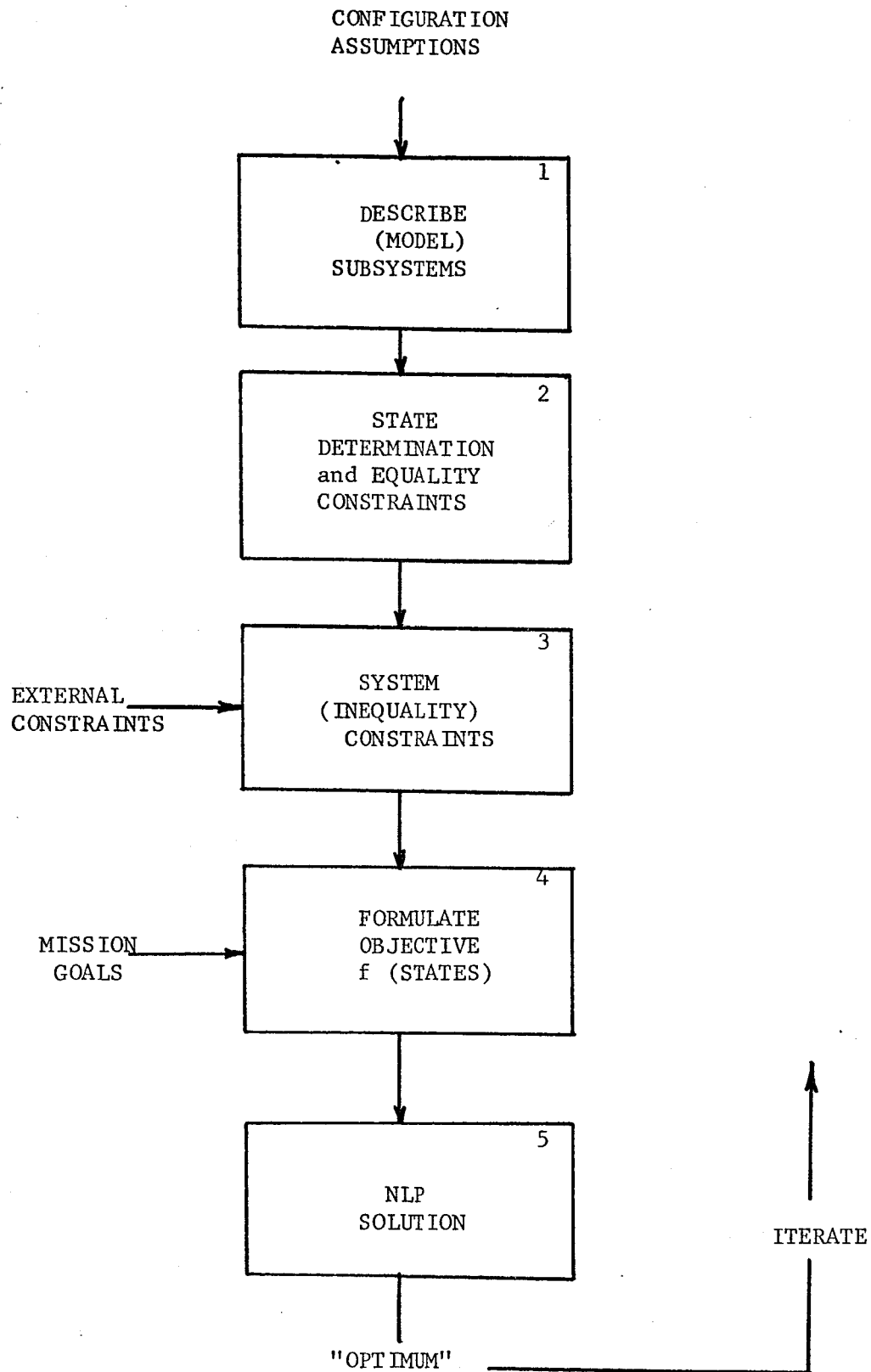
3. Subsystem Modeling

In order to best convey the meaning of the term " subsystem modeling", a fairly detailed explanation of the modeling for one of the subsystems (communications) will be given. Then, a synopsis of all the modeling results is presented in Table 4.

A. Subsystem Modeling Example

The Earth/Mars communication subsystem was modeled as a direct two way link in the microwave spectrum between a Mars roving vehicle (MRV) and an Earth communication station. A number of such models, with appropriate fixed parameters, would be required to describe the possible relay configurations which might be used.

The communication link is divided into an uplink to Mars and a downlink back to Earth. Uplink parameters associated with the rover were found to be negligible in comparison to similar downlink parameters, and were thus not considered directly.



MODELING AND OPTIMIZATION

Figure 30

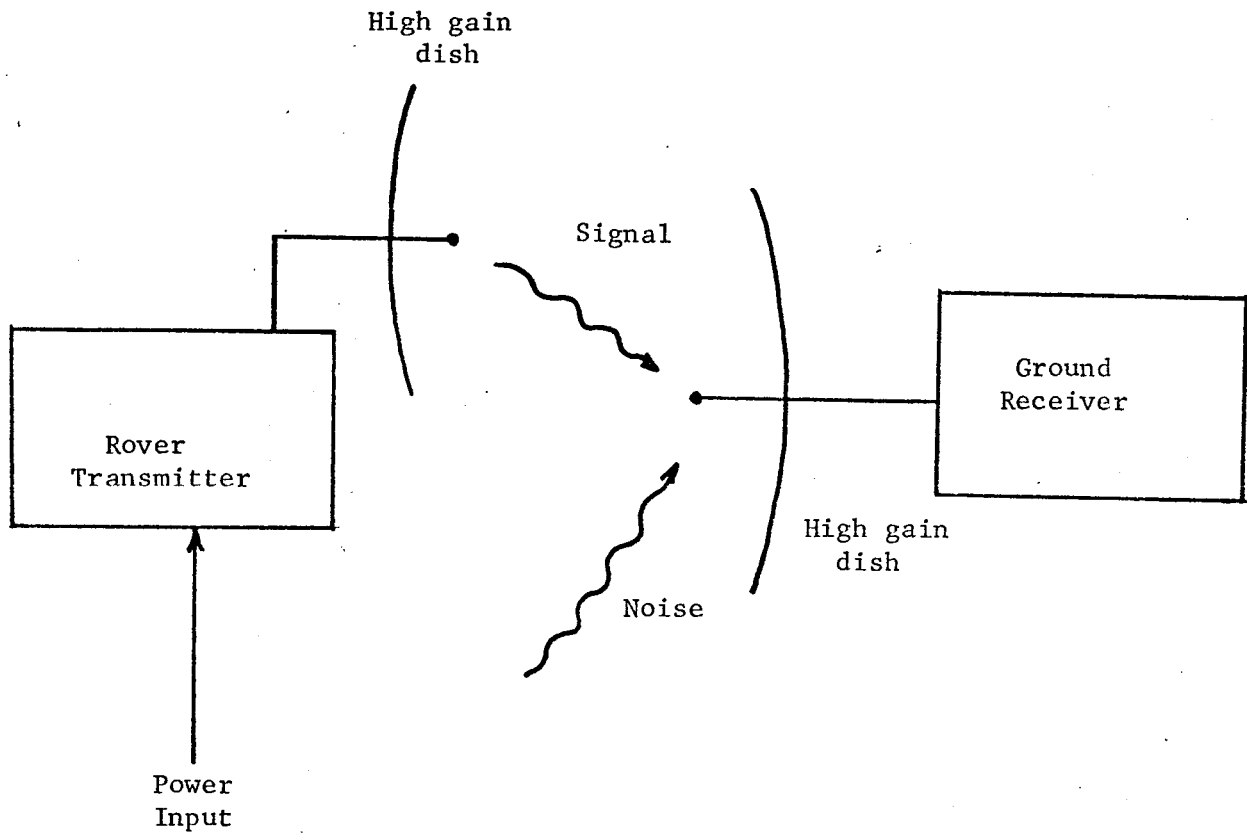
The downlink is composed of the spacecraft transmitter, a high gain parabolic dish antenna, a standby low gain omnidirectional antenna, a free space propagation path, a high gain parabolic dish receiving antenna, and an ultra low noise receiver, as shown in Figure 31.

The first step in the modeling task was to describe the subsystem mathematically in terms of link parameters. The list of parameters of interest in modeling the link is given in Table 4. The parameters can be divided into two classes: those which are fixed by nature, state of the art, or constraints; and those which are design dependent, and therefore a function of the design decisions made (e.g. link distance is fixed by nature, transmitter efficiency is fixed by the state of the art). However, data rate is free to vary over some range, as a function of the design chosen to implement the link.

Before proceeding further, it was necessary to make assumptions to specify the fixed parameters and constrain the model sufficiently to allow analysis:

1. The carrier is X-band microwaves of wavelength 3.3×10^{-2} meters, which have been shown to be especially well suited for high speed communications at Mars distances, Reference 7.
2. The ground station antenna is a 64 meter parabolic dish, Reference 8.
3. The rover antenna is a parabolic dish with a pointing error of 1° .
4. Uplink parameters are negligible.
5. The overall r.f. efficiency of the transmitter is 20%. This figure is obtained from a 25% TWT efficiency and a very low exciter efficiency, Reference 9.
6. The worst case link distance of 5.7×10^{11} meters is used.
7. Total equivalent noise temperature for the receiving system on Earth is the sum of the galactic and receiver noise temperatures, and was assumed to be 30°K , Reference 10.
8. The communication efficiency, a measure of the ability of a given modulation scheme to overcome additive channel noise, is 5%. This corresponds to a 20:1 signal to noise ratio in a typical PCM system, Reference 11.

The above assumptions specify many of the original list of parameters. To further reduce the number of unspecified parameters, equations relating the various parameters can



COMMUNICATION SUBSYSTEM:
DOWNLINK FUNCTIONAL DIAGRAM

Figure 31

PARAMETER	SYMBOL	UNITS
Data Rate	R	bits/sec
R.F. Power Output	P_t	watts
R.F. Efficiency	e	-----
Power Input	P_i	watts
Rover Antenna Diameter	D	meters
Rover Antenna Pointing Error	$\Delta\theta$	degrees
Carrier Wavelength	λ	meters
Weight (Mass)	W_c	kg
Volume	V_c	cubic meters
Heat Dissipation	Q_c	watts
Link Distance	L	meters
Noise Temperature	T	$^{\circ}\text{K}$
Receiver Antenna Diameter	D_r	meters
Communication Efficiency	(B_o/B)	-----

COMMUNICATION SUBSYSTEM:
DOWNLINK PARAMETER LIST

TABLE 4.

be found.

1. Conservation of energy allows two equations to be written.

$$P_t = e P_i$$

$$Q_c = (1-e)P_i$$

2. Subsystem weight was obtained as a function of power input alone from data associated with various prediction efforts in Mars communication, as shown in Figure 32, Reference 12.

From the data, a relationship of the form

$$W_c = aP_i + b$$

is found to approximate the functionality. For P_i expressed in watts and W_c expressed in Kg, the constants were found to be

$$a = 0.59 \text{ kg/watt and } b = 34.0 \text{ kg.}$$

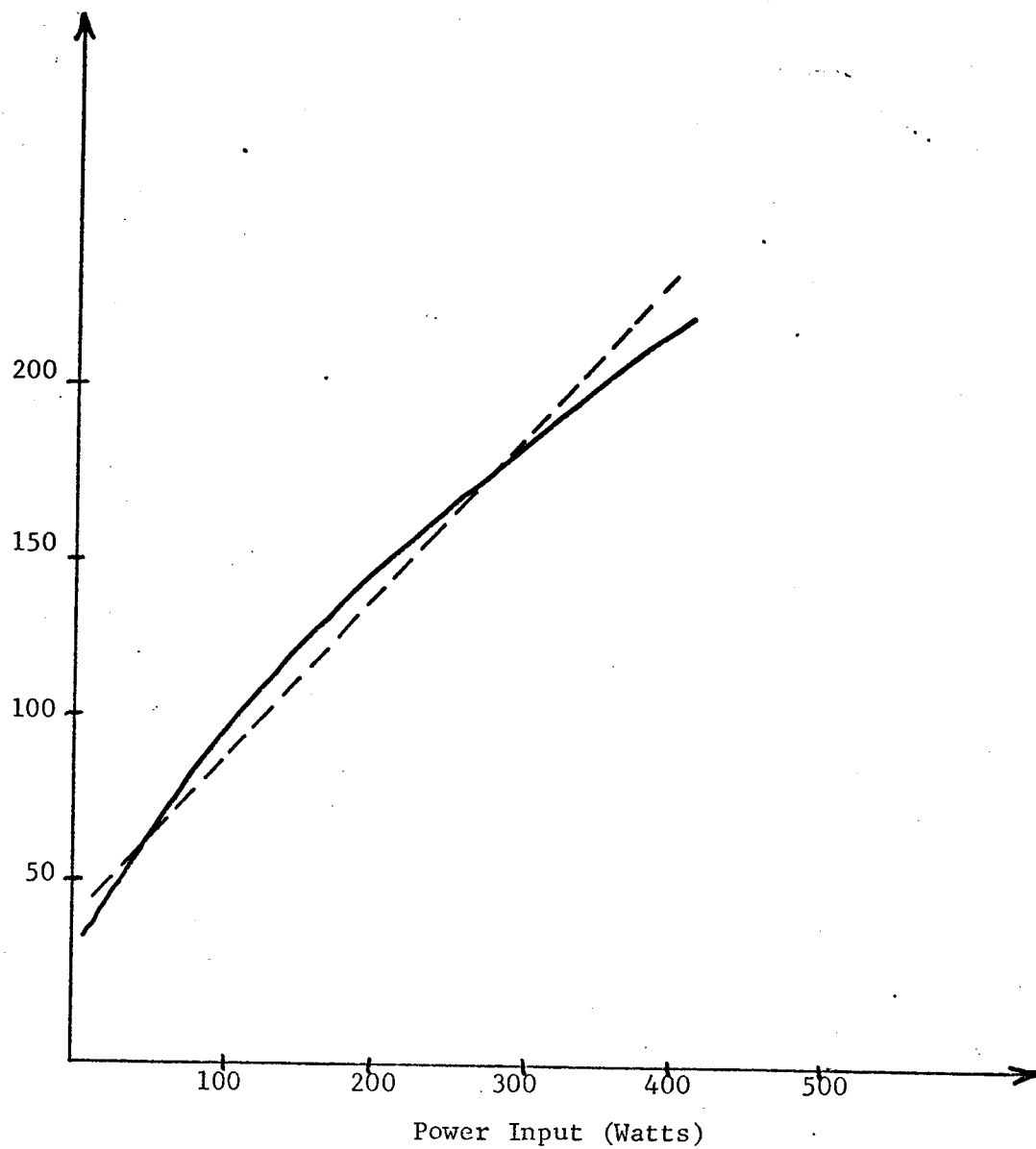
3. Similarly, volume was found to be related to power input in a like manner. The functionality was found to be approximately linear, Reference 12.

$$V_c = 8.3 \times 10^{-4} P_i + 4.8 \times 10^{-2} \text{ meter}^3$$

4. The weight of the antenna and its associated steering motors was estimated to be a function of antenna diameter, D , in meters, as:

$$W_{\text{ant}} = 2.0 D^2 + 5.0 \text{ kg, Reference 13.}$$

At this point, it was noted that there remain only three of the original parameters in Table 4 which have not been either specified by assumption or related to another specified parameter by the simplifying equations identified above: R , P_i , and D . In other words, a knowledge of these three parameters alone will, in the light of the basic assumptions listed, completely specify all of the parameters identified at the beginning of the modeling task as being necessary to uniquely



COMMUNICATION SUBSYSTEM:
GRAPH OF WEIGHT VS. POWER INPUT

Figure 32.

describe the entire subsystem. Given these three parameters, a subsystem could be built. However, not every subsystem would satisfy the requirements which this subsystem is being asked to satisfy. In other words, not any random choice of these parameters will produce a satisfactory subsystem. There must exist another equation which will provide a relationship which the defining parameters must satisfy. The sought after extra equation is the classic range equation for a noisy channel.

For a successful subsystem, the signal power received on Earth must be sufficiently large to overcome the noise. The received power is given by

$$P_r = P_t G_t L_p G_r ,$$

where

P_r is received signal power,

P_t is transmitted signal power,

G_t is transmitting antenna gain,

L_p is the space loss attenuation,

and

G_r is the receiving antenna gain.

Substituting known parameters, for P_r and P_i in watts, D in meters, the received power is found to be

$$P_r = 5 \times 10^{-19} D^2 P_i .$$

For the signal to overcome the noise, the following relation must be satisfied for PCM.

$$P_r = 10^{-23} (B/B_o) \cdot T \cdot R, \text{ Reference 11.}$$

where

B/B_o is the inverse of the communication efficiency,

T is the system noise equivalent temperature, $^{\circ}K$,

and

R is the data rate.

Substituting known parameters, assuming the equality, and combining the above two relations yields the desired relationship,

$$R = 42.0 D^2 P_i$$

Only choices of the three variables satisfying the above relationship will specify subsystems capable of communicating successfully with Earth.

As shown, the communication subsystem can be modeled on the basis of only two chosen parameters (states), as the third is determined by the range equation. If any of the assumptions made at the beginning of the analysis were to be relaxed, then additional state variables would be included to uniquely specify the subsystem.

B. Subsystem Modeling Results

The subsystems comprising the roving vehicle are:

1. science payload
2. power generation
3. communications
4. thermal control
5. navigation (position location in Mars coordinates)
6. obstacle avoidance (local obstacle detection and path selection)
7. computation and data handling
8. vehicle (frame, motors, packaging).

Table 5 summarizes the results of modeling the eight subsystems. The major assumptions shown in column B were made either because they were justifiable in terms of the conclusions of previous studies (e.g., X-band carrier wave for communication) or because it was necessary to constrain the number of options in order to arrive at a mathematical model. This second category of assumptions contains those which must be varied in additional runs of the NLP problem. The collection of all entries in columns C and D is the total set of design parameters. Using equality relations of these parameters, it is possible to establish the minimum number of states, column C. Note that there are three transcendental equations which cannot be used to reduce the number of states, and must appear as state equality constraints in the NLP problem.

TABLE 5.
RESULTS OF SUBSYSTEM MODELING

A subsystem	B major assumptions	C states	D other design parameters
science	equipment priorities, events in science stop	1 weight	power time required/stop volume
power	battery-RTG configura- tion	2 battery energy 3 RTG power 4 roving power 5 velocity	recharge time roving time (max.) weight volume
communica- tions	PCM transmission, X-band trans., antenna pointing- error	6 power 7 antenna diameter	bit rate weight volume
thermal control	radiator-heat pipe config., req'd. temp.=300°K	8 temp (p,n) 9 temp (r,n) 10 temp (p,d) 11 temp (r,d)	weight power radiator area insulation thickness cooling capacity
navigation	power, weight, attitude } constants error	- none -	
obstacle avoidance	scanning pattern path-selection algorithm type power } constants weight }	12 range 13 max. slope factor = (max. slope/ roving power)	max. slope % terrain passable path length ratio = (actual path length/ straight line distance)
computer	power } constants weight }	- none -	
vehicle	5 wheel RPI-MRV	14 wheel base	weight equipment package vol. width (track) height

state equations: one relating power subsystem states

two relating thermal control states

p = equipment package

r = radiator

n = night

d = day

4. System Modeling and Optimization

The design parameters are to be picked in such a way that the system best fulfills its purpose. The Martian rover has essentially two functions. The first is to rove the surface of the planet; the second is to gather and return scientific data. A reasonable objective function then is:

$$\text{maximize } f(\underline{x}) = (\text{distance roved}) \times (\text{science time}) .$$

On a per day basis, $f(\underline{x})$ can be written as a function of the design parameters as:

$$f(\underline{x}) = \frac{(T_{\text{Sci}} S V^2 T_{\text{Rov}}^2)/\text{PLR}}{(T_{\text{Sci}} S V T_{\text{Rov}} + T_{\text{Rov}} + T_{\text{Recharge}})^2}, \text{ where}$$

T_{Sci} = time required for one science stop

S = science stops/kilometer (a new state)

V = vehicle velocity

T_{Rov} = max. roving time before recharge

PLT = path length ratio

T_{Recharge} = recharge time from max. depth of discharge

The choice of states is limited by other constraints besides the three state equations. The two constraints that make optimal design of space systems a real challenge are total weight and volume limitations.

Given the choice of launch vehicle (this may be decided by monetary or availability considerations over which the designer has no control), one can write:

$$\sum \text{weights of all subsystems} \leq \text{payload capacity of launch vehicle}$$

$$\sum \text{volumes of all subsystems} \leq \text{volume of nosecone of launch vehicle.}$$

In addition, for the vehicle itself,

$$\sum \text{equipment volumes} \leq \text{vehicle equipment package volume.}$$

These equations establish the g_i 's (inequality constraints). At this point, the problem has been sufficiently mathematically formulated to attempt optimization.

A program solving the NLP problem using the sequential unconstrained minimization technique, Reference 14, has been written by Ron Janosko of the RPI-MRV project. At the present time, the program is being modified to handle the somewhat complex equations which resulted from subsystem modeling.

5. Future Work

A major effort will continue to be expended toward completing the present effort of optimizing the current MRV model. Then the model will be changed to conform with changes in assumptions that need to be made, and solutions will be obtained for all cases.

A study will be initiated to determine the sensitivity of the optimum solutions both to changes in the design parameters and model parameters. Design parameter changes represent changes made during actual design and construction of subsystems; and model parameter sensitivities indicate how inaccuracies in the model affect the optimal solution.

An attempt to separate the determination of mission goals, profiles, and system configuration from the optimization process will be made.

In addition, a more thorough examination of decision-making and computational requirements as a function of the design parameters will be undertaken.

Task C. Navigation, Terrain Modeling and Path Selection

The mission plan to undertake a systematic exploration of Mars requires that the roving vehicle can be instructed to proceed under remote control from its landing site to a succession of desired locations. This objective requires that the vehicle possess the capabilities: of sensing and interpreting the terrain to provide the information required by a path selection system, of selecting paths with due regard to safety and other considerations, and of knowing its location and that of its destinations. Tasks relating to these objectives have been defined and are under active study. The progress achieved to date is described in the sections immediately following.

Task C.1. Navigation Systems

The aim of the navigation task is to provide a continuous record of the position of the vehicle as it explores the Martian surface. It was decided to break this objective down into two main types of navigation systems. The Vehicle Navigation System provides a continuous estimate of the vehicle's position. However, this estimate contains some error which grows with time. The Satellite Navigation System provides a more accurate estimate of the vehicle's position at discrete instances of time. These are then used to correct the error in The Vehicle Navigation System. Referring to Fig. 32, it is possible to see how the entire navigation package is put together.

PROPOSED NAVIGATION SYSTEM

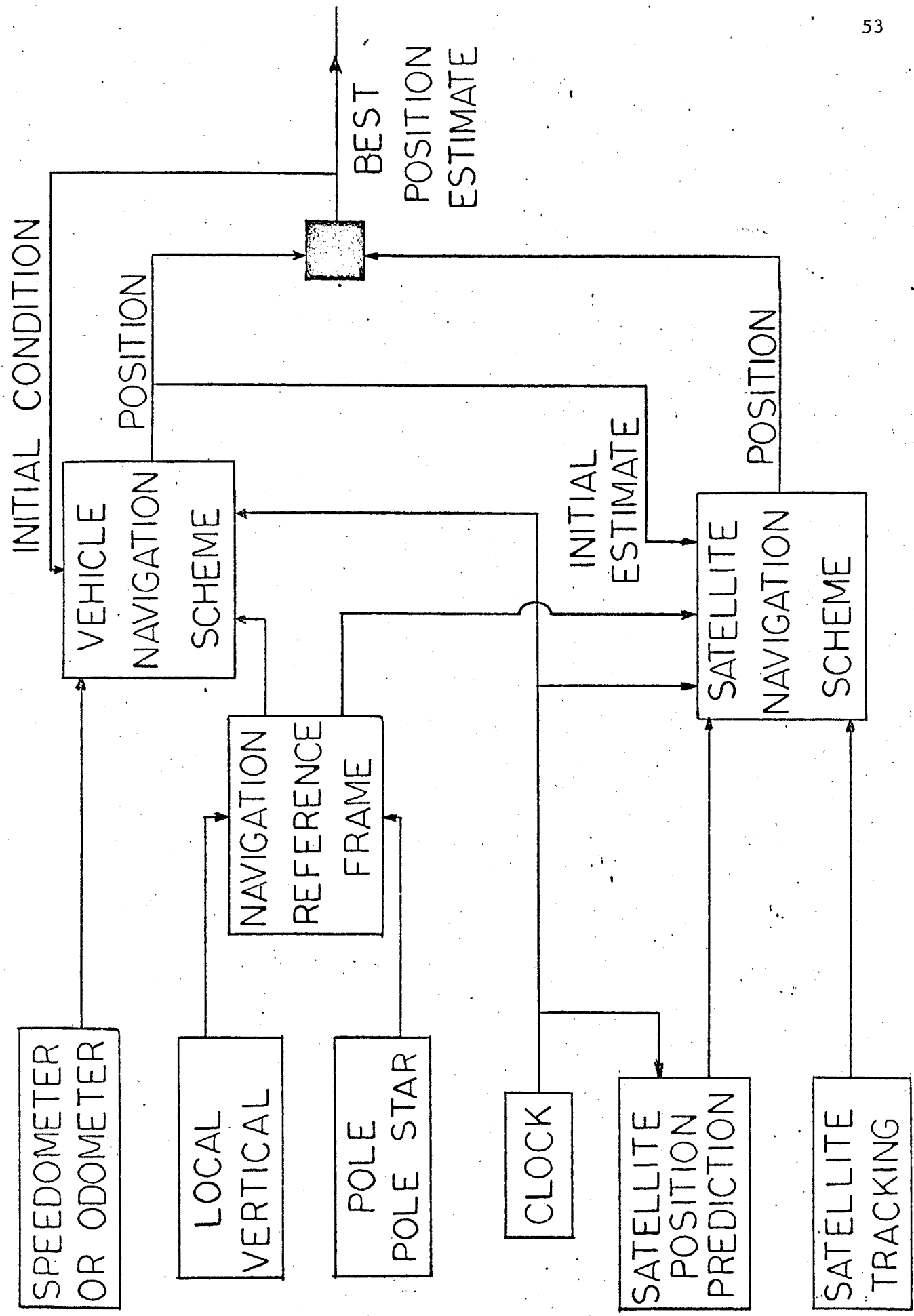


Figure 32.

The local vertical tracking block couples with the star and/or pole tracking block to generate a vehicle navigation reference frame. This frame is then used to transform the velocity measured in the body frame into the proper reference frame for use by the vehicle navigation scheme. The vehicle navigation scheme uses this transformed velocity and the on-board clock along with some initial condition of the estimated position and basically integrates the velocity to obtain an estimate of vehicle position as it travels on Mars.

The satellite navigation scheme uses a knowledge of the navigation reference frame, the clock, the output of a satellite tracking system, the prediction of the present satellite position and the present output of the vehicle navigation scheme to obtain an estimate of the present vehicle location. Here the estimate for the vehicle system is used as an initial estimate in an estimation scheme.

The outputs of both the vehicle navigation scheme and the satellite navigation scheme are combined to obtain a best estimate of the true vehicle position. This final estimate is then used as an initial condition for the vehicle navigation scheme. The output of the vehicle navigation scheme is available continuously where the satellite system output is only available at discrete instances where the satellite can be sighted by the rover.

At present work is progressing on the design of the satellite navigation system. The local vertical sensor and the star and/or pole tracking system and the vehicle navigation scheme have been completed during this last period. Work in these four areas is reported below.

Task C.1.a. Satellite Navigation System - R. E. Janosko
Faculty Advisor: Prof. C. N. Shen

During this period this task has attempted to minimize some of the errors inherent in the primary navigation system. That system assumed that the rover could track the orbiter and record the distance from the rover to the satellite. It was further assumed that the exact location of the satellite was known. From this information, the absolute location of the satellite and the location of the satellite with respect to the rover, it was then possible to solve for the location of the rover. An error analysis was then performed on this method of determining the rover's position. Nominal errors in the required measurements and in the location of the satellite led to a reasonable error in locating the rover, Reference 14.

The basis system studied is given in Figure 33, the I_1, I_2, I_3 are inertial axes centered in Mars, \bar{x} is the vector that locates the rover on the Martian surface, $\bar{s}_1, \bar{s}_2, \bar{s}_3$ are the three position vectors of the satellite, and ρ_1, ρ_2, ρ_3 are the three scalar distances from the rover to the satellite. For the present analysis it was assumed that the rover was fixed on the Martian surface and that Mars was not rotating.

In order to perform an error analysis on this scheme, perturbations were introduced in the measured quantities as well as in the components of the \bar{x} vector. These deviations in the \bar{x} vector were then algebraically solved for in terms of the errors in measuring

BASIC CONFIGURATION

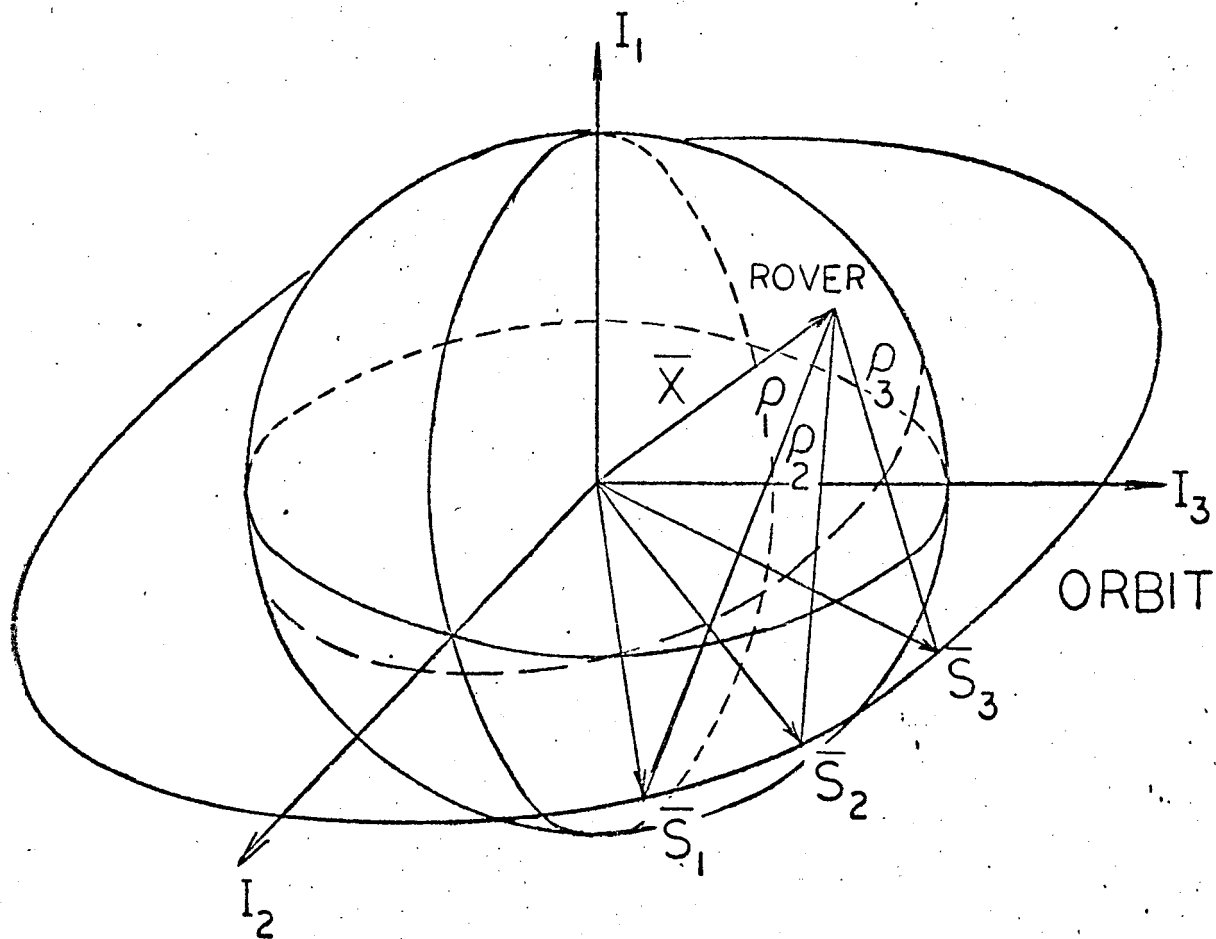


Figure 33.

the range and in locating the satellite.

These error equations were able to be written as

$$\Delta \bar{x} = \begin{bmatrix} (\bar{x} - \bar{s}_1)^T \\ (\bar{x} - \bar{s}_2)^T \\ (\bar{x} - \bar{s}_3)^T \end{bmatrix}^{-1} \begin{bmatrix} \rho_1 \\ \rho_2 \\ \rho_3 \end{bmatrix} \Delta \bar{\rho} + \begin{bmatrix} 1 \\ 1 \\ 1 \end{bmatrix} \Delta \bar{s} \quad (1)$$

where

- $\Delta \bar{x}$ is the rover error vector giving the error in the three component directions
- $\Delta \rho$ is the error in the range measurement (assumed equal for all three measurements)
- $\Delta \bar{s}$ is the error in locating the satellite (assumed equal in all directions)
- S is the error in the relative location of the satellite (assumed proportional to a clock error and about .1 s)

For Equation 1, a 1 km error in Δs and $\Delta \rho$ of 5 m., it was found that for 3000 km orbit $\Delta \bar{x}^T \Delta \bar{x}$ was about 3 km.² which is quite reasonable.

The final navigation error is thus able to be written as:

$$\Delta \bar{x} = [B(\bar{x}, \bar{s}_1, \bar{s}_2, \bar{s}_3)]^{-1} \{ \bar{\rho} \Delta \bar{\rho} + B(\bar{x}, \bar{s}_1, \bar{s}_2, \bar{s}_3) (1) \Delta s \}$$

where $\Delta \bar{x}$, $\Delta \rho$ and Δs are as previously defined.

$B(\bar{x}, \bar{s}_1, \bar{s}_2, \bar{s}_3)$ is a 3x3 matrix whose elements are functions of the rover location \bar{x} , and the three satellite locations \bar{s}_1 , \bar{s}_2 , and \bar{s}_3 .

$\bar{\rho}$ is a vector whose components are the three range measurements ρ_1, ρ_2, ρ_3 to the three satellite positions $\bar{s}_1, \bar{s}_2, \bar{s}_3$.

(1) is a vector where components are (1,1,1)^T

Note that the error in $\Delta \bar{x}$ is one-to-one with the error in locating the satellite.

Instead of minimizing the value $\Delta \bar{x}$ directly, we will minimize the trace of the correlation matrix of $\Delta \bar{x}$ or the mean squared error (MSE). This trace can be written as $E(\Delta \bar{x}^T \Delta \bar{x})$. If it is further assumed that the error in the satellite location and the error in the range measurement are independent and uncorrelated then the problem can be written as minimize

$$\text{MSE} = \bar{\rho}^T B^{-1T} B^{-1} \bar{\rho} \Delta \tilde{\rho}^2$$

where ρ and B , have been previously defined, and $\Delta \tilde{\rho}^2$ is the variance of the range error.

The error related to the range errors is a function of the rover location \bar{x} , which is arbitrary. If one were to look at reducing this error as a function of rover location we would unnecessarily restrict the area able to be explored by the vehicle. This error is also a function of the satellite position. However, this is a variable that can be controlled. It is possible to select an orbit so as to minimize the navigation error. For the present it was decided to assume that the orbit is circular and that the inclination doesn't enter into the error. This means that we can choose the altitude A , of the orbit. One also can choose the relative location between the satellite locations. To choose these locations it is possible to vary the angle α , where α is the angle between satellite vectors. This corresponds to deciding how often to take data. Figure 34 illustrates the simple problem chosen to test the method of minimizing the error vector. The variables in this case are A and α .

As mentioned previously, the error is a function of the rover location. To eliminate the problem of studying all rover locations and how the error varies at each, only the case where the rover is fixed, so that a line from the rover to the second sub-satellite point on the surface is perpendicular to the trace of the orbit on the surface, was studied. Further, the rover was located so that it is the maximum distance from the orbital plane that the rover can be and still see the satellite three times.

With the above as an outline indicating most of the mathematical background necessary, the problem could then be stated as

$$\min_{\alpha, A} \bar{\rho}^T B^{-1T} B^{-1} \bar{\rho} \Delta \tilde{\rho}^2$$

$$\text{subject to: } A_{\max} - A \geq 0$$

$$A - A_{\min} \geq 0$$

$$\beta - \alpha \geq 0$$

$$\cos \gamma \cos \alpha - \cos \beta = 0$$

$$\cos \beta - \sin \beta \frac{R}{R+A} = 0$$

where

$$B^{-1} = \begin{vmatrix} R \sin & R \cos & - (R+A) \cos & (R+A) \sin \\ R \sin & R \cos & - (R+A) & 0 \\ R \sin & R \cos & - (R+A) \cos & - (R+A) \sin \end{vmatrix}^{-1}$$

and

SPECIFIC GEOMETRY

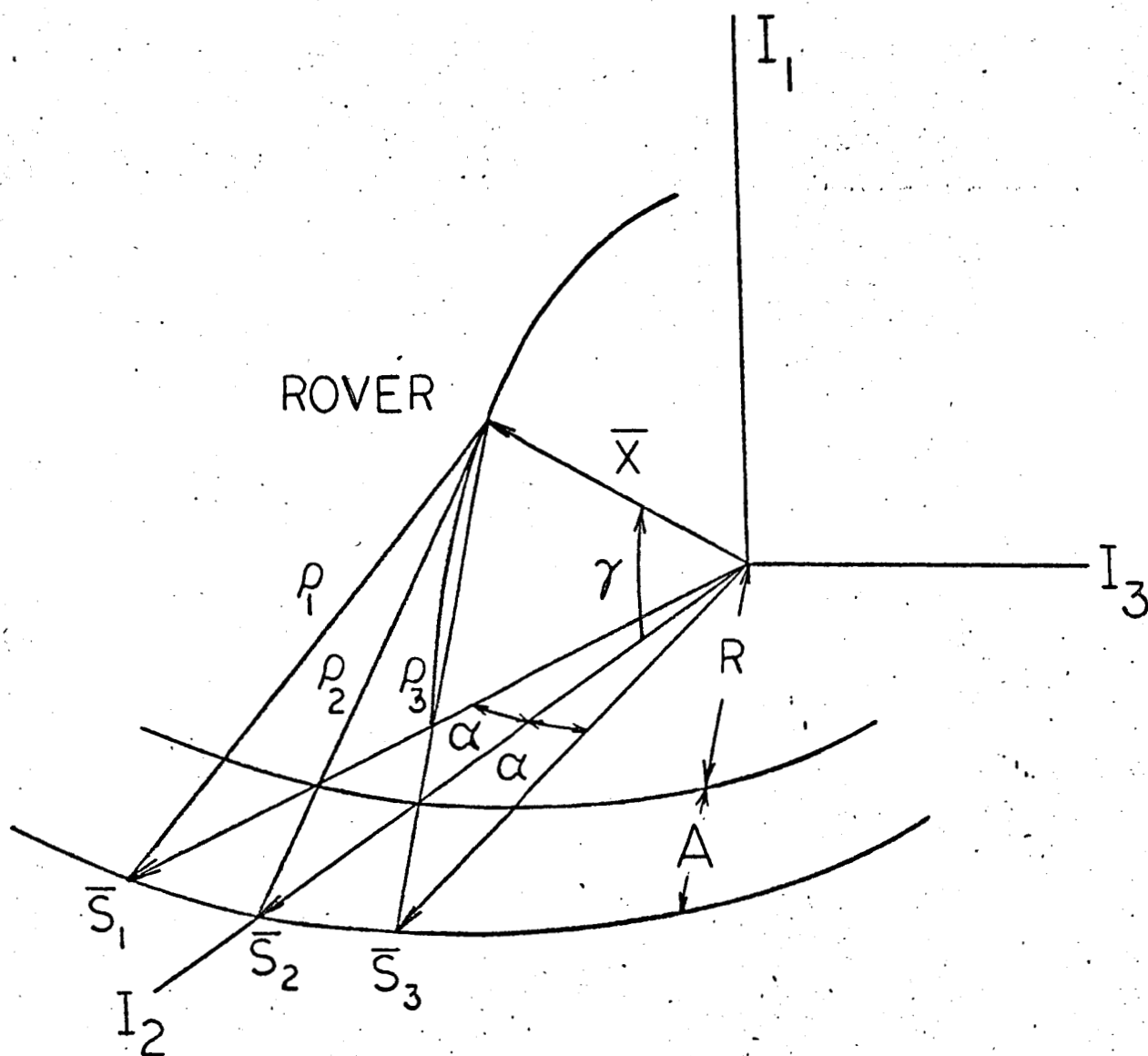


Figure 34.

$$\bar{\rho} = \begin{vmatrix} \rho_1 \\ \rho_2 \\ \rho_3 \end{vmatrix}$$

At this time the analytic solution to the above problem is completed. The optimal A is 2971.06 Km, the optimal α is 1.16×10^{-4} radians (a measurement interval of 0.28 sec). The minimum mse is then $6.08 \times 10^{-4} \text{ Km}^2$ for a $\Delta \tilde{\rho}^2$ of $2.5 \times 10^{-5} \text{ Km}^2$.

While the analytic solution to the problem was being investigated research was undertaken to see how the use of a laser range finder with its power requirements will effect the optimal solution. The laser will add additional constraints to the minimization problem.

The average power P_{av} , drawn by the laser must be less than or equal to the maximum power available to the laser subsystem. That is

$$P_{av} \leq P_{max}$$

where P_{max} is the maximum power available. Also the power received, P_r , must be greater than or equal to the minimum detectable power at the receiver. Or,

$$P_r \geq P_{min}$$

where P_{min} is the minimum detectable power. Further, to be realistic, the energy input to the laser E_{in} should be less than or equal to the energy rating of the laser E_L . If t is the time required to charge the laser, then the input energy E_{in} can be represented as

$$E_{in} = P_{av} t$$

and thus the constraint

$$E_L \geq P_{av} t$$

Letting the efficiency of the laser system be ϵ , the power transmitted in one pulse of the laser, P_t , can be represented by

$$P_t = \frac{\epsilon P_{av} t}{\tau} \quad (2)$$

where τ is the pulse width.

The problem now is to relate the power transmitted to the power received. The transmitted beam power P_t , and the power that is

incident on the target, P_T , are in a ratio proportional to the target, A_T , and the area that the transmitted beam has at the target range. This last area can be represented in terms of the average distance from the target to the transmitter, $\tilde{\rho}$, and in terms of the beam divergence angle θ_t . This power ratio is thus able to be written as

$$\frac{P_T}{P_t} = \frac{A_T}{\pi (\tilde{\rho} \theta_t)^2} \quad (3)$$

Likewise the ratio of power received by the receiver, P_r , to the reflected power from the target, P_T , is in the same proportion as their relative areas are, that is,

$$\frac{P_r}{P_T} = \frac{A_r}{\pi (\tilde{\rho} \theta_r)^2} \quad (4)$$

where A_r is the receiver area, and θ_r is the returned beam divergence angle. It should be mentioned here that it has been assumed that the satellite has been equipped with a retroreflecting surface so that almost all of the incident radiation onto the target area is reflected back in the direction of the transmitter/receiver group. If one of the natural satellites or a non-reflecting satellite is used instead then one must include the losses due to the scattering of the light by the non-retro-reflecting surface.

Besides the geometric losses, there is also the atmospheric absorption of some of the power, the slight losses at the retro-reflector (or large losses if not retroreflecting), and optical losses in the transmission and receiving of the laser beam. If ϕ represents the one way atmospheric loss, ϕ_T represents the factor correcting for the reflective loss, and η represents the overall optical efficiency of the system, then the transmitted power can be related to the receiver power rather accurately by

$$\frac{P_r}{P_t} = \frac{\eta \phi_a^2 \phi_T A_r A_T}{\pi^2 \theta_r^2 \theta_t^2 \tilde{\rho}^4} \quad (5)$$

which is obtained from equations (3) and (4) when the loss factors are included.

Equation (5) can now be used to relate the time to charge the laser and the power received. Using equation (2) in equation (5) the following equation results:

$$P_r = \frac{\eta \epsilon \phi_a^2 \phi_T A_r A_T P_{av} t}{\pi^2 \theta_r^2 \theta_t^2 \tau \tilde{\rho}^4}$$

The time between sightings must now be made to correspond to the time to charge the laser. This can be done by relating the period of the orbit to the time it takes to travel an arc length equal to α degrees. This relationship can be given by the following formula that holds for a circular orbit, Reference 16,

$$t_b = \alpha \frac{(A + R)^{3/2}}{207.0}$$

where t_b represents the time between sightings in seconds and A and R are in kilometers and α in radians. It is now required that the time between sightings be greater than the time used to charge the laser. This can be represented by

$$t \leq \alpha \frac{(A + R)^{3/2}}{207.0}$$

After a detailed investigation of laser rangefinders in the literature, we found that it was possible to form a relationship between the signal-to-noise ratio and the root mean square (RMS) range error. For a pulsed laser this relationship can be given by, Reference 17,

$$(\Delta \rho^2)^{1/2} = \frac{Kc}{2b} \left[\frac{1}{2(S/N)} \right]^{1/2} \quad (6)$$

where c is the speed of light in kilometers/sec, b is the pulse detector bandwidth in hertz, K is a dimensionless constant depending on the shape of the bypass characteristics and equals approximately 0.4 and (S/N) represents the signal-to-noise ratio in db. It was further possible to relate the (S/N) to the receiver power by the following equation which holds for a photomultiplier tube detector, Reference 18,

$$S/N = 10 \log \left[\frac{\left(\frac{qn}{h\nu} \right) P_r}{4 b q \left[1 + P_B/P_r + (I_d/P_r) \left(\frac{h\nu}{qn} \right) \right]} \right] \quad (7)$$

where q is the electron charge (coul.)
 h is Planck's constant (joules-sec)
 n is the quantum efficiency
 ν is the frequency of radiation (sec^{-1})
 P_B is the background power falling on the detector (watts)
 b is the bandwidth in hertz
 I_d is the dark current (amps)

Equations (6) and (7) can now be combined to yield

$$(\Delta \tilde{\rho}^2)^{1/2} = \frac{Kc}{2b} \left[\frac{0.05}{\log \left[\left(\frac{qn}{hv} \right) P_r \right] - \log \left[4b_q \left\{ 1 + P_B/P_r + (I_d/P_r) \left(\frac{hv}{qn} \right) \right\} \right]} \right]^{1/2}$$

In this section all of the constraints and the objective function are not in the standard nonlinear programming format. This standard format can be written as

$$\min: \bar{\rho}^T B(\bar{x}, \bar{s}_1, \bar{s}_2, \bar{s}_3)^{-1T} B(\bar{x}, \bar{s}_1, \bar{s}_2, \bar{s}_3)^{-1} \bar{\rho} \Delta \tilde{\rho}^2$$

subject to:

The equality constraints

$$\cos \beta - \sin \beta - \frac{R}{R+A} = 0$$

$$\cos \gamma - \cos \alpha - \cos \beta = 0$$

$$P_r - \frac{\eta \epsilon \phi_a^2 \phi_T A_r A_T P_{av} t}{\pi^2 \theta_r^2 \theta_t^2 \tau \tilde{\rho}^4} = 0$$

$$\Delta \tilde{\rho}^2 - \frac{(Kc)^2}{2b} \left[\frac{0.05}{\log \left[\left(\frac{qn}{hv} \right) P_r \right] - \log \left[4b_q \left\{ 1 + P_B/P_r + \left(\frac{I_d}{P_r} \right) \left(\frac{hv}{qn} \right) \right\} \right]} \right] = 0$$

and the inequality constraints

$$\alpha - \beta \geq 0$$

$$A_{\max} - A \geq 0$$

$$A - A_{\min} \geq 0$$

$$P_{\max} - P_{av} \geq 0$$

$$P_r - P_{\min} \geq 0$$

$$P_{av} t - E_1 \geq 0$$

$$t - \frac{\alpha(A+R)^{3/2}}{207.0} \geq 0$$

Also $\tilde{\rho} = (\rho_1 + \rho_2 + \rho_3)/3$, that is $\tilde{\rho}$ is the average range measured, and B and $\tilde{\rho}$ are as previously defined.

The minimization is to be carried out with respect to the variables

$\alpha, \beta, A, \gamma, P_r, \Delta \tilde{\rho}^2, t, P_{av}$. All other quantities in the above equations are treated as constants and their values must be specified before the problem can be solved. The analytical solution to this total problem is not yet complete. It is anticipated that this problem will be solved by February 1972 by which time additional constraints specifying the area of surface investigation will also be included.

Task C.1.b. Vehicle Navigation System - H. M. Chen
Faculty Advisor: Prof. C. N. Shen

The objective of this sub-task is the design and analysis of a surface navigation system for a Mars Roving Vehicle. The major emphasis during past period has been directed to a detailed error analysis of the proposed navigation scheme.

During the past period when designing a rover navigation system, an attempt was made to avoid using conventional navigation methods which use a gyro-platform with accelerometers because they are ineffective for low speeds and high vibrations, a direct velocity sensor, Reference 19, was devised to measure the velocity relative to the Martian surface in a vehicle body-bound frame. The velocity measurement was then transformed to a non-inertial reference frame for computation. To establish the reference frame, the vehicle has to measure continuously, a unit vector \hat{u}_v , pointing away from the Mars center. One of the axes of the frame, x_1 , is aligned with the vector \hat{u}_v . The second axis is placed perpendicular to the plane formed by the pole-star and local-vertical directions in the direction of the vector $\hat{u}_p \times \hat{u}_v$. The third axis is orthogonal to both the first two axes and forms a right-handed triad. By integrating the velocity components along these three axes, the vehicle computer is able to continuously track the value of radius $r(t)$, latitude $\lambda(t)$, and longitude $\phi(t)$, with respect to a Mars geographic coordinate system as the vehicle travels from a given initial point with the value (r_0, λ_0, ϕ_0) .

Due to the errors of the initial position estimates, the velocity measurement, the optical star-tracking device and the local-vertical sensor, the computer errors in $r(t)$, $\lambda(t)$ and $\phi(t)$ are found to be proportionally increasing with the distance traveled by the rover. It is then concluded that the system needs re-initiation periodically by using some outside independent information, e.g., the rover position estimates from the satellite update system, Reference 15.

There are two kinds of singularity problems in this system when the rover is near the Mars poles. They are the reference frame singularity problem and computational singularity problem. The former is due to the closeness of the pole-star vector and the local-vertical at high latitude area. To establish a more accurate reference frame in the area $\lambda > 70$ degrees, it may be suggested that additional measurement such as consecutively observing three known stars which are near the Mars equator and about 120 degrees apart, should be obtained. Concerning the computational singularity problem a region called POLE AREA is defined for the latitudes from $\lambda = 88^\circ$ to $\lambda = 90^\circ$. This POLE AREA is then a circular, almost flat region with a radius less than 120 km's. Within the POLE AREA, it would be proper to stop the above

surface navigation system and use landmarks, sun tracking, satellite or even place a beacon as a reference.

Comparison with other navigation schemes

After a review of the literature it was possible to compare other candidate navigation schemes by means of the table following. Table 6 compares four candidate schemes. The system proposed in the earlier part of the section is the pole star-local vertical/velocity sensor system. The other three systems are commonly used navigation systems.

As a result of this rough comparison it was decided that the gyro/accelerometer inertial system and the body bound gyro system could be dropped from consideration as candidate systems. This was because of their short independent operation times and because of the large error sources that were inherent in the systems themselves. Further it was decided that a hybrid system using basically the odometer gyrocompass system updated by the pole star location could combine the best of the remaining two systems. A more thorough discussion is given in the technical report that was written in the area and is summarized in the next section.

The above comparison suggests that a possible feasible and reliable system might be the one described as follows. For the physical platform, use a horizontally stabilized platform which is orientated with respect to the local vertical only. A north or south seeking gyrocompass is mounted on a pivot fixed to the platform, such that the gyrocompass is free to rotate with respect to the normal of the platform. A pole star sensor, which is also mounted on the platform the same way, is used periodically to update the north or the south of the gyrocompass.

The distance traveled by the rover is measured by using angle pick-offs on the two driving wheels. Weight the angle measurements by some function of the steering angle when the front wheels are turned. Measure the horizontal deflection angle ϕ of the tail wheel arm to calculate the lateral slide of the vehicle. The horizontal deflection angle ϕ_T of the arm caused by the steering angle θ alone was reported in Reference 19. Once $\phi_T(\theta)$ is evaluated, the lateral slide S_{B1} of the vehicle can be calculated as

$$S_{B1} = S_{B2} \tan (\phi - \phi_T)$$

when S_{B2} is the weighted odometer reading within some short time interval (say one minute, or equivalently 20 meters) when ϕ and ϕ_T can both be considered as constants.

This distance is measured in the vehicle body frame. In order to transform it to the local reference frame for use by the vehicle navigation system, the pitching angle β and the rolling angle γ of the platform and the yawing angle α of the gyrocompass have to be measured. The transformation is accomplished by means of the equation

TABLE 6
CANDIDATE SYSTEMS

	POLE-STAR LOCAL-VERTICAL VEL. SENSOR SYSTEM	GYROCOMPASS / ODOMETER SYSTEM	GYRO/ACC. INERTIAL SYSTEM	BODY- BOUND GYRO SYSTEM
PLATFORM NEEDED	STABLE w/ L.V.	STABLE w/ L.V.	STABLE w/ N.E. & L.V.	NONE
NAVIGATION REFERENCE	P.S. SENSOR L.V. SENSOR	TWO-DEGREE -FREEDOM GYRO WITH PENDULAR MASS, VERTICALLY DAMPED. L.V. SENSOR	3 SINGLE -DEGREE- FREEDOM GYROS	2 BODY- MOUNTED TWO-DEGREE -FREEDOM GYROS L.V. SENSOR
NAVIGATION MEASURE -MENTS	"VELOCITY" ON BODY FRAME BY TAIL-WHEEL VEL. SENSOR. PLATFORM GIMBAL ANGLES	"DISTANCE" ON BODY FRAME BY WHEEL ROTAT- ION ANGLE PICK-OFFS. PLATFORM GIMBAL ANGLES	"ACCELERATION" COMPONENTS ALONG L.V., N. & E. BY 3 ORTHOGONALLY PLACED ACCELEROMETERS	GYRO GIMBAL ANGLES & ANGLE RATES. VEHICLE "ACCELERATION" ON BODY FRAME
ERROR SOURCES	P.S. & L.V. SENSOR ERRORS BUT "STABLE". VEL. SENSOR BIAS & PROP. ERRORS.	L.V. SENSOR ERROR GYRO DRIFTS ODOMETER BIAS & PROP. ERRORS; SIDE-SLIDE	"UNSTABLE" GYRO DRIFTS PLATFORM TILT	GYRO DRIFTS GIMBAL ANGLE & RATES MEASUREMENT ERRORS ACC. MEASURE- MENT ERROR
INDEPENDENT OPERATION TIME	LONGEST	LONG	SHORT	PROBABLY SHORTEST
COMPUTATION	SIMPLE	SIMPLE	NOT COMPLICATED	COMPLICATED
CURRENT FEASIBILITY STUDY CONCLUSION	FEASIBLE	FEASIBLE	NOT FEASIBLE	UNKNOWN

$$\begin{bmatrix} S_E \\ S_N \\ S_V \end{bmatrix} = A(\alpha) B(\beta) C(\gamma) \begin{bmatrix} S_{B1} \\ S_{B2} \\ 0 \end{bmatrix}$$

where S_E , S_N , S_V = transformed distance components along the E, N and L.V. directions respectively. The matrix A, B and C are defined as

$$A(\alpha) = \begin{bmatrix} \cos \alpha & \sin \alpha & 0 \\ -\sin \alpha & \cos \alpha & 0 \\ 0 & 0 & 1 \end{bmatrix}$$

$$B(\beta) = \begin{bmatrix} 1 & 0 & 0 \\ 0 & \cos \beta & -\sin \beta \\ 0 & \sin \beta & \cos \beta \end{bmatrix}$$

$$C(\gamma) = \begin{bmatrix} \cos \gamma & 0 & \sin \gamma \\ 0 & 1 & 0 \\ -\sin \gamma & 0 & \cos \gamma \end{bmatrix}$$

Now, if $S_E(k)$, $S_N(k)$ and $S_V(k)$ are used to denote the transformed distance measurements in the Kth time interval, the updated position of the vehicle at the end of the ith interval can be calculated as follows:

$$\begin{bmatrix} \phi(t) \\ \lambda(t) \\ r(t) \end{bmatrix} = \begin{bmatrix} \phi_0 \\ \lambda_0 \\ r_0 \end{bmatrix} + \sum_{k=1}^i \begin{bmatrix} S_E(k) / r(k) \cos \lambda(k) \\ S_N(k) / r(k) \\ S_V(k) \end{bmatrix}$$

where $[\phi(t), \lambda(t), r(t)]^T$ is the rover position at time t, and (ϕ_0, λ_0, r_0) is the initial position. The time interval (0,t) has been divided into i equal subintervals which are assumed to be small.

To consider the output accuracy of the above modified system, the following possible error sources are investigated. The distance component S_{B2} is measured by two angle pick-offs which are mounted on the driving wheels. Due to slippage, sinkage and wheel deformation, Reference 20, etc., a 5% proportional error would be a reasonable guess. Also some amount of bias error may exist due to poor calibration. When the vehicle is turning, improper weighting on the angle

pick-off outputs is another source of error. The lateral movement S_{B1} which is related to S_{B2} apparently has a larger error. The lateral deflection angle ϕ may be a very poor measurement if the arm-wheel assembly is not light, Reference 19. The angle measurements α , β , γ are comparatively accurate for transformation purposes, if the sampling time intervals are chosen to be very small. Hence as a first approximation, the α , β , γ measurement errors will be neglected. It should be understood that although these angular measurements can be made accurately, the measurements β and γ contain the platform error and/or the local vertical sensor error, and the measurement α contains gyro misalignment and drift errors. Assume that the normal to the platform plane does not follow the true local vertical but deviates from it a small angle ϵ_v , and the gyro drifts from the true north or south by a small angle ϵ_g . To show the consequence of the error sources stated above, the system equation is perturbed to yield the following:

$$\begin{aligned}
 \begin{vmatrix} \Delta S_E \\ \Delta S_N \\ \Delta S_V \end{vmatrix} &= ABC \begin{vmatrix} \Delta S_{B1} \\ \Delta S_{B2} \\ 0 \end{vmatrix} + AB \begin{vmatrix} -\sin \gamma & 0 & \cos \gamma \\ 0 & 0 & 0 \\ -\cos \gamma & 0 & -\sin \gamma \end{vmatrix} \begin{vmatrix} S_{B1} \\ S_{B2} \\ 0 \end{vmatrix} \Delta \gamma \\
 &+ A \begin{vmatrix} 0 & 0 \\ 0 & -\sin \beta & -\cos \beta \\ 0 & \cos \beta & -\sin \beta \end{vmatrix} C \begin{vmatrix} S_{B1} \\ S_{B2} \\ 0 \end{vmatrix} \Delta \beta \\
 &+ \begin{vmatrix} -\sin \alpha & -\cos \alpha & 0 \\ \cos \alpha & -\sin \alpha & 0 \\ 0 & 0 & 0 \end{vmatrix} BC \begin{vmatrix} S_{B1} \\ S_{B2} \\ 0 \end{vmatrix} \Delta \alpha
 \end{aligned}$$

where the Δ quantities are interpreted as the associated errors, and the non- Δ quantities can be interpreted as the associated true values. It is clear that

$$\Delta \alpha = \epsilon_g$$

$$\Delta \beta = \epsilon_v \cos \omega$$

$$\Delta \gamma = \epsilon_v \sin \omega$$

If ϵ_v and ϵ_g are considered as small gaussian random variables with zero means; the angle ω is a random variable uniformly distributed on $[0, 2\pi]$, and the quantities ΔS_{B1} and ΔS_{B2} are taken as gaussian random but with non-zero means, it then follows that $[\Delta S_E, \Delta S_N, \Delta S_V]^T$ is a random vector which is a function of the random variable $\Delta S_{B1}, \Delta S_{B2}, \epsilon_v, \epsilon_g$ and ω .

To get more insight into the above analysis, an example is given as follows: Assume that the rover travels eastward for 2000 meters, in a straight path with constant speed, on a horizontal terrain such that

$$\alpha = \frac{\pi}{2} \quad \beta = \gamma = 0$$

and the lateral movement

$$S_{B1} = 0$$

Also assume that the instrument errors have zero means and the following standard deviations

$$\text{s.d. of } \epsilon_g = 1/50 \text{ radian}$$

$$\text{s.d. of } \epsilon_v = 1/50 \text{ radian}$$

$$\text{s.d. of } S_{B2} = 5\% \text{ of } S_{B2}$$

Then, from the perturbed error equation, we get

$$\begin{vmatrix} \Delta S_E(K) \\ \Delta S_N(K) \\ \Delta S_V(K) \end{vmatrix} = \begin{vmatrix} \Delta S_{B2}(K) \\ - S_{B2}(K) \epsilon_g \\ - S_{B2}(K) \epsilon_v \cos \omega \end{vmatrix}$$

where the interger K denotes the Kth measurement of the distance. If we can claim that with a total of n measurements in equal time intervals, the associated measurement errors in different time intervals are uncorrelated, then the mean square position errors at the end of the 2000-meter trip are apparently*

$$\sum_{k=1}^n \begin{vmatrix} E [\Delta S_E^2(K)] \\ E [\Delta S_N^2(K)] \\ E [\Delta S_V^2(K)] \end{vmatrix} = \sum_{k=1}^n \begin{vmatrix} \text{Var} [\Delta S_{B2}(K)] \\ S_{B2}^2(K) \text{Var} (\epsilon_g) \\ \frac{1}{2} S_{B2}^2(K) \text{Var} (\epsilon_v) \end{vmatrix}$$

*Note that in this example S_{B2} is equal to 2000 meters divided by the total interval n.

$$= \left| \begin{array}{l} 0.05 \times \frac{2000}{n} \\ \left(\frac{2000}{n} \right)^2 \left(\frac{1}{50} \right)^2 \\ \frac{1}{2} \left(\frac{2000}{n} \right)^2 \left(\frac{1}{50} \right)^2 \end{array} \right| = \left| \begin{array}{l} \left(\frac{100}{n} \right)^2 \\ \left(\frac{40}{n} \right)^2 \\ \frac{1}{2} \left(\frac{40}{n} \right)^2 \end{array} \right| \text{ meter}^2$$

Note that the result is valid only for the particular number n . For example, if $n = 100$, the root mean square errors at the end of the trip are 10, 4, 2.8 (meters) in E, N and L.V. directions respectively. For larger n , the errors in different intervals are correlated, thus cross product terms should be added to the above result which we will not elaborate here. Instead, let's consider the problems associated with making n as large as practical so that the accumulated error will be small. It can be seen that the main cause of error correlation in our system is mechanical response time, specifically the response of the platform. For example, if the platform is initially tilted in some direction (some specific values of ξ_v and ω), it will remain tilted so that its mean direction in the near future is in approximately the same direction as its original orientation due to its inertia. Hence within some short time interval the noise cannot be considered as white. Therefore, finding a large n is equivalent to building a platform which is light in weight and with a small time constant of response. It is then understood that to divide the platform system into a pilot platform and load platform might be an attractive alternative.

The main conclusions that can be drawn thus far are summarized below.

It has been shown that a non-inertial reference frame is feasible for surface navigation. The reference frame aligns its axes with the local vertical, local north and local east. With this set of coordinates a dead reckoning type of navigation can be used utilizing distance measurements obtainable from the rover wheel variant. An error analysis of this system has been made with the recommendation that the surface navigation system be periodically re-initiated because its error grows with distance traveled.

The future work in the area of surface navigation will concern itself with landmark navigation and, in particular, with stereoscopic maps of the surface.

Task C.1.c. Preliminary Design of An Automatic Device for the Location of the Pole Star and/or True Pole of Mars
Faculty Advisor: Prof. C. N. Shen

For surface navigation of an unmanned vehicle on the planet Mars, the location of the Martian pole star can be used to help generate the needed reference frames. Since an unmanned vehicle's initial surface orientation is unknown, there would be some

difficulty in locating the pole star. The object of this task is to design an automatic system for the unmanned vehicle whose purpose is to locate the pole star of Mars and to supply this information to the navigational equipment.

The automatic system operates on the concept that if a unique group of stars can be found in the heavens, a geometrical relationship can be derived from this group that allows the generation of the location of the pole star. This is accomplished through the use of a pattern recognition system. The system designed in this project operates on this principle and will locate the pole star and/or any point in the heavens desired. The pole star location generated by the system is more than accurate enough for most navigational needs.

- (1) Identification of the Pole Star and the approach for its location. The determination of celestial coordinates of the pole of Mars and the mathematical approach to location of pole star and/or true pole of Mars has been described in References 15 and 25.
- (2) Description of basic star locating/tracking device. The basic device for locating and then tracking a binary reference star is illustrated in Fig. 35.

(a) Telephoto lens -- The telephoto lens is used to gather light from all stars in a specific angular field of view (about 20°), determined by the lens construction, and to direct it into a small focal plane. Instead of picking up all objects in its field of view with equal intensity, as is common in telephoto lenses, this lens is constructed in such a manner that a star in the center of its field will be picked up as a slightly greater intensity image than a star of equal magnitude on the edge of its field. The reason for this will be explained later.

(b) Collimator -- The collimator takes the light emerging from the telephoto lens and forms it into a tightly collimated light beam.

(c) Prism -- Upon leaving the collimator, the light beam encounters a prism made of dense flint glass, forming a right angle with the prism face first met. Upon leaving the prism, the light beam diverges as an immediate result of the variation of the refractive index of the optical glass with wavelength. There will be an approximate angular separation of 1.65° degrees between the two extremes in the visible spectra.

(d) Mirrored optical path -- To obtain a distance of separation of about two centimeters between the two extreme wavelengths, an optical pathlength of about 0.7 meters is required. This is accomplished through the use of a mirrored box, into which the emerging beam from the prism enters. Inside the box, the diverging beams of light

BASIC STAR LOCATOR

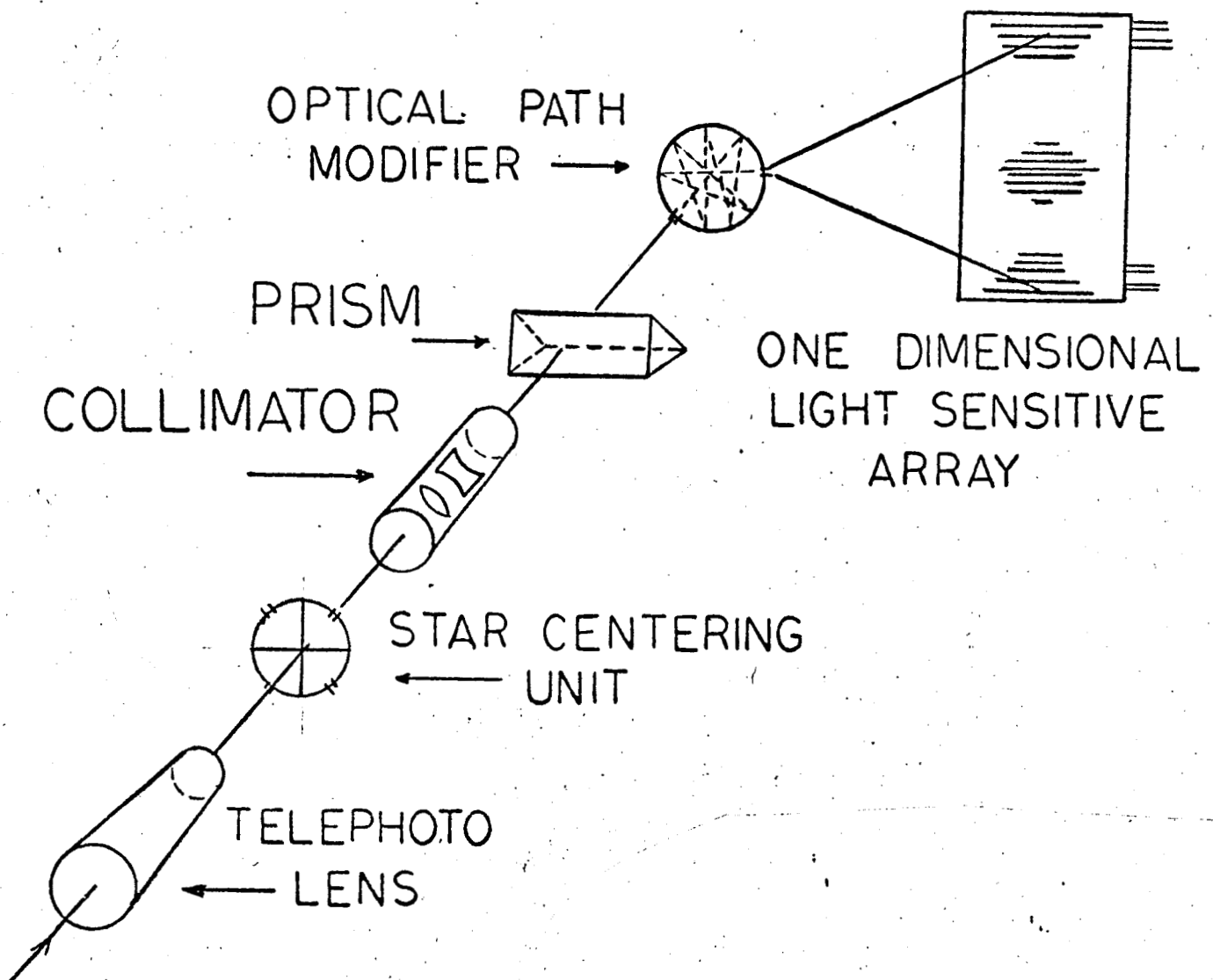


Figure 35.

are reflected along an optical path of the desired length and at the end of this path they leave the box and fall upon a one dimensional array of light sensitive devices. Thus a high intensity light beam has been dispersed along a light sensitive array giving a distribution of light intensity related to the distribution of wavelength in the original beam, at a cost of having less light intensity per unit area than the original beam (though the total light intensity is constant).

(e) Photo-detector --

1. Background material. The time rate of light energy is referred to as luminous flux. The luminous flux is the characteristic of radiant energy which produces visual sensation. The unit of flux is the lumen, which is the flux emitted in a unit solid angle by a uniform point source of one candela, which produces a total luminous flux of 4 lumens, Reference 21.

In measuring stellar magnitudes photoelectrically, the flux in lumens L from a star of magnitude M which is received by a telescope having a diameter of d inches can be expressed as follows:

$$2.5 \log_{10}(L) = 7.57 - 30 + 5 \log_{10}(d) - M$$

For a telescope with a diameter of five inches and a star of magnitude three, $L = 1.68 \times 10^{-9}$ lumens, Reference 21.

2. Comparison of Photo-Detectors. To find a photo-detector which would perform satisfactorily with this magnitude of luminous flux, a study of photodetectors was performed. The approximate range of power or luminous flux for which various types of detectors are useful is given in Reference 22.

3. Limitations on Desired Photo-Detector. As a result of this study, it was decided to use silicon photojunction cells. Assuming an 8% loss of intensity in the telephoto lens, 4% in the collimator, 2% in the mirrored unit and 1% in the prism, the photojunction cells are still capable of handling the job. A silicon photodiode is basically a p-n junction, exhibiting a nonohmic characteristic. Reverse biasing the cell, it operates as a photoconductive device and its output is developed across a series load resistor. In photo-voltaic applications, the cell is used to convert radiant power directly into electrical power. Due to its greater sensitivity, the photoconductive mode of operation will be used, References 21, 22 and 23.

After a discussion with staff members in the Electrophysics Department at R.P.I., it was decided that if there was no need to worry about impulses of light and

the resulting transients, i.e., the star is viewed for 1 msec or more, and the device is operated at a low current level, a one dimensional array of diodes may be fabricated having a diode width of approximately .2 mil/unit. Thus a one dimensional array that is two centimeters long could contain, if desired, approximately four thousand units, with the leads coming in from above and below the array.

Assuming that an array of photojunction cells may be fabricated to operate at a level of 10^{-12} lumens, the number of elements in the array is limited by the minimum amount of light required by one unit. Using the assumed losses in the optical devices,

$$\frac{(1.68 \times 10^{-9}) \times .92 \times .96 \times .98 \times .99 \text{ lumens}}{10^{-12} \text{ lumens/unit}} = 1450 \text{ units}$$

the limit would thus be a 1450 unit array. Since there is a spread of approximately three thousand angstroms over the range of interest, the number of units in the array is arbitrarily chosen as five hundred.

4. Operation of Photo-Detector. For a first check on the identity of the observed star, the outputs of all the array elements are summed and this sum is related to the star's magnitude. If too low a magnitude is indicated, the star is rejected and the device will begin scanning for another star. If the magnitude is great enough, the output from each array element is compared against predetermined standards corresponding to each of the desired reference stars dispersed spectra. If the observed spectra does not correspond to one of the preprogrammed spectra, the star is rejected and the device will begin scanning for another star. If the spectra does correspond to that of one of the binary reference stars, a digital signal identifying the star will be generated and a signal will be sent the star tracker unit to maintain the location of this star.

(f) Positioning device for tracking of reference stars -- The star tracking unit, upon receiving the track signal will move into place between the telephoto lens and the collimator. It will proceed to position the star at the optical center of the telephoto lens, the point where the effective intensity of the star will be the greatest (due to the construction of the lens). This will be accomplished through the use of a segmented, light sensitive disk (CdS). Constructed of four identical wedgeshaped segments, the output of each segment is related to the intensity of light incident upon it. Through the use of a servo-mechanism system, the direction of the telescopic lens is adjusted to give equal outputs from all segments corresponding to equal light intensities on all four segments. This occurs when the star is exactly centered in the device.

(3) Location of Pole Star.

(a) Location of second reference star -- Once the first reference star is located, a modified sweep path will be used to locate the second reference star. A second unit, identical with the first one just described will be positioned at an angle, with respect to the first unit, equal to the angular separation between the already located (now known) reference star and one of the other two reference stars. The second unit will sweep a constant radius circular path around the first unit. If the second reference star is located and identified, the second unit will track it and thus maintain its location. If it is not found, the angle of the first unit, with respect to the second unit, will be changed to equal the angular separation between the already found reference star and the remaining reference star. The modified sweep path will again be used, now locating and identifying the second reference star.

(b) Generation of the location of the Pole Star and/or true Pole from locations of reference stars -- Having located and identified two reference stars, it is necessary to use them to locate either the pole star or the point in the heavens over the true pole. The two star locating units are mounted on a platform on the roving vehicle. They are gimballed to move in two directions only, one direction being parallel to and the other being in a plane perpendicular to the surface of the platform. A fictitious reference frame, xyz, is established on the platform.

In the star charts, the right ascension and declination of a star is measured with respect to a specific vernal equinox, Reference 24. Since this is a relative measurement, the right ascension and declination of the reference stars can be measured with respect to the point in the sky where the fictitious y axis is directed towards at a specific time. If this is done, the angular measurement of the gimbal in the xy plane corresponds to the right ascension and the angular measurement of the remaining gimbal corresponds to the declination of the reference star in terms of this fictitious frame. Knowing the right ascensions and declinations of the two reference stars in this fictitious reference frame, it is possible to compute the right ascension and declination of the pole star, (or point in the heavens) with respect to this frame. Since the rest of the navigation package is also located on this platform, this gives to it the needed location of the pole star.

(c) Pole Star location error -- Errors in the location of the two binary reference stars will result in an error in the generated location of the pole star and/or true pole. Considering the fabrication techniques of today, the reference stars should be located by the locating/tracking device to

less than 0.1 degrees of their correct locations. Introducing these errors will result in the generation of a pole star location that should be well within the tolerances for most navigational needs, Reference 25.

- (4) Conclusion. The navigational approach to locating the pole star and/or true pole using binary reference stars is feasible, generating the pole star location exactly if the reference star locations are exact and not generating unreasonable errors in the pole star location for small errors in the reference star locations. The pattern recognition system is shown in the body of this report to be capable of operating on the light intensity emitted by the reference stars. Once the reference star is located, the method for maintaining its location and generating its coordinates in the vehicle reference frame is easily applied with a high degree of accuracy, being limited by fabrication techniques.

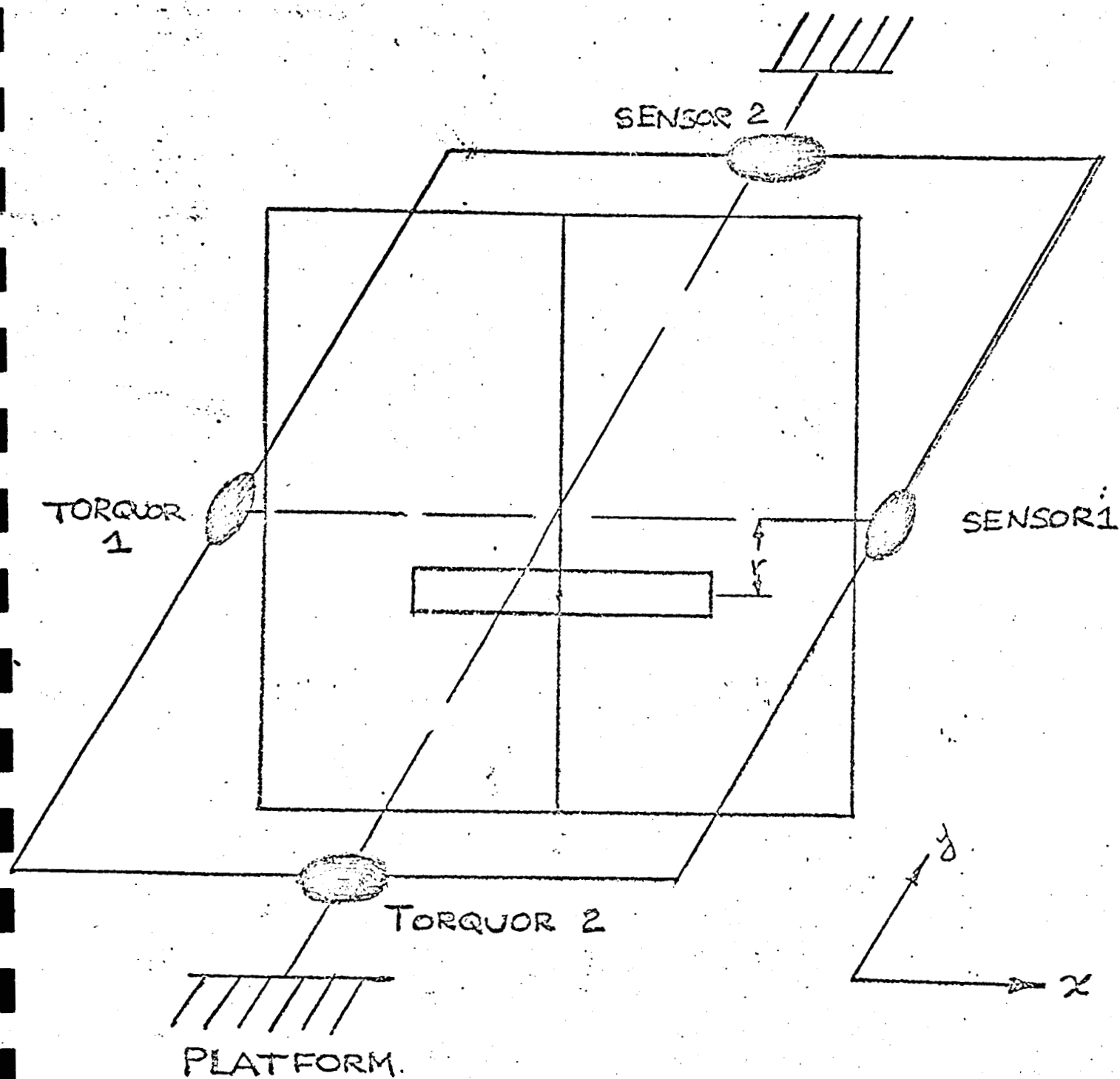
Looking at the total system, a pole star location error of less than one tenth (0.1) of a degree should be entirely feasible if care is taken in the construction of the system and if the platform on which it is mounted is kept reasonably stable with respect to the Martian surface.

Task C.1.d. Local Vertical Sensor -- Mark Rodamaker
Faculty Advisor: Prof. C. N. Shen

One of the requirements of the vehicle navigation system described under Task C.1.b. is a subsystem capable of defining the local vertical. The objective was to design an accurate, disturbance insensitive, and physically realizable device. The gyro pendulum, shown in Figure 36, was chosen because it could be tuned to produce very small errors even when large inputs of velocity, acceleration and jerk (i.e. acceleration of acceleration) were to be encountered.

The final design calls for a thin disk rotor of radius 2 cm. spinning at 188,000 rpm with a c.g. to gimbal axis offset (r) of 0.0535 cm. If a value of $3.66 \frac{m}{sec^2}$ is assumed for the martian gravitational acceleration, then these parameters predict a natural precessional frequency, ω_g , of $10^{-3} \frac{radians}{sec}$.

The analytic equations of a gyro pendulum, (eqns. (2) and (3) of References 15, 26 may be expressed in terms of ω_g and the inputs if $\omega_g = \frac{mgr}{H}$, where m is the mass of the rotor, g is the Martian gravitation, r is the offset and H is the angular momentum of the rotor. The inputs are the velocity, acceleration and jerk components in the horizontal plane. If these inputs can be found or approximated, then the performance of the gyro pendulum is specified. Since the true inputs which are related to the vehicle's velocity and suspension system and the terrain are mainly unknown quantities at this time, it was necessary to estimate the inputs based on an approximate vehicle vibration technique. By September of 1971, however, better values may be available as the RPI MRV vehicle dynamic simulation



THE GYRO PENDULUM

Figure 36.

analysis is presently underway. At the present time, the following maximum values were chosen:

$$V_{\max} = .445 \text{ m/sec}$$

$$a_{\max} = 8 \text{ m/sec}^2$$

$$\text{jerk}_{\max} = 144 \text{ m/sec}^3$$

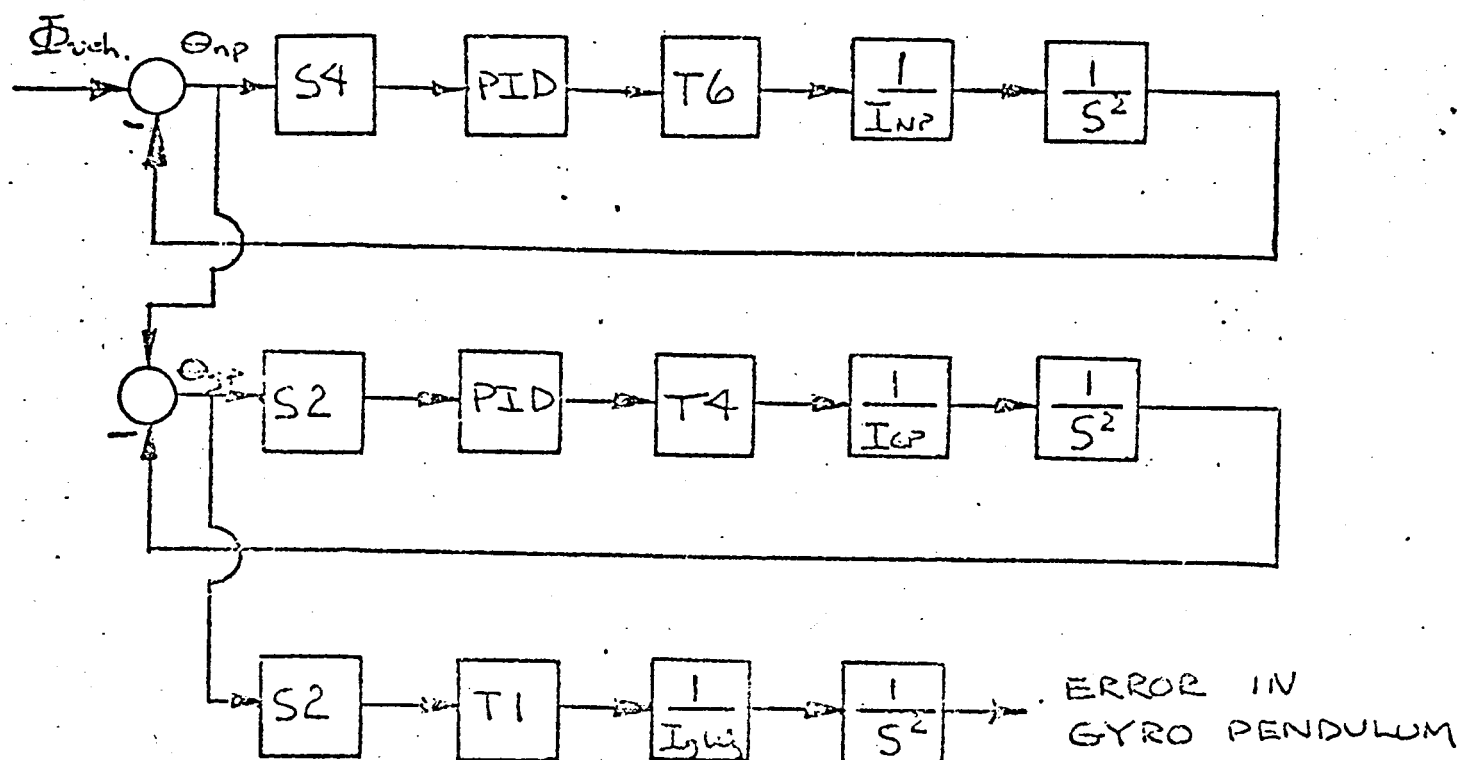
These inputs were assumed to be impulsive to permit a reasonable solution of the analytical equations. Furthermore, the impulse mode represents a worst case. With these estimates a maximum error of 1.39° is predicted if $\omega_g = 10^{-3} \frac{\text{radians}}{\text{sec}}$.

Almost all of this error was due to the jerk term. This term is probably the least accurate of the input terms which is unfortunate. In actual operation, errors would probably be less than 0.1° due mainly to the fact that a positive jerk must be followed by a nearly identical negative jerk and vice versa with a quite short time interval between them. The net response is the sum of the two responses which should be very small compared to the maximum amplitude of one response by itself. This is very low disturbance sensitivity and appears to satisfy the objective of the preliminary design.

Once a preliminary local vertical sensor was fixed, work was extended into the area of platform design since the task of providing a local vertical was only a subtask to providing a vertical platform for the navigation package. Time was too short for an analysis of the entire system, but conceptual plans were made which should point the way for future work.

One outcome of this brief investigation is that it would be desirable if a platform within a platform could be constructed. This arrangement isolates the gyro pendulum from the gross rotations of the vehicle if the gyro pendulum is mounted on the inner platform. As shown in Figure 37, the input to the gyro platform is the error in the navigating platform which should be much smaller than the rotation of the vehicle. Also, the input to the gyro pendulum is only the error in the gyro platform which is due to the previously reduced input from the navigation platform. In addition, there are many adjustable parameters in the system which should allow high degree of accuracy when the system is finally built. The entire system is shown in Figure 38 to demonstrate one way of arranging the components.

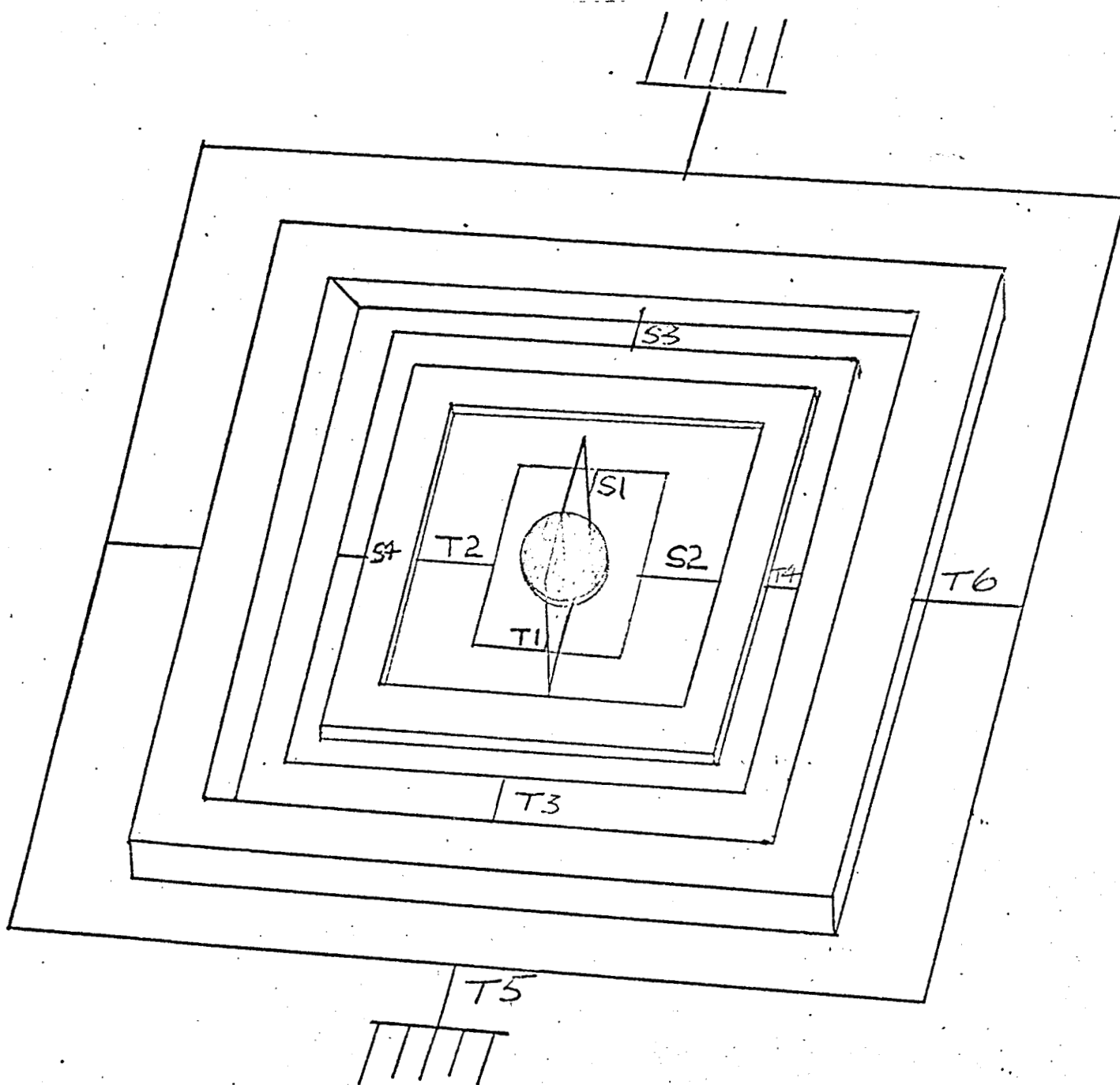
In conclusion the task of designing a local vertical indicating device has been accomplished. The resulting design appears feasible to construct and highly accurate in operation. Further refinement of system accuracy and parameters may be possible when the operating environment is better defined. Eventually, this device must be constructed and all the physical problems inherent in meeting the



- $S 4$ = Sensor 4 etc.
 $T 6$ = Torquor 6 etc.
 PID = Proportional plus Integral plus Derivatives
 Inp = Moment of inertia of navigation platform
 $\frac{1}{S^2}$ = $\int \int dt^2$
 I_{GP} = Moment of inertia of gyro platform
 I_g = Moment of inertia of gyro pendulum
 ω_g = Spin angular velocity of gyro pendulum

SINGLE AXIS BLOCK DIAGRAM OF COMBINED SYSTEM

Figure 37.



THE COMBINED GYRO PENDULUM-PLATFORM SYSTEM

Figure 38.

specifications must be solved. This actual physical construction along with continued platform study should comprise the majority of future work on this task.

Task C.2. Terrain Modeling and Path Selection - A. M. Rautio, C. Pavarini
Faculty Advisor: Prof. S. Yerazunis

It is desired that, once landed, the vehicle be able to proceed autonomously from the landing site to predetermined locations on the martian surface. This objective requires the development of a system by which the vehicle will be able to sense the terrain in the direction of travel and to choose a safe path toward a distant objective.

Past work in this task area has produced a terrain modeling system and path selection algorithm involving an ideal, discrete, line-of-sight electromagnetic sensor, Ref. 27.

Beyond this point the following objectives were defined:

- (1) Determination of the effect of given amounts of sensor error upon the range data and subsequently on the vehicle's conception of the unknown terrain.
- (2) Evaluation of the error sensitivity of the path selection algorithms so as to produce quantitative measures of value whereby future alternative path selection algorithms can be compared. The fact that choosing the "best" path is no longer a deterministic matter when range information is obtained by an inaccurate sensor is of prime importance in this phase of the study.
- (3) Once the implications of phases (1) and (2) have been drawn and studied, the generation of sensor parameter requirements necessary in order to sufficiently describe an unknown terrain can be undertaken.

During the first half of the year, primary emphasis was directed to the first of these objectives. At this time, the criticality of short range terrain sensing was recognized and the priority of effort was turned to this task, postponing effort on the second and third objectives defined above.

Effect of Sensor Errors on Long Range Terrain Modeling

The effect of sensor error on long range terrain interpretation has been described in detail in Ref. 28.

In brief, azimuthal angle sensor errors were determined to be minor and emphasis was directed primarily to the evaluation of elevation angle errors.

Initial work revealed that elevation angle errors give rise to errors in range data whose magnitude is dependent upon:

- (1) The amount of elevation angle error.
- (2) The terrain being modeled.

Since a deterministic numerical analysis was impossible due to the dependence of the resulting gradient errors upon the type of terrain being modeled, a computer program which simulated the vehicle's data acquisition and terrain modeling system was written. Two programs were constructed, their difference being the method by which the actual terrain could be inputted into the simulation. Their description follows:

- (1) Continuously defined terrain - The surface is introduced in the form of a combination of gaussian hills and inclined planes. This program enables one to compare the ranging and gradient data obtained with an ideal sensor, an imperfect sensor, and actual terrain slopes and gradients.
- (2) Point-wise defined terrain - This program makes use of a terrain model which can be generated through a contour map on which the sensor location is chosen and azimuth lines are drawn. The intersection of the azimuth lines and contour lines are inputted into the simulation in terms of distances from the sensor and elevations relative to the sensor. Consequently, the terrain is composed of a set of connecting polygons whose intersections with sensor beams can be computed exactly.

Both programs enabled the user to introduce sensor inaccuracies in the form of elevation angle alignment error and imperfect range determination. The elevation angle error was modeled by a normal distribution of error about the correct angle. This was believed to be a realistic simulation of the inaccuracies of an actual servo-mechanism, namely, (1) a D.C. or bias error which can be accounted for, (2) a known distribution of error and (3) a completely random error. In the case of the ranging error, also modeled by a normal distribution about the correct value, the standard deviation of the error was made proportional to the range itself, therefore simulating the deterioration of accuracy with increasing distance from the sensor.

It was concluded that by dividing a terrain into its principle components and studying the effect of sensor errors on each, an idea of the inaccuracy present in the complete model of an unknown terrain could be generated. Hence, the study was initiated on the simplest of all terrains, the horizontal plane. The computer simulation was run for a sensor height of 10 feet and a maximum range capability of 1500 ft. Nine azimuth lines were used (scan of 40 degrees) with an elevation scan of .03 radians (-.0325 to -.0025 radians measured from the horizontal). Using an elevation increment of .0025 radians, five runs were made with the standard deviation of the normally distributed elevation angle error taking on values of 5%, 10%, 20%, 30%, 40% and 50% of the increment angle.

The deviations of the resulting gradient calculations were tabulated and the mean error and standard deviation about zero were computed, Table 7.

The inability to affix to the resulting errors in the gradient determination any known distribution envelope presented a major difficulty. It was concluded that only general trends could be deduced from these simulations since an accurate prediction of resulting gradient errors would entail considerably more simulation and computation time. Such a commitment does not appear advisable at this time and an alternate approach appears to have more potential. As an alternative the modeling of the elevation angle error was changed to a "chopped" normal distribution, whereby it was assumed that all errors would fall between ± 2 standard deviations from the correct value.

This assumption, by establishing upper and lower bounds on the error, enabled worst case gradient errors to be evaluated for the case of a flat terrain. A worst case terrain was constructed utilizing the extreme values. As can be seen in Figure 39 either a positive or negative maximum of the in-path slope error could be achieved. A worst case azimuth was then concluded as being a jagged surface of alternating positive and negative in-path slopes. In the cross-path slope calculation, the worst case results when both adjacent azimuths are mirror images of the azimuth along which the gradient calculations are being computed. Further investigation proved that the worst case cross-path slope was identical when either of the two corresponding points on the adjacent azimuth were used in the calculations.

Having generated a worst case terrain model, the extreme values utilized were then substituted back into the gradient equations, and the assumption was made that the small angle approximations were valid. Worst case approximations for the positive and negative in-path slopes and their corresponding cross-path slopes and gradients were then generated as functions of β_2 , the elevation angle of the point whose gradient is being calculated, $\Delta\beta$, the elevation angle increment, and σ , the standard deviation of the normally distributed elevation angle error, Table 8.

Upon investigation the following conclusions were made for the case of a flat terrain:

- (1) The in-path slope error is linearly dependent upon β_2 , increasing as β_2 becomes more negative, that is, as the data point in question moves closer to the vehicle.
- (2) The cross-path slope error is constant with respect to β_2 .
- (3) As a result of (1) and (2), the gradient error is an increasing function of β_2 (in the negative direction).
- (4) Upon the plotting of the magnitude of gradient error with various elevation angle increments and standard deviations, it was noted that for a given σ the gradient error increases as the elevation angle increment is decreased, that is, when the scanning mesh is tightened.

TABLE 7

GRADIENT ERROR ANALYSES AS A FUNCTION OF SENSOR (ELEVATION ANGLE) ERROR

Gradient Error Analysis - Flat Plane

Normally distributed elevation angle alignment error

Elevation angle increment ($\Delta\beta$) = .0025 radians

σ (rad.)	% $\Delta\beta$	mean error (degrees)	S.D. about zero error (degrees)	# of samples
.000125	5	.139	.159	140
.0025	10	.260	.298	140
.0005	20	.708	2.67	138
.00075	30	1.16	2.24	132
.0010	40	1.36	2.04	138
.00125	50	4.05	9.63	140

Revised Gradient Error Analysis

Gradient values greater than 3 S.D. discarded

					Discarded Values
.0005	20	.397	.497	136	22.2
					21.25
.00075	30	.863	1.187	128	9.4
					10.3
					12.0
					12.0
.001	40	1.13	1.46	133	6.5
					6.6
					6.3
					9.1
					9.0
.00125	50	2.85	5.57	136	57.8
					56.2
					31.7
					34.97

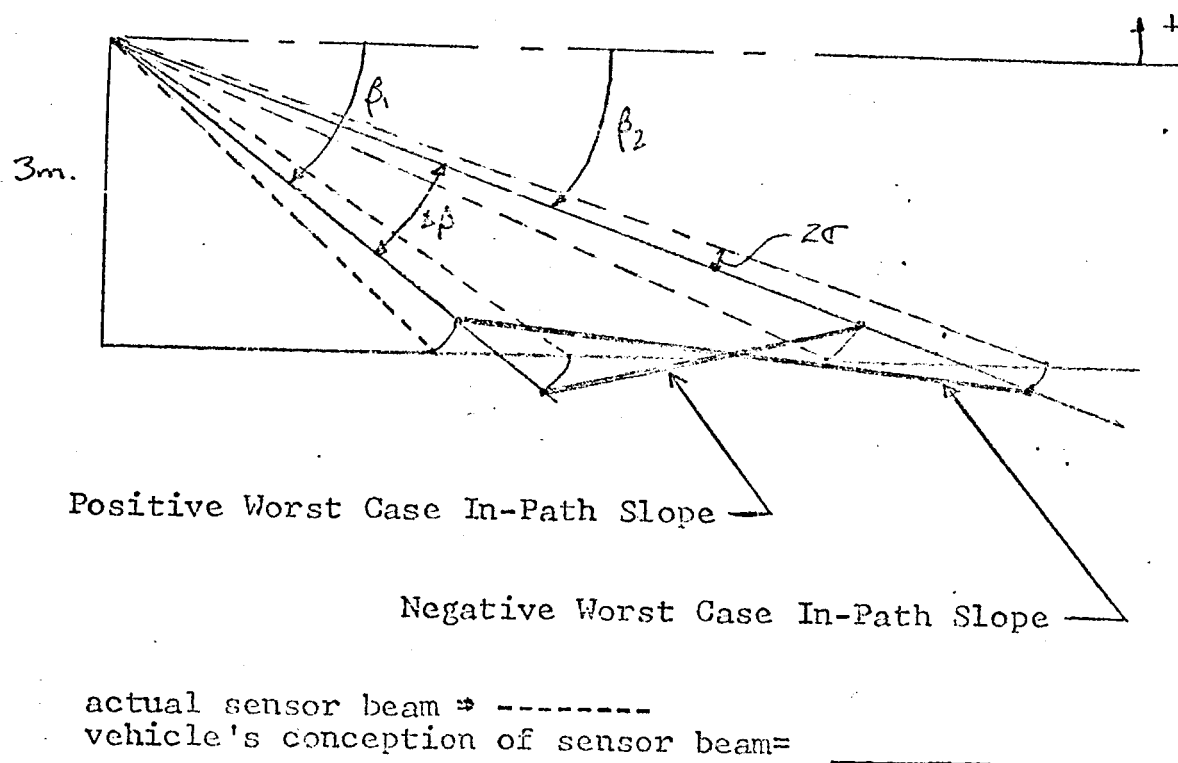


FIGURE 39
WORST CASE TERRAIN GRADIENT INTERPREATION

TABLE 8

Worst-Case Approximations
of Gradient Errors
(Flat Terrain)

Positive Extreme-

$$\text{In - Path Slope (SI)} = \frac{2\sigma(2\beta_2 - \Delta\beta)}{4\sigma - \Delta\beta}$$

$$\text{Cross-Path Slope (SC)} = \frac{(SI - 2\sigma)\Delta\beta}{\Delta\theta(\beta_2 - 2\sigma)}$$

Negative Extreme-

$$\text{In-Path Slope (SI)} = \frac{(2\sigma)(\beta_2 - \Delta\beta)}{4\sigma + \Delta\beta}$$

$$\text{Cross-Path Slope (SC)} = \frac{\Delta\beta(2\sigma + SI)}{\Delta\theta(\beta_2 + 2\sigma)}$$

$$\text{Gradient} = \sqrt{(SI)^2 + (SC)^2}$$

Work to this point has been confined to the analysis of elevation angle alignment error when modeling a horizontal flat terrain. Although this terrain would appear to be idealistically simple, it does represent a case of considerable modeling difficulty. Planes which slope toward the sensor (upgrades) will incur less error in the gradient calculations than the flat plane case. This is due to the fact that, for a constant range of error about the correct elevation angle, resulting range differences between the extreme cases of maximum error decrease as the slope of the plane is increased. Conversely, down-grades represent terrains on which error will result in even greater misinterpretation than in the case of the flat terrain.

Imperfect ranging does not induce errors which are dependent upon the terrain itself as in the elevation angle case. Ranging error is, however, dependent upon the resolution of the laser beam, which is in fact a function of the physical characteristics of the terrain. The simulation of this dependence was not attempted in this study. Therefore, it can be concluded that if the range capabilities of the sensor decay linearly with distance from the sensor, the resulting error in gradient calculations are analogous in form to those determined in the analysis of the elevation angle alignment error. However, if it is considered that the range determination accuracy is relatively constant within a given range, then the decay of gradient information is more rapid as sensor readings are taken closer to the vehicle.

Short Range Terrain Modeling

The ability of an autonomous roving vehicle to pursue an exploration of the planet Mars depends on the development of an effective short range terrain modeling system applicable in the range of 3 to 30 meters from the vehicle. Such a system which would search for obstacles and other hazards would have to be compatible with the long range terrain modeling and path selection system.

Although it had been hoped that a system analogous to the long range system described above might be effective, the following deficiencies were noted:

1. The system was overly sensitive to both elevation angle and ranging errors at short distances.
2. The gradient outputs were inaccurate and of little value since for a fixed elevation angle increment, the data points were separated by fractions of meters.

While some of the deficiency could be eliminated by adjusting the elevation angle increment, it had the disadvantage of reducing the amount of terrain information gathered. As an alternative, it was decided that a new approach to define the character of the terrain would be more fruitful.

The obstacles to be considered include:

1. Obtrusions -- involving critical clearances such as boulders and steps.

2. Depressions -- involving excessive slopes, crevices.
3. Slopes -- involving gradients exceeding vehicle climbing ability or stability limits.
4. Soil characteristics -- a hazard which cannot be detected by a sensor such as a laser rangefinder.

The original terrain modeling system concentrated on the detection of slopes. In the short range case, the system must be able to detect obtrusions, depressions as well as unacceptable slopes. For the purposes of this study, obstacle criteria were based on the MRV described under Task A. A maximum step of 0.5 meters and a maximum crevice width of 1 meter were assumed. The question of slope determination has been deferred for later consideration.

The rationale behind the proposed scheme is to determine the relationship between sequential range measurements and their interpretation as to the existence of an obstacle.

To detect the existence of a step obstacle, at least two beams must strike the step with the next beam touching the upper edge of the step as a minimum, Figure 40. With this as a criterion and assuming level terrain and a three meter sensor height, an elevation angle increment not greater than 0.008 radian must be employed.

A similar logic is applied to the crevice problem where successive range points can be separated by a distance which does not exceed the vehicle's crevice crossing capability. For the one meter assumptions made above, a maximum elevation angle increment of 0.0034 radian is required. The significance of this approach to the problem is that the successive data points define bounds on the terrain which may conceivably exist as shown on Figures 41 and 42. A terrain modeling scheme based on this concept would have to interpret sequential range measurements as potential obstacles and to penalize a potential path accordingly.

In addition to the detection of the potential obtrusion and depression, it is necessary that some estimate of the general slope of the terrain on which these obstacles are located be obtained. As of this writing it is proposed that a slope determination scheme based on a scale large compared to the obstacles per se (perhaps the order of magnitude of the vehicle) may be effective.

It is proposed in Ref. 28 that the following short range system be investigated. Consider each azimuth line separately and obtain range data in terms of elevation which are subsequently converted into altitudes and distances with respect to the vehicle position. Range distances between successive data points are computed. Assuming worst case vertical steps, comparison is made with the step climbing ability of the vehicle. A comparable test is made for separation distance with a penalty to be incurred if maximum crevice width is exceeded. Following these calculations, an estimate of the general slope of the terrain would be obtained to be used as a reference by which the corresponding altitudes and separations for the real terrain can be calculated. This calculation would reflect the fact that a simple altitude or separation may or may not be an obstacle depending on whether the terrain is generally sloping upward or downward.

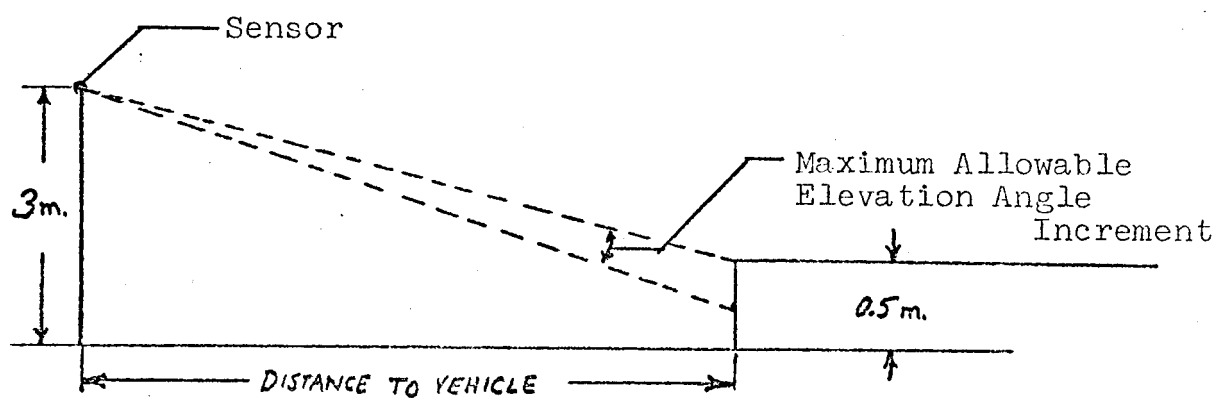


Figure 40: Vehicle Step Perception

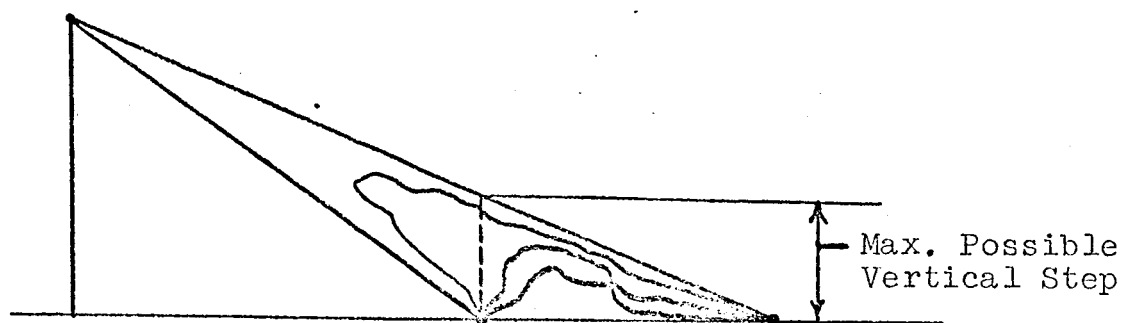


Figure 41. Possible Positive Terrain Configurations

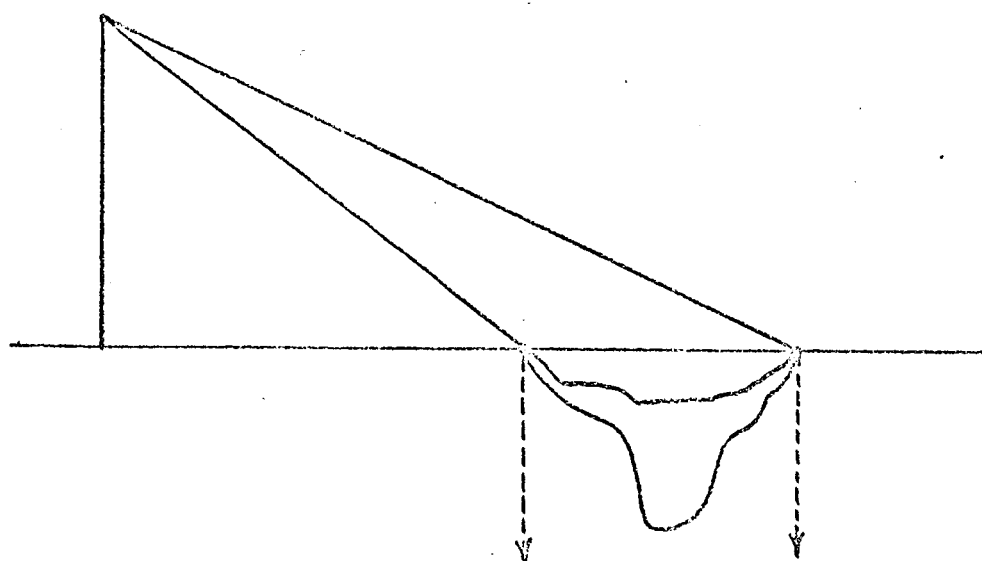


Figure 42: Possible Negative Terrain Configurations

This information would have to be combined with an appropriate decision rule by which the necessary safety-energy-distance tradeoffs can be made between alternative paths.

As future work, it is intended to refine this short range terrain modeling system and to assess the effect of sensor error on the reliability of the system to interpret the terrain. Beyond this point, the system would have to be joined with the long range terrain modeling concept so that simulations of path trajectories over a variety of terrains with alternative path selection decision making alternatives can be conducted. The ultimate objective is to define a terrain sensing and modeling system and a path selection algorithm for an autonomous roving vehicle. Such a design should include specification of devices, their error limitations and the consequences of alternative error limitation specifications.

Task D. Chromatographic Systems Analysis

One important phase of the initial missions to Mars is the search for organic matter and living organisms on the martian surface. The present concept for attaining this objective consists of chemically treating samples of the atmosphere and surface matter and thereafter analyzing the resulting products in a combination gas chromatograph/mass spectrometer. It is the objective of this task to generate fundamental engineering design techniques and concepts for use in optimizing the design of the chromatographic separating system.

Because of the complexity of the system and the number of independent parameters, a system analysis based on the mathematical simulation of the chromatograph is being undertaken. This technique uses mathematical models, which incorporate fundamental parameters, to explore various concepts and to direct experimental research.

In prior work, several variations of a basic mathematical model have been discussed. This earlier work has involved numerical solutions of the system equations and various preliminary studies. In addition, the construction of an experimental test facility to verify the system equations was begun.

Currently the project involves effort in three areas:

1. Completion of the test facility.
2. Verification of the system equations using experimental data.
3. Development of reliable methods for predicting fundamental parameters of the equations.

Task D.1. Test Facility - G. L. Benoit
Faculty Advisor: Prof. P. K. Lashmet

To experimentally evaluate the mathematical models, a test facility was constructed by renovating and modifying a Perkin-Elmer, Model 154C vapor fractometer previously used in chemical kinetic studies. After preliminary experiments, the system was further modified, the final

system being shown schematically in Figure 43. The chromatograph is composed of six subsystems:

1. Carrier gas control. The flow rate of helium is regulated and metered before entering the composition detectors. A preheater coil is provided to warm the carrier gas to the chromatograph temperature. Flow rates range to about 200ml/min (STP).
2. Composition detection. Two microthermistors acting as thermal conductivity detectors are provided, one for each end of the chromatographic column. These detectors, which have time constants in the order of 0.04 second, and which are sensitive to changes in chemical composition, form the variable legs of two separate wheatstone bridges. Associated with the detectors are the detector controls and a light-beam oscillograph for recording the detector signals.
3. Column. Facilities are provided for a single chromatographic column or two columns arranged in series. The columns may be 3.2 or 6.4 mm in diameter and up to one meter in length.
4. Sample injection. Liquid samples may be injected with a microsyringe through a septum in the injection block where they are vaporized into the carrier gas stream. Gas samples may be injected either by gas syringe or through a precision mini-sampling valve.
5. Oven. The detectors, columns, and sample injection equipment are mounted within a forced circulation oven capable of maintaining constant temperatures in the range of room temperature to 225 deg C.

This task has been completed and a technical report, Reference 29, which describes the physical characteristics of the system has been issued.

Task D.2. System Model Verification - G. L. Benoit
Faculty Advisor: Prof. P. K. Lashmet

A mathematical model, composed of a system of partial differential equations, was presented earlier, Ref. 30. This task has as its objective the development of a procedure for comparing the theoretical representations with experimental data. Solutions to linearized approximations of the differential equations obtained by classical techniques were reported earlier, Ref. 31, 32. Because of their complexity, the equations were solved by assuming the sample was injected as an impulse. Preliminary experimental evidence shows this assumption is not strictly correct and prior theoretical studies, Ref. 35, have shown that deviations from an impulse input can appreciably affect the predicted results. Hence to compare the mathematical model with the data, the impulse solution is convoluted

SYSTEM FLOW DIAGRAM

92

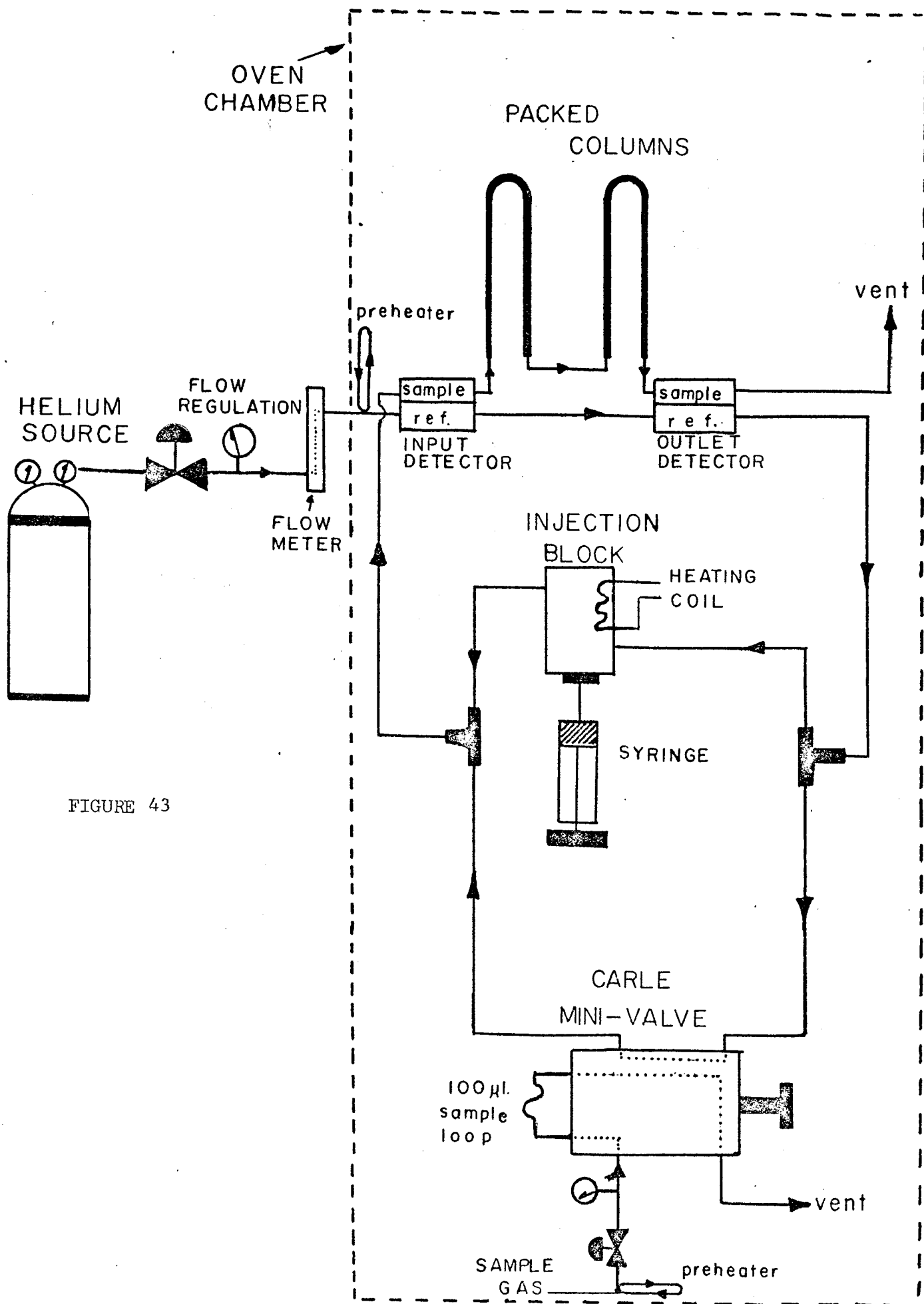


FIGURE 43

with the actual input function to provide a predicted response or chromatogram:

$$\text{Output } (\theta) = \int_0^{\theta} X(\lambda) Y(\theta - \lambda) d\lambda$$

where: θ = a dimensionless time

$Y(\theta)$ = theoretical impulse response

$X(\theta)$ = measured concentration of sample at column inlet.

Output (θ) = predicted concentration of sample at column exit.

This operation assumes system linearity which is consistent with the derivation of the impulse response.

For simplicity in developing the data reduction and comparison techniques, the equilibrium adsorption model, Ref. 31, was used in this study. This model assumes that at each point in the column, the gas phase is in equilibrium with the solid adsorbent which is equivalent to an infinitely long column. This assumption leads to a simple exponential solution to the governing equations:

$$Y(\theta) = (1/2) \sqrt{\frac{\beta Pe}{\pi \theta^3}} \exp \left[-\frac{Pe}{4\beta} (\theta - \beta)^2 / \theta \right]$$

where:

$$\beta = 1 + (1/mR_0)$$

$$\theta = \text{dimensionless time} = vt/L$$

$$v = \text{carrier gas velocity}$$

$$t = \text{time}$$

$$L = \text{column length}$$

$$Pe = \text{the Peclet number which is a dimensionless measure of sample diffusion in the carrier gas.}$$

$$mR_0 = \text{a thermodynamic parameter, peculiar to the specific chemical species and adsorbent used.}$$

The dimensionless Peclet number is predictable since it depends only upon the system configuration and fluid mechanics. The thermodynamic parameter mR_0 is specific to the system used and is determined from the system data using a curve fitting technique.

The numerical procedure which was developed has the following features:

1. Normalizes all experimental data so that the areas under the input and output chromatograms are both unity. This minimizes the effects of calibration differences between the two composition detectors.
2. Convolutes the input data with a system model which can be specified.
3. Estimates the thermodynamic parameter mR_0 by positioning the maximum point of the predicted chromatogram at the time when the maximum concentration appears in the experimental data.
4. Plots the generated curves as well as the experimental data for visual comparison.
5. Generates statistical information such as variances and means for numerical comparison.

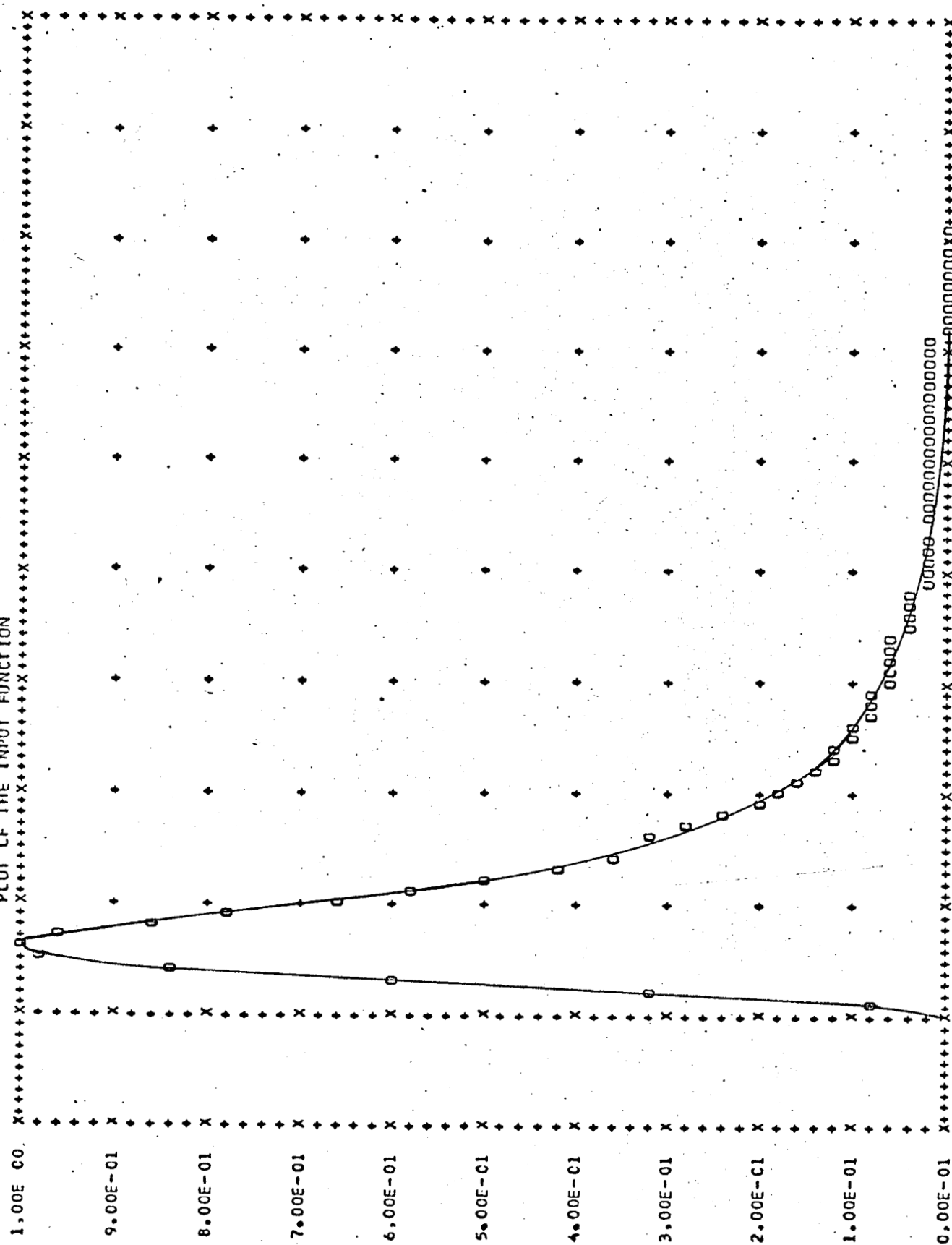
Initial studies were conducted with the following systems:

<u>Component</u>	<u>Column</u>	<u>Helium Flowrate</u>	<u>Temperature Range</u>
Isobutane	Chromasorb 102	38 ml/min	20°C
Ethylene	Chromasorb 102	38 ml/min	20°C
Nitrogen	Molecular Sieve, 5A	35 ml/min	20°C
Oxygen	Molecular Sieve, 5A	35 ml/min	20°C
Acetone	Chromasorb 102	24 ml/min	125°C
Acetone	Chromasorb 102	43 ml/min	100-200°C
Ethylene	Chromasorb 102	43 ml/min	28-175°C

The physical constants of the columns were the same: length - 1 meter; inside diameter - 2.2 mm; and particle size - 60/80 mesh (0.250/0.177 mm.). Typical results using the equilibrium adsorption model are given in Figures 44 through 49.

The input pulse for acetone, which was injected as a liquid using a microsyringe and then vaporized, is shown in Figure 44. Figure 45 compares the predicted impulse response and the convolved response with the experimental data for the column at 100°C. As the temperature is increased to 150°C, agreement between the data and the convolved response improves as seen in Figure 46. Figure 47, a magnification of Figure 46, shows the small differences between the predicted and actual performance for this system. Ethylene was injected as a gas using the sampling valve with the resultant pulse of Figure 48. Agreement between the predicted and observed performance for this system was not as satisfactory as seen in Figure 49. However, use of the input pulse and convolution shows marked improvement over use of the simple impulse response.

PLOT OF THE INPUT FUNCTION

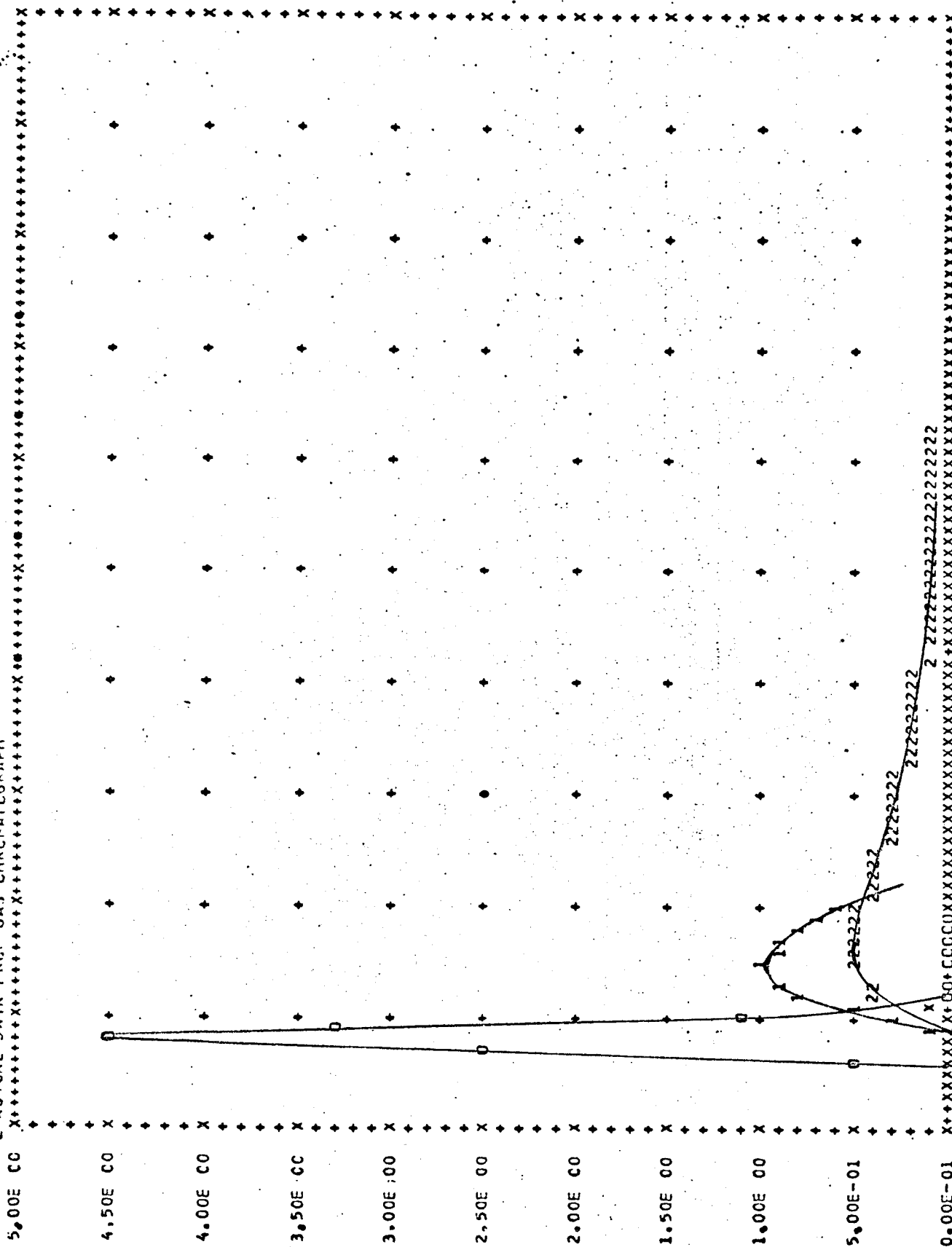


-8.00E-01 0.00E-01 8.00E-01 1.60E 00 2.40E 00 3.20E 00 4.00E 00 4.80E 00 5.60E 00 6.40E 00 7.20E 00

THIS IS A PLOT OF Y/A VS. DIMENSIONLESS TIME FOR M RO= C.223200 AND A PECLET NUMBER= 7806.000000

FIGURE 44. Injection Pulse for Acetone

PLOT OF SYSTEM RESPONSE 0=IMPULSE RESPONSE, 1= CONVOLVED RESPONSE TO INPUT FUNCTION
2=ACTUAL DATA FROM GAS CHROMATOGRAPH



4.80E 00 5.60E 00 6.40E 00 7.20E 00 8.00E 00 8.80E 00 9.60E 00 1.04E 01 1.12E 01 1.20E 01 1.28E 01

THIS IS A PLOT OF Y/A VS. DIMENSIONLESS TIME FOR M RO= 0.223200 AND A PECLET NUMBER= 7806.000000

FIGURE 45. Chromatograms for Acetone at 100°C

PLOT OF SYSTEM RESPONSE 0=IMPULSE RESPONSE, 1= CONVOLVED RESPONSE TO INPUT FUNCTION

2=ACTUAL DATA FROM GAS CHROMATOGRAPH

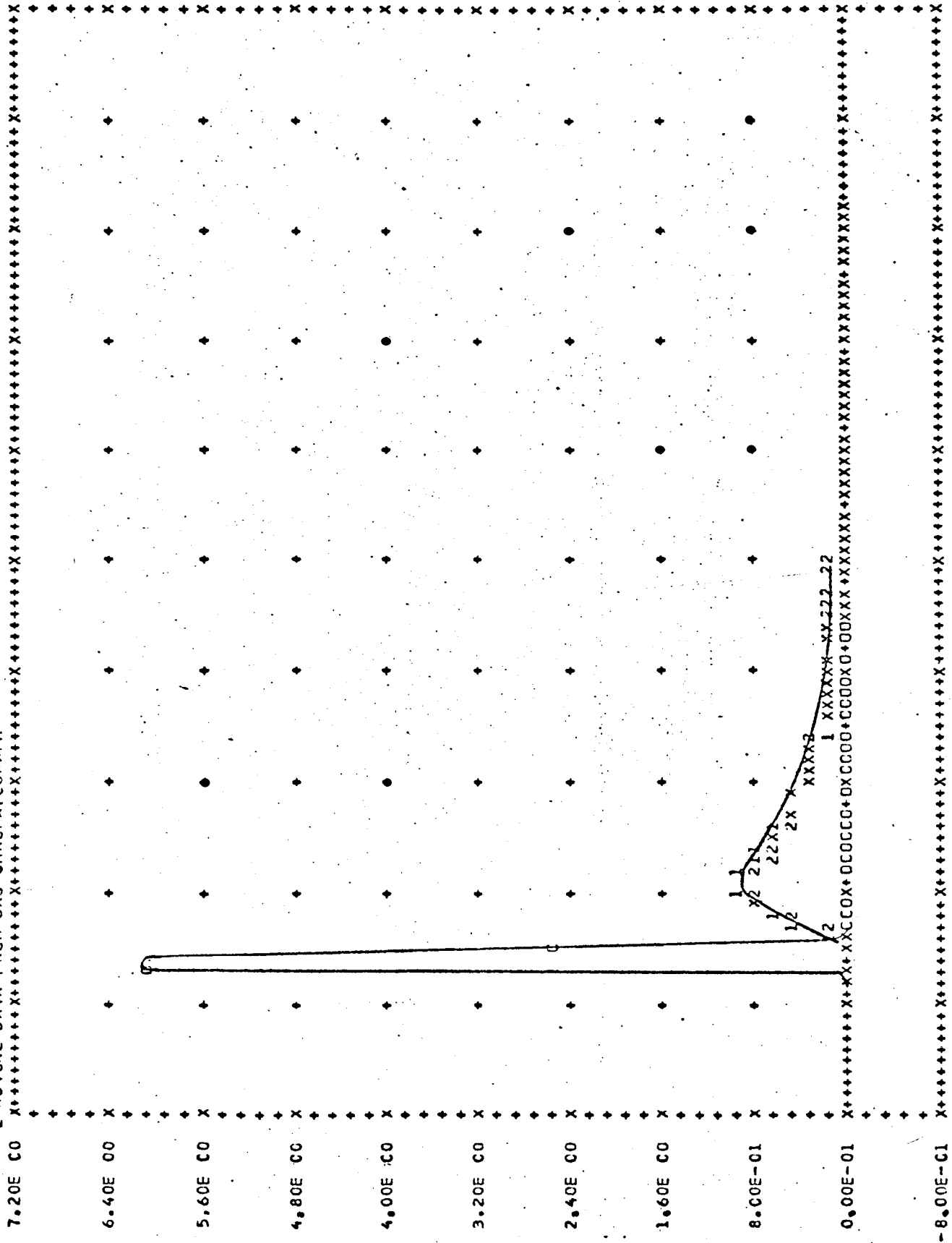
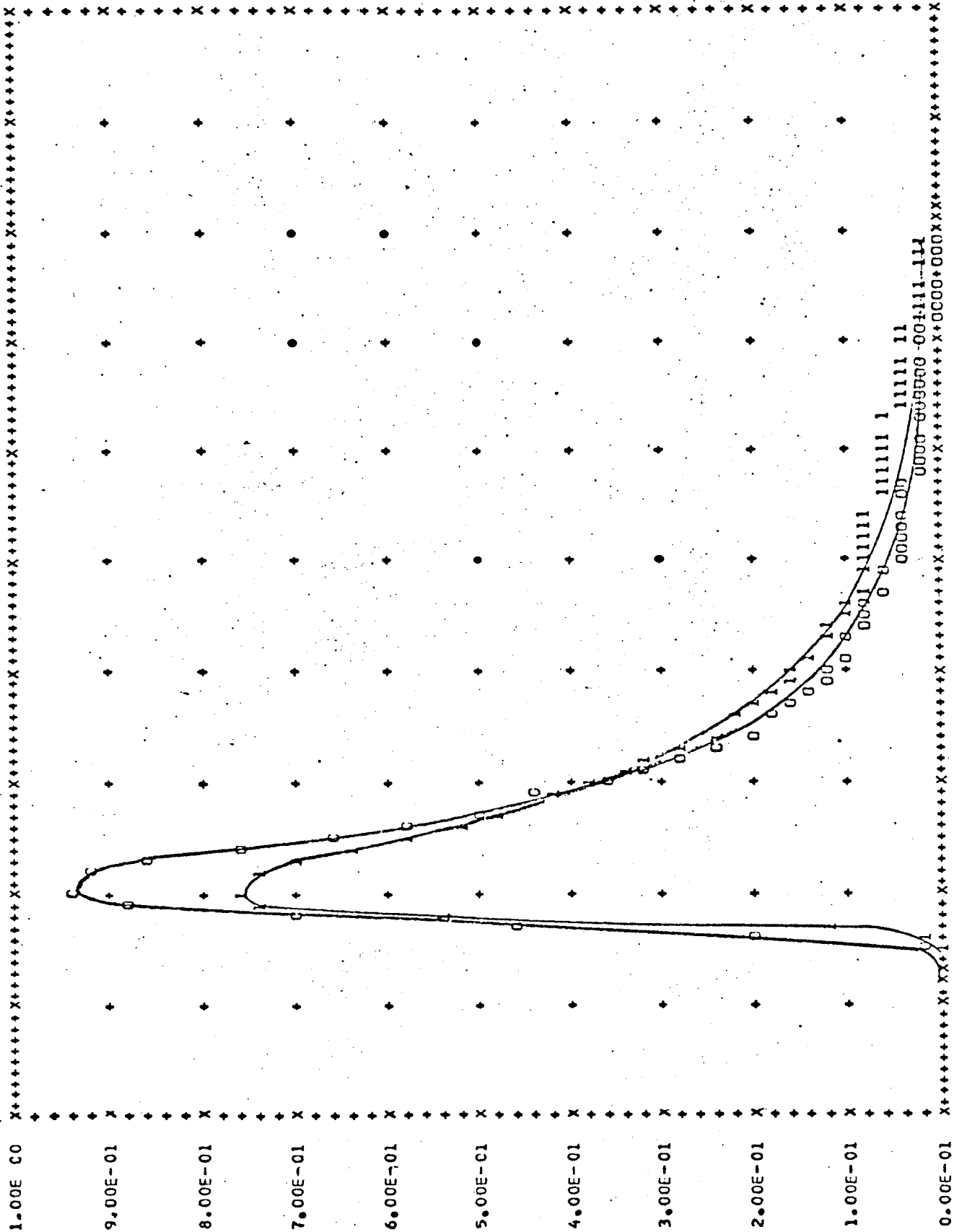


FIGURE 46. Chromatograms for Acetone at 150°C

ACETONE AT 150 DEG C, 43 CC/MIN FLOW RATE, ON A CHROMASORB 102 COLUMN



8.00E-01 1.60E 00 2.40E 00 3.20E 00 4.00E 00 4.80E CC 5.60E CC 6.4CE 00 7.20E 00 8.00E 00 8.80E 00

THIS IS A PLOT OF Y/A VS. DIMENSIONLESS TIME FOR M RO= 1.098462 AND A PECLET NUMBER= 7806.000000

FIGURE 47. Chromatograms for Acetone at 150°C

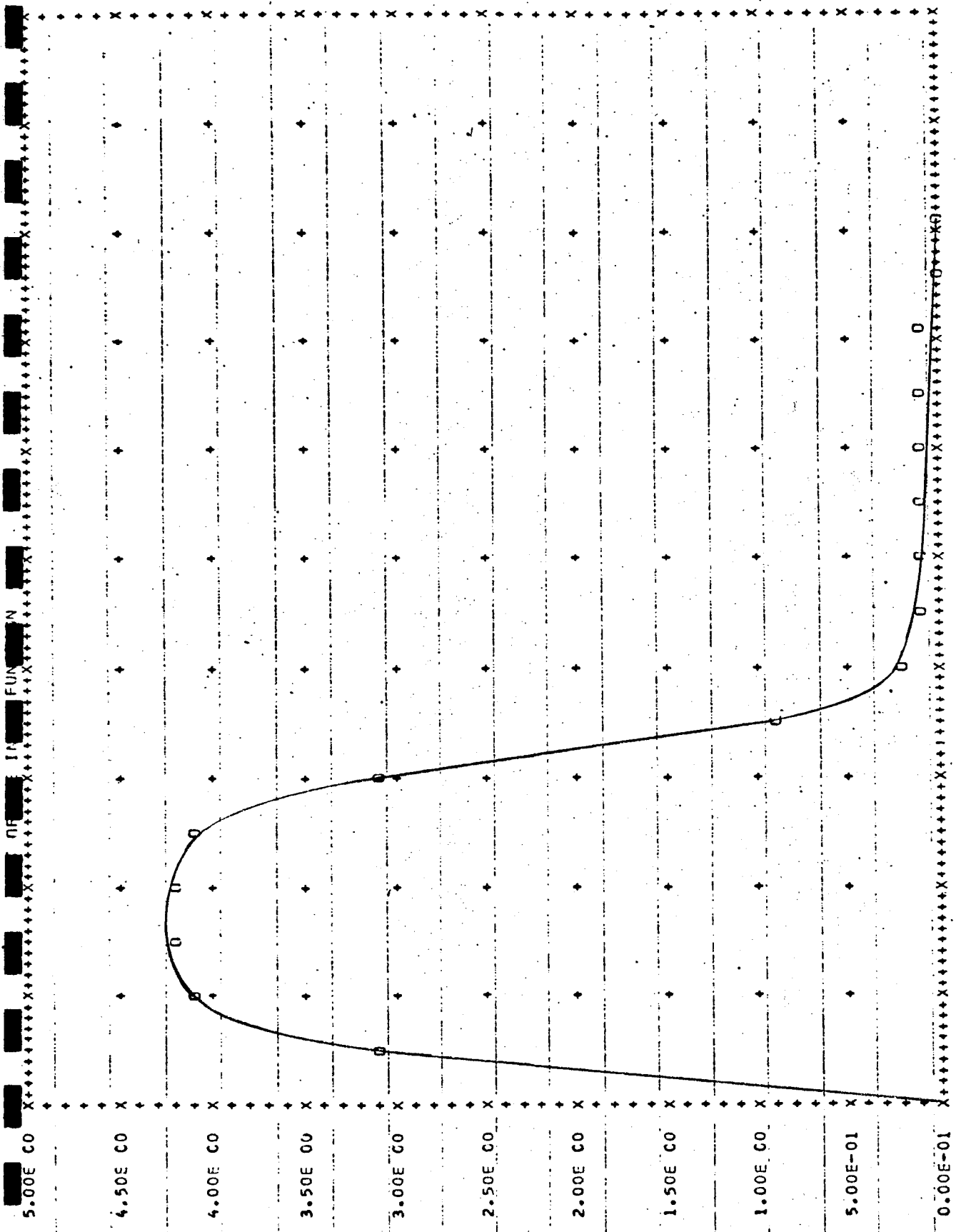


FIGURE 48. Injection Pulse for Ethylene

0.00E-01 8.00E-02 1.60E-01 2.40E-01 3.20E-01 4.00E-01 4.80E-01 5.60E-01 6.40E-01 7.20E-01 8.00E-01

THIS IS A PLOT OF Y/A VS. DIMENSION/JLFS TIME FOR M RC= 0.200907 AND A PECLFI NUMBER= 7189.657CC9

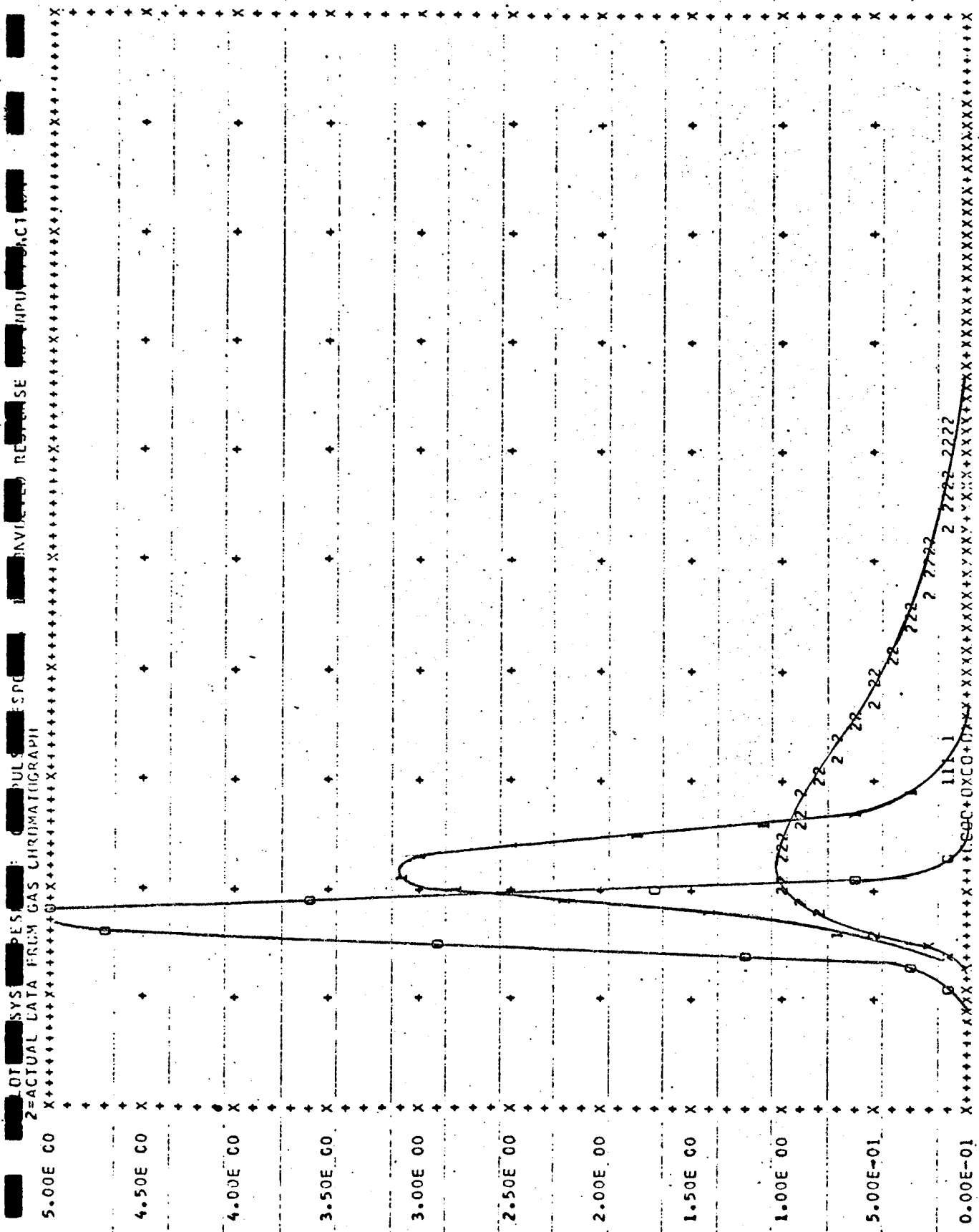


FIGURE 49. Chromatograms for Ethylene at 175°C

Results for both the acetone and ethylene systems show improved representation by the equilibrium adsorption model as the system temperature is increased. It appears that an unknown transport mechanism which is temperature sensitive as well as material dependent is responsible for the differences between the data and the prediction. Because the solid is a porous polymer, it is possible that an original assumption of a thin adsorbed layer on the adsorbent surface and no intraparticle diffusion is not valid. This might account for the differences between the observed behavior of the acetone and ethylene systems because ethylene is a smaller molecule and would tend to exhibit larger intraparticle diffusion effects. The use of the more complicated model, Ref. 32, which includes the effect of finite column length, as expressed as a dimensionless transport parameter N_{tOG} offers a possible area of study. The term N_{tOG} which is a measure of the approach to equilibrium adsorption is relatively temperature-insensitive but interactions between the various parameters Pe , mR_0 , and N_{tOG} may be sufficient to account for this behavior. These topics will be investigated thoroughly in future work.

In summary, the data reduction program in its present form is capable of simulating the gas chromatograph and comparing predicted behavior to actual system data. The equilibrium adsorption model is found to represent data fairly well provided the input pulse is considered, although further work in the model development is warranted. The task on developing a data reduction and analysis procedure is complete and further details have been reported, Ref. 34. Future work will include further model development using the procedure to compare theory with experiment.

Task D.3. Transport Parameter Estimation - P. K. Lashmet

Mathematical representation of the chromatograph requires a priori estimates of the transport parameters Pe and N_{tOG} as well as other properties which depend upon the complexity of the mathematical model. Approximate methods for estimating N_{tOG} have been discussed earlier, Ref. 30, so this task has had as its immediate objective the development of a suitably accurate method for estimating the Peclet number Pe .

The Peclet number, which is a dimensionless measure of diffusion in the direction of carrier gas flow, is defined as

$$Pe = vL/D$$

in which v = mean velocity of the carrier gas

L = length of chromatographic column

D = effective diffusion coefficient

This Peclet number is a function of the fluid mechanics of the system as well as the physical properties of the chemical sample and carrier gas.

Prior attempts to compute the Peclet number from theoretical considerations and other measured transport properties of the system were not completely successful, Ref. 35. It was found during an investigation of the numerical techniques that the step size and error criterion specified in solving the applicable differential and integral equations lead to serious loss of significant figures and a resulting numerical instability. Furthermore, review of recently reported experimental work shows appreciable deviations between data and accepted correlations. Because these correlations are used in deriving the numerical procedure and in checking the technique, the numerical investigation is being delayed until a critical review of the available literature is completed. In addition to this formal work, it is planned to obtain experimental data in the test facility which will yield Peclet numbers. A column packed with non-adsorbing glass beads is available for this purpose.

Because of the availability of new data and these apparent discrepancies, completion of this subtask has been delayed. It will be continued during the next year and should be completed by December 1971. After completion of this portion of the task, the properties of the other parameter N_{tOG} will be further investigated. Because the mathematical models are not particularly sensitive to values of N_{tOG} expected in the projected systems, this portion of the basic task is not critical at the present time.

In summary, a main objective of the Chromatographic Systems Analysis - the development and verification of system models - is well underway. In addition to further work in model development, effort will be initiated in the following areas during the coming year:

1. Effect of chromatograph design upon the design and performance of the overall analytical system (GC/MS).
2. Evaluation of design parameters upon chromatographic system performance especially in multicomponent gases and possible applications to adaptive strategies for system improvement on Mars.

Although the presently available models deviate appreciably from actual data under certain conditions, they are adequate for initiating these proposed overall systems studies.

REFERENCES

1. Rayfield, W.P., and G.N. Sandor, "Rensselaer's Roving Vehicle for Mars," Proceedings of the First Western Space Congress, Santa Maria, California, October 27-20, 1970.
2. Rayfield, W.P., "Mars Roving Vehicle Configuration," RPI Technical Report MP-16, Rensselaer Polytechnic Institute, Troy, N.Y.
3. Baxter, George A., "Wheel Design for an Extraterrestrial Roving Vehicle," Masters Project Report, June, 1970, Rensselaer Polytechnic Institute, Troy, N.Y.
4. Simon, Richard L., "Design of a Toroidal Wheel for a Martian Roving Vehicle," R.P.I. Technical Report MP-21, NASA Grant NGL 33-018-091, May, 1971, Rensselaer Polytechnic Institute, Troy, N.Y.
5. Koehler, Raymond, "Steering and Differential Control Systems for a Mars Roving Vehicle," Masters Project Report, June, 1971, Rensselaer Polytechnic Institute, Troy, N.Y.
6. Zangwill, W.I., Nonlinear Programming: A Unified Approach, Prentice Hall, 1969.
7. "An Exploratory Investigation of a 1979 Mars Roving Vehicle Mission," Jet Propulsion Laboratory, 1970.
8. Petrovich, N.T. and Kamnev, Ye. F., "Problems of Space Radio Communications," NASA TT F-366, January 1966, pg. 183.
9. Renzetti, et al., "Projected NASA/JPL Deep Space Network Capabilities in the 1970's," Stepping Stones to Mars Meeting, March 28-30, 1966, p. 144.
10. Krassner and Michaels, Introduction to Space Communications, McGraw Hill, 1964, pp. 144, 200.
11. Carlson, A.B., Communications Systems, McGraw Hill, 1968, p. 354.
12. "Voyager Spacecraft Systems Study, Phase II, Final Report," Vol. I, General Electric Space Department, Doc. 64SD4376, 1964.
13. Stiffler, J.J., "Telecommunications," Vol. V of Series Space Technology, NASA, SP-69, 1966.
14. Fiacco and McCormick, "The Sequential Unconstrained Minimization Technique for Nonlinear Programming, a Primal Dual Method," Management Science, Vol. 10, No. 2, January 1964.
15. Frederick, D.K. et al, "Analysis and Design of a Capsule Landing System and Surface Vehicle Control System for Mars Exploration"- A Progress Report for July 1, 1970 to December 31, 1970, RPI Technical Report MP-18, Rensselaer Polytechnic Institute, Troy, N.Y., January 1971.
16. Battin, Richard H., Astronautical Guidance, McGraw-Hill Book Company, New York, N.Y., 1964.

17. Watkins, M.C., "Laser Tracking/Ranging Measuring System," Proceedings SPIE Laser Range Instrumentation Seminar, El Paso, Texas, October 1967.
18. Quelle, F.W., "Alternatives to Q-spoiled Ruby Rangefinders," Proceedings SPIE Laser Range Instrumentation Seminar, El Paso, Texas, October 1967.
19. Wilson, J.V., "Instrumentation Study of Primary Navigation System," Rensselaer Polytechnic Institute Technical Report MP-13, Troy, New York.
20. Moore, J.W., "Surface Navigation on Mars," National Space Meeting, Moffett Field, California, February 1970.
21. "Phototubes and Photocells; Technical Manual PT-60," R.C.A., Lancaster, Pa., 1963.
22. DiDomenico, Svelto, "Solid-State Photo Detector: A Comparison Between Photodiodes and Photoconductors," Proceedings of the IEEE, February 1964, pp. 136-144.
23. Melchior, Lynch, "Signal and Noise Response of High Speed Germanium Avalanche Photodiodes," IEEE Transactions on Electron Devices, December 1966, pp. 829-838.
24. Wm. Smart, "Spherical Astronomy," Cambridge Press, 1965.
25. Rieback, D.J., "Preliminary Design of an Automatic Device for the Location of the Pole Star and/or True Pole of Mars," Rensselaer Polytechnic Institute Technical Report MP-20, Troy, New York.
26. Rodamaker, Mark C., "Design and Analysis of a Local Vertical Sensor for a Mars Roving Vehicle," Engineering Project Report, Rensselaer Polytechnic Institute, May 1971.
27. Pavarini, C. and Chrysler, J., "Terrain Modeling and Path Selection by an Autonomous Martian Exploratory Vehicle," Rensselaer Polytechnic Institute Technical Report MP-14, Troy, New York, June 1970.
28. Rautio, A.M., "An Analysis of the Effect of Sensor Errors on a Long Range Terrain Modeling System and a Study of Short Range Terrain Modeling for an Autonomous Roving Vehicle," Engineering Project Report, Rensselaer Polytechnic Institute, Troy, New York, June 1971.
29. Baer, S.R., and Benoit, G.L., "Chromatographic Test Facility," RPI Technical Report MP-19, Rensselaer Polytechnic Institute, Troy, New York, March 1971.
30. Sliva, T.F., "Chromatographic Systems Analysis: First-Order Model Evaluation," RPI Technical Report MP-1, Rensselaer Polytechnic Institute, Troy, New York, August 1968.
31. Voytus, W.A., "Chromatographic Systems Analysis: Moment Analysis of the Equilibrium Adsorption Model," RPI Technical Report MP-19, Rensselaer Polytechnic Institute, Troy, New York, June 1969.
32. Taylor, P.N., "Chromatographic Systems Analysis: Second-Order Model Development," M. Eng. Report, Rensselaer Polytechnic Institute, Troy, New York, June 1970.

33. Krum, R.C., "Chromatographic Systems Analysis: Sample Injection Problem," RPI Technical Report MP-10, Rensselaer Polytechnic Institute, Troy, New York, June 1969.
34. Benoit, G.L., "Reduction of Chromatographic Data and Evaluation of a GC Model," RPI Technical Report MP-22, Rensselaer Polytechnic Institute, Troy, New York, June 1971.
35. Reichman, D.E., "Chromatographic Systems Analysis: Transport Parameter Estimation," M. Eng. Report, Rensselaer Polytechnic Institute, Troy, New York, August 1970.